INEEL/EXT-02-00060

INEEL Advanced Radiotherapy Research Program Annual Report 2001

J. R. Venhuizen

April 2002

Idaho National Engineering and Environmental Laboratory
Bechtel BWXT Idaho, LLC

INEEL/EXT-02-00060

INEEL Advanced Radiotherapy Research Program Annual Report 2001

J. R. Venhuizen

April 2002

Idaho National Engineering and Environmental Laboratory
Idaho Falls, Idaho 83415

Prepared for the
U.S. Department of Energy
Office of Science
Under DOE Idaho Operations Office
Contract DE-AC07-99ID13727

ABSTRACT

This report summarizes the major activities and accomplishments of the Idaho National Engineering and Environmental Laboratory (INEEL) Advanced Radiotherapy Research Program for calendar year 2001. Applications of supportive research and development, as well as technology deployment in the fields of chemistry, radiation physics and dosimetry, and neutron source design and demonstration are described. Contributions in the field of chemistry include analysis of biological samples and continued effort focused on development of a blood-boron analyzer based on infrared spectrometry. Contributions in the fields of physics and biophysics include development of advanced patient treatment planning software, feasibility studies of accelerator neutron source technology for Neutron Capture Therapy (NCT), and completion of major modifications to the research reactor at Washington State University to produce an epithermal-neutron beam for NCT research applications.

CONTENTS

FIGURES

APPLICATION OF INFRARED SPECTROSCOPY FOR THE DETERMINATIOIN OF BORON IN BIOLOGICAL FLUIDS

CONSTRUCTION OF AN EPITHERMAL NEUTRON BEAM FOR PRECLINICAL BNCT RESEARCH AT WASHINTON STATE UNIVERSITY

FIGURES (Continued)

CONSTRUCTION OF AN EPITHERMAL NEUTRON BEAM FOR PRECLINICAL BNCT RESEARCH AT WASHINTON STATE UNIVERSITY (CONTINUED)

FIGURES (Continued)

CONSTRUCTION OF AN EPITHERMAL NEUTRON BEAM FOR PRECLINICAL BNCT RESEARCH AT WASHINTON STATE UNIVERSITY (CONTINUED)

PRELIMINARY NEUTRONIC PERFORMANCE ASSESSMENT OF AN EPITHERMAL NEUTRON BEAM FOR PRECLINICAL BNCT RESEARCH AT WASHINGTON STATE UNIVERSITY

DEVELOPMENT OF ADVANCED MULTI-MODALITY RADIATION TRANSPORT SOFTWARE

FIGURES (Continued)

DEVELOPMENT OF ADVANCED MULTI-MODALITY RADIATION TRANSPORT SOFTWARE

MOLECULAR TARGETED RADIOTHERAPY DEMONSTRATION SOFTWARE

FILTERED EPITHERMAL PHOTONEUTRON BEAM PARAMETER STUDIES FOR NEUTRON CAPTURE THERAPY APPLICATIONS

FIGURES (Continued)

FILTERED EPITHERMAL PHOTONEUTRON BEAM PARAMETER STUDIES FOR NEUTRON CAPTURE THERAPY APPLICATIONS (CONTINUED)

TABLES

PRELIMINARY NEUTRONIC PERFORMANCE ASSESSMENT OF AN EPITHERMAL NEUTRON BEAM FOR PRECLINICAL BNCT RESEARCH AT WASHINGTON STATE UNIVERSITY

FILTERED EPITHERMAL PHOTONEUTRON BEAM PARAMETER STUDIES FOR NEUTRON CAPTURE THERAPY APPLICATIONS

TABLES (Continued)

FILTERED EPITHERMAL PHOTONEUTRON BEAM PARAMETER STUDIES FOR NEUTRON CAPTURE THERAPY APPLICATIONS
(CONTINUED)

ACRONYMS AND ABBREVIATIONS

API	Application Programming Interface
ARTP	Advanced Radiotherapy Program
ATR	attenuated total reflectance
BNCT	Boron Neutron Capture Therapy
BNL	Brookhaven National Laboratory
Bq	Becquerel
BSH	borocaptate sodium
cGy	centiGray
cm	centimeter
CPU	central processor unit
CRADA	Cooperative Research and Development Agreement
CT	computed tomography
CY	calendar year
DBMS	database management system
DC	direct current
DDP	dose-depth plots
DI	deionized
DICOM	radiological scanner electronic image format
DOE	Department of Energy
DORT	Discrete Ordinates Radiation Transport
DRR	digitally reconstructed radiograph
DVH	dose-volume histograms
E	energy
eV	electron volt
FDA	Food and Drug Administration
FIA	flow injection analysis
FiR 1	Finnish Research Reactor
FNT	fast neutron therapy
FT	Fourier transform
FTIR	Fourier Transform Infrared
FTIRS	Fourier Transform Infrared Spectroscopy
FWHM	full width half maximum
FY	fiscal year
g	gram
GUI	graphical user interface
HPGe	high-purity germanium
HTML	hyper-text markup language
Hz	hertz
IAC	Idaho Accelerator Center
ICP-AES	inductively coupled plasma-atomic emission spectrometry
ICP-OES	inductively coupled plasma-optical emission spectrometry

ACRONYMS AND ABBREVIATIONS (Continued)

IDE	Integrated Development Environment
in	inch
INEEL	Idaho National Engineering and Environmental Laboratory
IR	Infrared
IRE	Internal reflectance element
IRLED	IR-light emitting diode
ISU	Idaho State University
JDBC	Java database connectivity
keV	kilo-electron volt
kg	kilogram
kW	kilowatt
lb	pound
LDRD	Laboratory Directed Research and Development
LINAC	linear accelerator
LLNL	Lawrence Livermore National Laboratory
ma	milliampere
mC	millicolumb
MC	Monte Carlo
MCNP	Monte Carlo N-Particle
MeV	Million-electron volt
MINERVA	Modality-Inclusive Environment for Radiotheraputic Variable Analysis
MHz	Megahertz
mL	milliliter
mm	millimeter
mrad	millirad
ms	millisecond
MSU	Montana State University
MTR	molecular targeted radiotherapy
MW	Megawatt
mW	milliwatt
NCT	neutron capture therapy
NIST	National Institute of Standards and Technology
NTL	Neutron Therapies, Limited Liability Company
NURBS	Non-Uniform Rational B-Spline
ODBC	Open database connectivity
PC	personal computer (control computer)
PET	positron emission tomography
PLS	partial least squares

ACRONYMS AND ABBREVIATIONS (Continued)

ppm	parts per million
RTOG	Radiation Therapy Onocology Group
Rtpe	Radiation treatment planning environment
s	second
SC	Office of Science
SERA	Simulation Environment for Radiotherapy Applications
SPECT	single photon emission computed tomography
TE	thermoelectric
TIRADE	Transport Independent Radiotherapy Environment
TRIGA	Transient Reactor Irradiator-General Atomics
UCD	University of California, Davis
UCLA	University of California, Los Angeles
UML	unified modeling language
UW	University of Washington
VHP	Visible human project
VTT	Valtion Teknillinen Tutkimuskeskus (Technical Research Centre of Finland)
W	watt
WSU	Washington State University
2D	two-dimensional
3D	three-dimensional
μCi	microcurries
μg	microgram
μJ	microJoule
μL	microliter
μm	micron or micrometer
μs	microsecond
μS	microSievert
μW	microwatt

INEEL ADVANCED RADIOTHEAPY RESEARCH PROGRAM ANNUAL REPORT 2001

INTRODUCTION AND EXECUTIVE SUMMARY

The Idaho National Engineering and Environmental Laboratory (INEEL) Advanced Radiotherapy Research Program completed its 15th year under the sponsorship of the U.S. Department of Energy (DOE), Office of Science (SC). The program underwent a major external peer review during CY 2001. As a result of this review, many ongoing activities were continued, a few others were reprioritized, and a new activity focused on collaboration with Lawrence Livermore National Laboratory (LLNL), in the field of advanced treatment planning software development, was initiated during the fourth quarter. This report includes detailed articles describing major INEEL activities and accomplishments during the year.

A primary program goal has been, and continues to be, participation in the establishment of neutron capture therapy (NCT) as a clinically useful innovative radiotherapy in and of itself, or as an adjunct to fast-neutron therapy (FNT). In addition, a new task involving the development of advanced multi-modality computational dosimetry and treatment planning software with an initial emphasis on molecular targeted radionuclide applications was introduced during the year. The various program goals are accomplished through applications of supportive research and development and technology deployment in the fields of chemistry, radiation physics and dosimetry, and neutron source design and demonstration. Many activities have been performed in close collaboration with other DOE national laboratories and major universities. Where a benefit to the U.S. NCT effort is realized, the INEEL also maintains formal cooperative arrangements with certain foreign collaborators, specifically in The Netherlands, Finland, Sweden, and Argentina. Finally, in light of the stated goals of DOE for technology transfer and commercialization, some aspects of the Program are operated in partnership with private U.S. industry through a Cooperative Research and Development Agreement (CRADA), as well as through several technology licensing agreements. These arrangements have resulted in substantial leveraging of DOE-SC funding, especially in the important area of boron agent development.

The historical INEEL role as a center for quantitative boron analysis and radiation treatment planning software development and deployment continued during 2001. Biological samples and boron agent samples submitted to the INEEL by DOE-supported NCT research organizations were analyzed for boron content in accordance with well-established standards, and the results were reported back to the submitting organizations. For the first three quarters of the year, work continued on a real-time infrared blood-boron analyzer that will be able to sample the boron content of a patient's blood by infrared absorption spectrum techniques, since the absorption spectrum contains a feature common to all boron hydride compounds. The internationally recognized INEEL SERA (Simulation Environment for Radiotherapy Applications) computational dosimetry and treatment planning software system continued to be supported during the year. The initial release of SERA occurred in 1998, considerable refinement and additional feature development took place in 1999 and 2000, and the distribution version was stabilized in 2001. NCT and FNT research centers worldwide serve as benchmarking and testing institutions for SERA, providing extremely valuable feedback and suggestions for improvement.

With the completion of SERA, work has now begun on the new multimodality radiotherapy treatment planning system, in collaboration with LLNL. This effort will take advantage of the many benefits of using the Java programming language to create a "next-generation" system for a wide variety of research applications.

With the completion of the DOE-sponsored epithermal-neutron boron NCT (BNCT) clinical trials at Brookhaven National Laboratory (BNL), INEEL attention has shifted toward the continued development of new neutron source technologies useful for NCT and NCT-augmented FNT, and toward additional basic research focused on the clinical introduction of improved boron agents. This has been done in connection with a longstanding relationship established with a CRADA partner, Neutron Therapies, Limited Liability Company (NTL), as well as under separate collaborations with the University of Washington (UW) fast-neutron radiotherapy program, and with DOE-sponsored radiobiological research efforts conducted by the Washington State University (WSU) School of Veterinary Medicine. Human biodistribution studies of one alternate boron agent continued through most of 2001 at UW under a Food and Drug Administration (FDA) approved protocol, with in-kind technical support from the INEEL. These studies are in preparation for the possible future initiation of separately funded human trials of BNCT-enhanced FNT for certain lung tumors and high-grade brain tumors using the UW clinical fast-neutron facility. In addition, some small-animal radiobiology studies were conducted to provide an initial assessment of a new fast-neutron beam configuration at UW that was jointly developed by INEEL and UW to improve the performance of the UW facility for NCT-augmented FNT applications. Furthermore, construction of a new epithermal neutron beam facility for preclinical research at WSU was completed during the year in a collaborative effort of INEEL and WSU, with a significant funding component from internal WSU sources.

Finally, in addition to the baseline NCT activities supported directly at the INEEL by DOE-SC, further supportive, but separate, collaborative BNCT-related university research is sponsored by the INEEL Laboratory Directed Research and Development (LDRD) Program. Two INEEL/university NCT projects were completed during the year under this type of sponsorship. These were: 1) development by INEEL and Idaho State University of a concept for an electron accelerator based epithermal-neutron source for BNCT; and, 2) investigation, by the University of Tennessee, of the application of Positron Emission Tomography (PET) to the quantitative imaging of boron agents *in vivo*, with incorporation of the resulting information into the treatment planning process via the SERA system. The first of these projects is documented in this report, while the second is documented separately[a].

---

[a] M..K. Kahn, L.F. Miller, G.W. Kabalka, T.F. Nichols, "Improving Existing BNCT Dosimetry by use of Registered PET and MRI Images", Proceedings of the ANS Radiation Protection and Shielding Division 12th Biennial Topical Meeting, April 14-18, 2002, American Nuclear Society, Chicago Illinois.

ANALYTICAL CHEMISTRY

W. F. Bauer and B. M. White

Idaho National Engineering and Environmental Laboratory, Idaho Falls, ID

INTRODUCTION

There were two basic analytical chemistry related functions during 2001. The first of these functions was simply the determination of boron in a variety of biologically related samples using inductively coupled plasma atomic emission spectroscopy (ICP-AES). The second function was the continuation the task examine the feasibility of using some novel infrared devices to create a device to measure blood boron as boron hydrides *in vivo*, and is described in the next article, Application of Infrared Spectroscopy For The Determination of Boron in Biological Fluids.

DETERMINATION OF BORON IN BIOLOGICAL SAMPLES

During 2001, 675 new samples were received for analysis. With samples from FY 2000 and the additional QA samples, the total samples analyzed came to 1,195. Of the samples received, 648 were from dogs and/or rodents from the Boron Neutron Capture Therapy and related programs in Dr. P. Gavin's group at Washington State University (WSU), 3 were of stock solutions to be sent to WSU and assorted other preparations from Dr. F. Hawthorne's group at University of California, Los Angeles (UCLA), 16 were from the trials being done in conjunction with Neutron Therapies, Limited (NTL) at the University of Washington (UW), and 2 were from NTL (San Diego). The anticipated level of samples from WSU never materialized in 2001 for various reasons. As the neutron beam comes on line, the anticipated number of samples from WSU will increase dramatically. During 2002, samples are expected from UCLA, WSU, UW, Southwest Texas State University, and from George Kabalka at the University of Tennessee. Many of the samples from WSU are actually in support of the researchers from the other institutions.

APPLICATION OF INFRARED SPECTROSCOPY FOR THE DETERMINATION OF BORON IN BIOLOGICAL FLUIDS

W. F. Bauer[1], A. Suazo[2] and C. Rae[1]

1. **Idaho National Engineering and Environmental Laboratory, Idaho Falls, ID**
2. **Manitou Springs High School, Manitou Springs, CO (Summer Research Assistant)**

INTRODUCTION

Infrared spectroscopy has been suggested as a potential tool for boron determinations in Boron Nuclear Capture Therapy (BNCT) related studies. Many of the boron delivery agents being considered for BNCT are polyhedral borane derivatives[1-5]. The B-H stretch for these compounds generally occurs in the 2400-2650 cm^{-1} region, a spectral region with little interference. Using this spectral region, detection limits as low as 2.5-5 μg B/g in blood plasma have been reported[1-4]. Infrared analysis for B is rapid and selective, however, as discussed previously[6], it is limited by the achievable detection limits. The strong absorbance by water throughout most of the mid-infrared spectral region limits the pathlength that can be used in the sample cell to something less than a few 10s of microns. Liquid handling cells with such short pathlengths are hard to deal with, and difficulties in filling and cleaning the cells while achieving reproducible pathlengths are commonplace. Attenuated total reflectance (ATR) is one method that has been used in infrared (IR) spectroscopy to overcome the issues associated with short, non-reproducible pathlengths[7].

In ATR, the infrared beam from the spectrometer is passed into an internal reflectance element (IRE) at an angle. Because of the differences in the refractive index of the IRE and the surrounding medium at the interface, the beam is reflected back into the crystal. The resulting evanescent wave penetrates the region between the IRE and the sample to a depth of ~1-2 μm per reflection. Therefore, as long at the surface of the IRE is covered with the sample to a depth of > 1-2 μm, the effective pathlength is always reproducible.

The authors are attempting to use attenuated total reflectance and some novel new infrared sources to build a benchtop laboratory instrument whose sole purpose is to measure boron from polyhedral borane compounds in biological samples. The instrument to be developed will be portable and capable of analysis of liquids and, possibly, solid samples. This year's work focused upon the application and potential limitations of the ATR technique using a simple cell design with Fourier Transform Infrared Spectroscopy (FTIRS), and characterizing different infrared sources to be used in a simple filter photometer that would be designed to determine boron in biological samples routinely.

EXPERIMENTAL METHODS

Solutions of GB-10 were prepared by simple dilutions from 10,000 μg $^{10}B/g$ as GB10 stock solutions (Neutron Therapies, Inc.). Solutions of sodium mercaptoundecahydrodo-decaborate (BSH), ^{10}B enriched BSH, and $Li_2B_{12}H_{12}$ were prepared by weighing the dry salt from an Idaho

National Engineering and Environmental Laboratory (INEEL) archive sample and diluting with deionized water (18 megaohm). Standards were prepared at 5, 10, 20, 30, 40, 50, 100, 150, 200 and 250 µg B/mL. Concentrations of the stock solutions and some of the diluted samples were confirmed by inductively coupled plasma-optical emission spectroscopy (ICP-OES)[8].

The ATR cell used for the FTIR studies was the Foundation Series Multi-Reflection HATR accessory (Thermo Spectra-Tech, Shelton CT) with a ZnSe internal reflection crystal mounted in a trough plate for liquid samples. A Wilmad (Buena, NJ) VariPath transmission cell with CaF_2 windows was used for the transmission measurements. Infrared spectra were acquired on a BioRad (Hercules, CA) FTS 60 or a Bruker Equinox 55 FTIR spectrometer. Scans were acquired on the FTS 60 equipped with a wide-band mercury cadmium telluride (MCT) detector at 4 cm^{-1} resolution, and were typically an average of 32 scans at a mirror velocity 10 kHz. Scans acquired on the Equinox 55 were also acquired at 4 cm^{-1} resolution with a MCT detector, but consisted of an average of 128 scans with a mirror velocity of 20 kHz. Three spectra were collected for each standard by running through the entire sequence of standards for each analyte three separate times. In this way, many of the factors that influence baselines, such as the repeated handling and cleaning of the ATR cell and time, are included into the calibration curve. Data processing, including peak integration, peak height determinations, and partial least squares (PLS) analyses was performed in Grams/AI (Thermo Galactic). All determinations were made after a 2-point background correction at 2607 and 2392 cm^{-1}. Integration and PLS analysis were performed from 2610-2390 cm^{-1}.

Flow injection analysis (FIA) was carried out with an experimental apparatus as shown in Figure 1. This apparatus consisted of a PulseIR or ReflectIR (Boston Electronics Corporation) thermal source (Figure 2) controlled with a pulse generator programmed via an RS232 connection with the control computer (PC). Although the ReflectIR source is collimated to a large degree due to the housing, additional BaF_2 lenses were used to further focus and collimate the beam. The beam then passed through a Micro Demountable Flow-Thru Cell (Spectra-Tech) with CaF_2 windows, and was focused with a BaF_2 lens through a bandpass filter onto a PbSe detector (Electro-Optical Systems, Inc.) thermoelectrically cooled to –30°C. The carrier stream was simply deionized water pumped at 1 mL/min with a peristaltic pump. The sample was loaded into a 100 µL sample loop and injected into the carrier stream for analysis. Analog output from the PbSe detector was digitized with a PCI-MIO-16e multifunction card (Digital Instruments) using the source pulse as a trigger for the data acquisition. Source control and data collection operations were performed with LabView software on the control computer (PC).

RESULTS AND DISCUSSION

ATR-FTIR Spectroscopy

Previously, the ability of ATR-FTIRS to determine B with reasonable accuracy and precision was demonstrated[6]. Detection limits determined from the standard deviation of the y-intercept were ~5 µg ^{10}B/mL as GB10. GB10 is only one of many compound types containing multiple B-H bonds that are being considered for use in BNCT. To optimally design a filter photometer

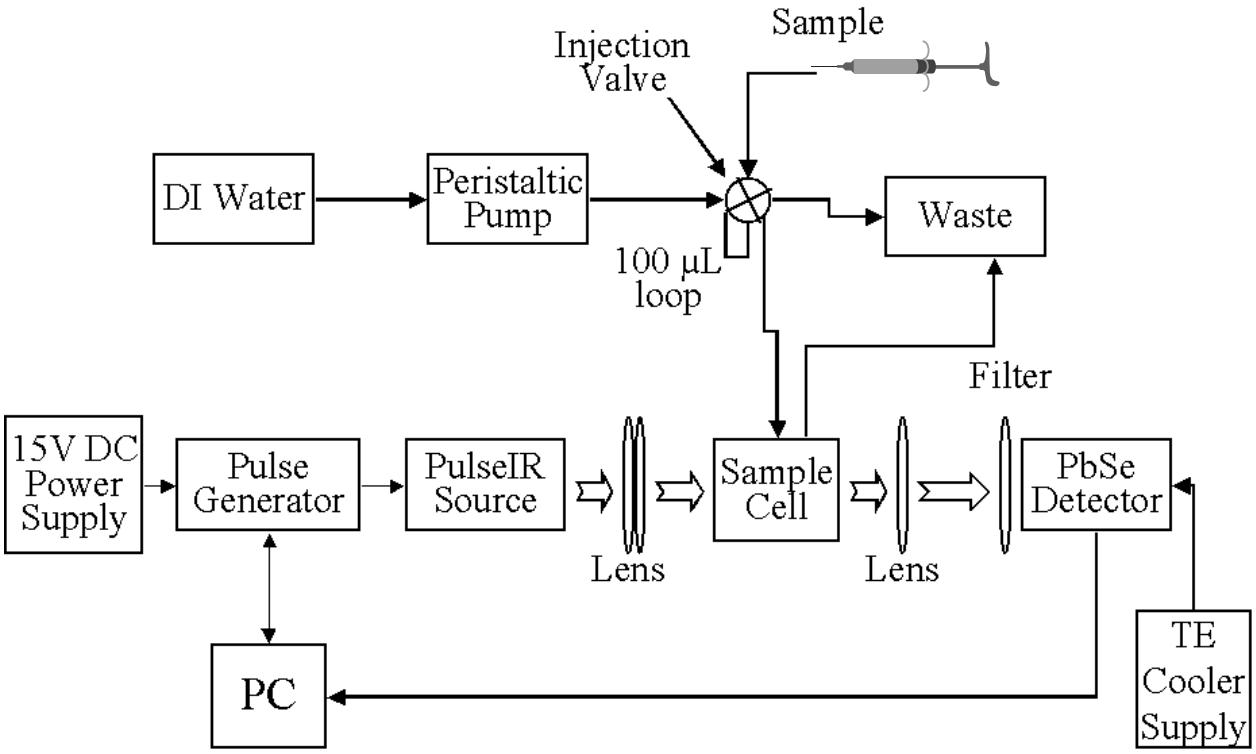

Figure 1. Simple schematic of infrared filter photometer for determination of boron in biological fluids by flow injection analysis.

Figure 2. ReflectIR pulsed thermal sources on left with CaF_2 windows and a continuous miniature IR source (LC-IR-12k) with elliptical reflector to help collimate the beam shown on right.

for B analysis, it will be important to fully understand the spectral characteristics and behavior of other B compounds of interest in the 2400-2650 cm^{-1} spectral region. The availability of a variety of compounds is somewhat limited, however, at the INEEL, there are multiple ^{10}BSH, BSH and $Li_2B_{12}H_{12}$ samples available.

The standards of BSH, ^{10}BSH, $Li_2B_{12}H_{12}$ and GB10 were run on the Bruker Equinox 55 FTIR using the ZnSe ATR cell. A problem was encountered with the BSH standards as the BSH reacts with the surface of the ZnSe surface, presumably via exchange of a Se and the sulfhydryl group of BSH. Figures 3 and 4 demonstrate the kinetics of this reaction using a 5 µg B/mL BSH solution. The apparent concentration of B rapidly increases over the first couple of minutes and then increases much more slowly. The reaction does not appear to be complete by 17 minutes. By this time, the peak has more than doubled. The reaction does not appear to be due to any of the oxidation products of BSH[9-11], as the same results were obtained with aged solutions and freshly prepared solutions. This reaction could potentially be viewed as an advantage in that it concentrates the boron compound on the surface, allowing much lower detection limits. Unfortunately, the reaction is relatively slow for analytical purposes. The BSH is bound rather tightly to the surface of the ZnSe IRE and can only be removed by several minutes of exposure to a sodium hydroxide solution.

To collect data for the calibration curves of BSH, scanning was initiated after a 10 second delay from the time the sample was put in the cell. After data collection, the cell was cleaned by exposure to the sodium hydroxide solution. The cleaning was repeated until no BSH was apparent in the spectrum of blank deionized (DI) water. Even with this cleaning, the calibration curves were nonlinear at the lowest concentration levels as demonstrated in Figure 5. Fitting to a quadratic equation was still not adequate to describe the curve. The lower concentration range of the curve appears to be dominated by the kinetics of the BSH reaction with the ZnSe surface. The lower concentration measurements are also much more precise, possibly owing to the number of surface sites being reacted in the same period of time at the different concentration levels. Use of peak areas rather than the peak heights did not improve the precision. In fact, the precision was somewhat worse, possibly indicating that some baseline abnormalities may play a role in the poor reproducibility. This would not be unexpected, as peaks with such a small net absorbance may be easily influenced by any minor spectral variability. The shape of the curve in Figure 4 does not appear to conform to a simple rate law suggesting either more than one type of binding site on the ZnSe IRE or there may be consecutive reactions. In either case, each site or reaction has its own rate. This added level of uncertainty could also contribute to the lower precision at the higher concentrations.

Even without knowing the exact reaction dynamics of the BSH with the ZnSe IRE, a calibration can be obtained using the method of PLS[12]. This multivariate approach to calibration utilizes the entire spectral range rather than just the peak height or peak area to determine concentration. The PLS calibration accommodates shifting baselines and can accommodate some nonlinearities. Figure 6 plots the predicted concentrations vs. the actual concentrations for the PLS calibration of ^{10}B as BSH using the same spectra as in Figure 5. The six factors used to describe the data set with the PLS appears to adequately describe the nonlinearities shown in Figure 5, as well as to describe the variations in the baselines that contribute to the imprecision. Interestingly, at 40

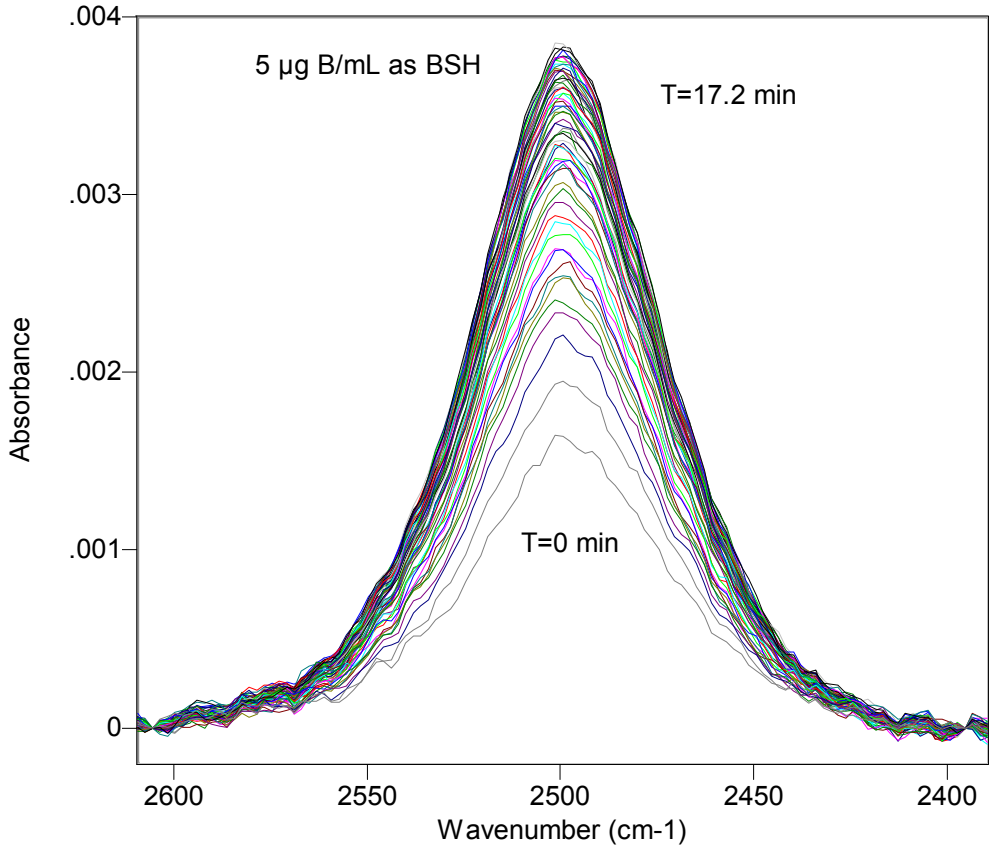

Figure 3. Reaction of BSH with ZnSe is demonstrated with 5 µg ^{10}B/mL as BSH.

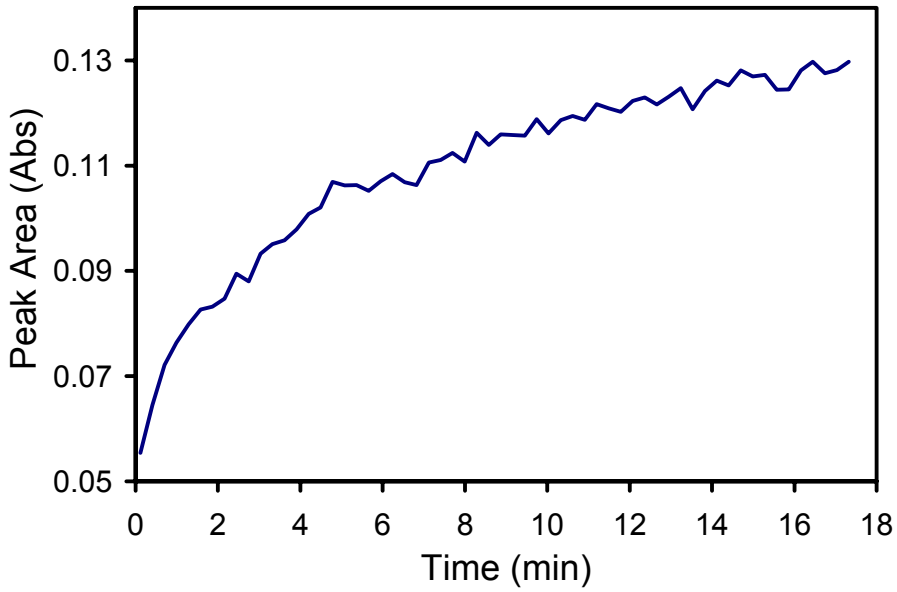

Figure 4. Summary of the data in Figure 1 showing the increase in peak area with time of exposure for 5 µg ^{10}B as BSH on a ZnSe ATR element (n = 32 scans).

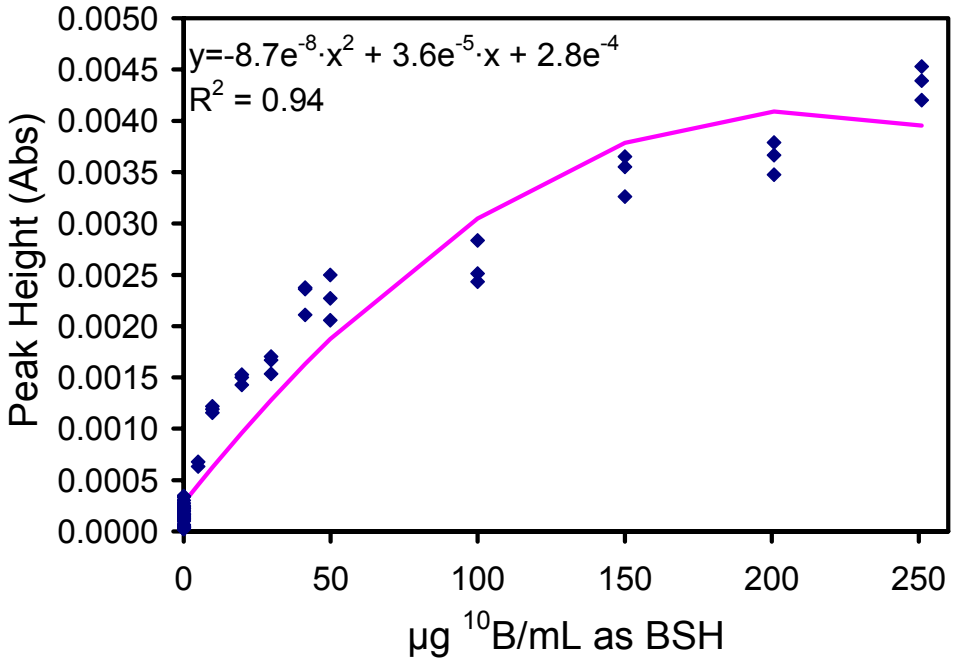

Figure 5. Boron concentration plotted vs. peak height for BSH determined by FTIR ATR with a ZnSe crystal. At the low concentration end, sorption of BSH to the ZnSe crystal dominates.

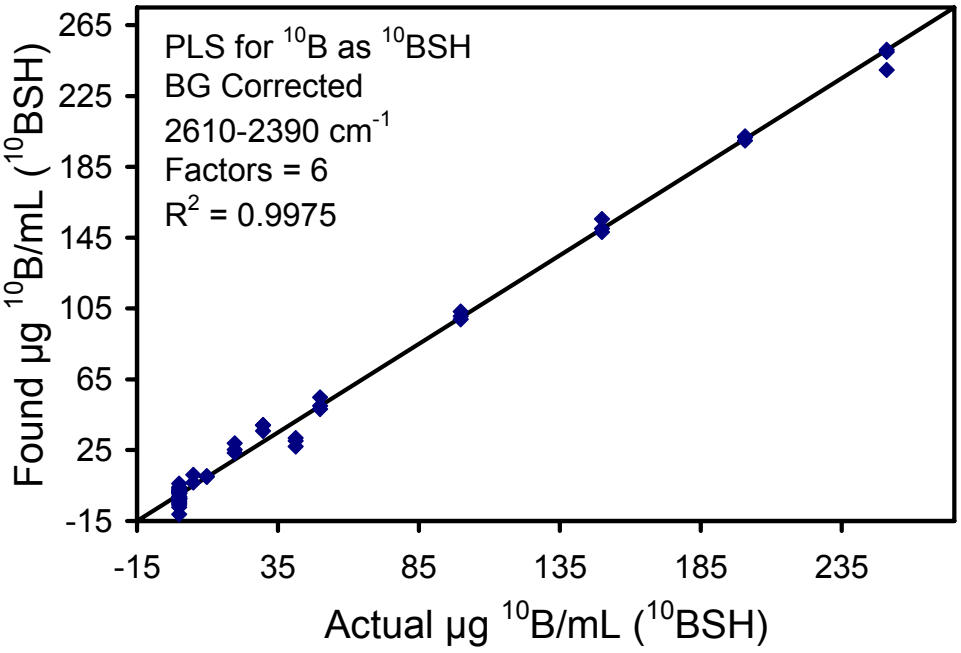

Figure 6. Same data as in Figure 5 using PLS calibration model.

μg ^{10}B/mL, the ^{10}B concentration is underestimated and the error largest. This appears to be where two portions of the curve shown in Figure 5 meet. In any case, the R^2 is 0.9975, and the estimated detection limit using three times the standard deviation of the y-intercept of the curve plotted in Figure 6 is 2.1 μg/mL. Similar results were obtained with the natural abundance boron BSH.

The calibration curves for ^{10}B as GB10 and B as $Li_2B_{12}H_{12}$ are typified by the calibration curve for $Li_2B_{12}H_{12}$ using peak heights shown in Figure 7. The R^2 is greater than 0.98, and the detection limits determined at three times the standard deviation of the y-intercept typically range from 7 to 8 μg B/mL when using peak heights. Peak areas tended to be slightly worse with the detection limits ranging from 8-11 μg B/mL. Again, because of the extremely low observed absorbance values, any variations in the spectral background can have a negative effect upon the results. If the spectral shapes of these backgrounds can be modeled by a multivariate calibration method, then higher precision and lower detection limits can be achieved. Figure 8 shows the results of the PLS calibration using the same spectra as used for Figure 7. The R^2 is raised to > 0.99 and the detection limits are in the 2.5-3.2 μg B/g range.

Because of the nature of absorbance spectroscopy, a calibration, once developed, should be universal since the absorption coefficients at each wavelength are constants. Figure 9 depicts the results for the determination of boron concentrations for a set of standards prepared with GB10 in late 2001 using a PLS calibration made with a different set of standards prepared and analyzed in September, 2000 on a different FTIR instrument. The calibration was developed using spectra collected with the ATR cell mounted in the FTS 65. The spectra of the standards analyzed as unknowns were collected ~1 year later on the Equinox 55. The correlation between the two sets of spectra is quite good as the R^2 is greater than 0.99. However, the slope and y-intercept indicate that there is slight bias and offset. The reason for the bias is unknown, but may be related to the different apodization functions used to process the interferograms[13,14]. Although, due the naturally wide peaks of the analyte relative to the instrument resolution, any differences caused by the apodization functions will be at a minimum. The FTS 65 and Equinox 55 interferograms were processed with Happ-Genzel and weak Norton-Beer apodization functions, respectively. Calibration transfers are often adversely affected by some unknown instrument function, however, the calibrations can easily be corrected with a normalization function determined from a set of standards, or by slightly more involved methods if necessary[15].

Development of an Infrared Filter Photometer for B determinations

Previous work with IR light emitting diodes (IRLEDs) indicated that there was some possibility that they may be suitable for use in a filter photometer dedicated to boron determination. However, because of their low power output (2 mW) and the large degree of attenuation by the optical components and water, it was decided that they were not the most suitable technology for this application at this time. The output wavelengths of the IRLEDs were also optimized for carbon dioxide and hydrocarbon determinations. Boron determinations were only possible by virtue of the wide bandpass of the IRLED that encompassed the B-H stretch in the tail. The search for alternative small IR sources led to some very simple miniature thermal sources. These sources are relatively inexpensive at < $70, and come in pulsed and continuous output versions. The main advantage that the IRLED has over the pulsed thermal sources is that it can

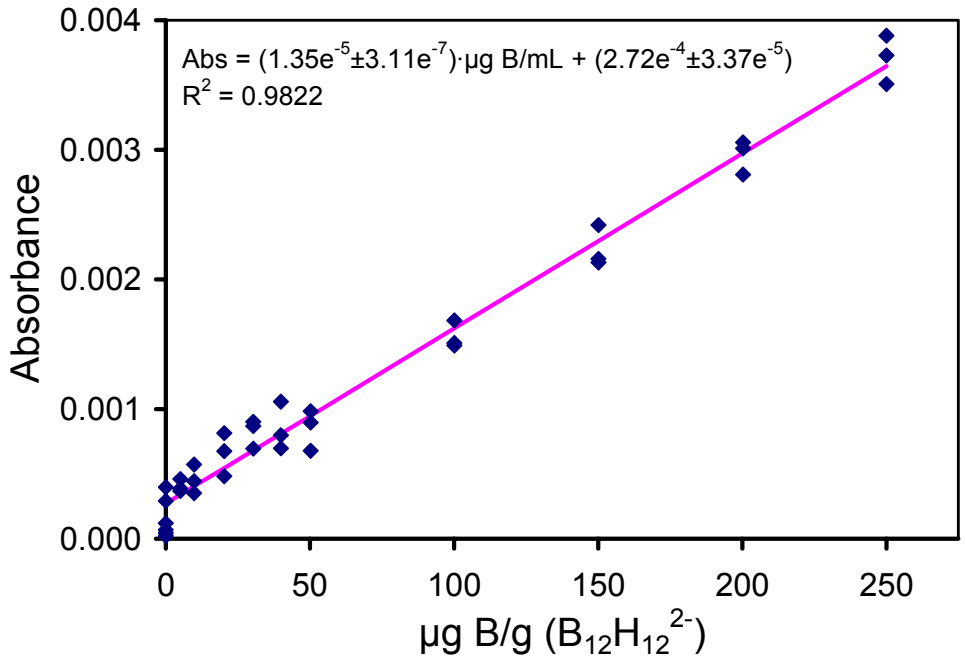

Figure 7. Boron concentration plotted vs. peak height for $B_{12}H_{12}^{2-}$ determined by FTIR ATR with a ZnSe crystal.

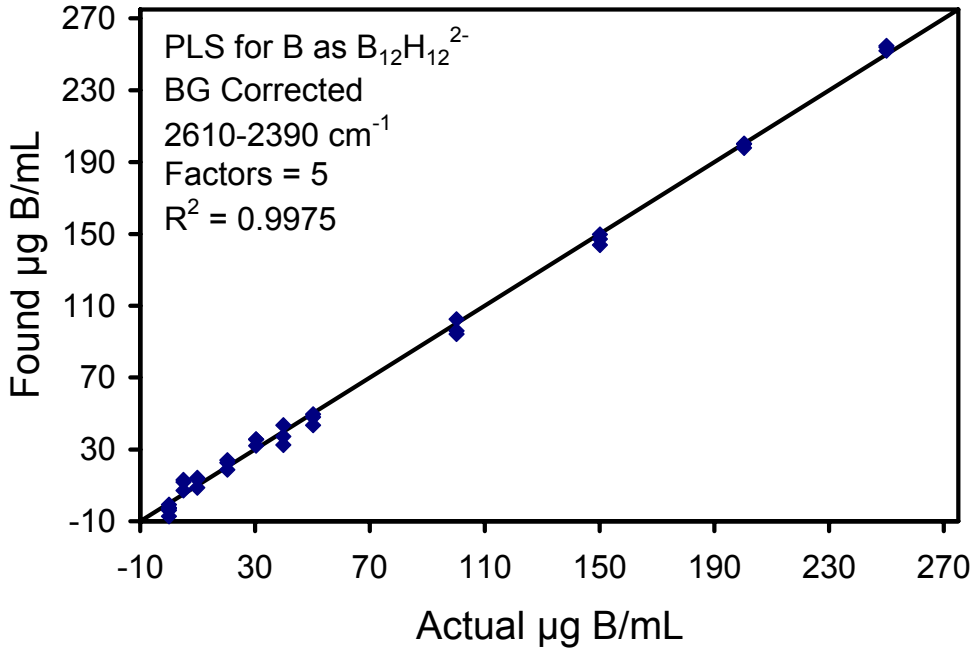

Figure 8. Same data as in Figure 7 using PLS calibration model.

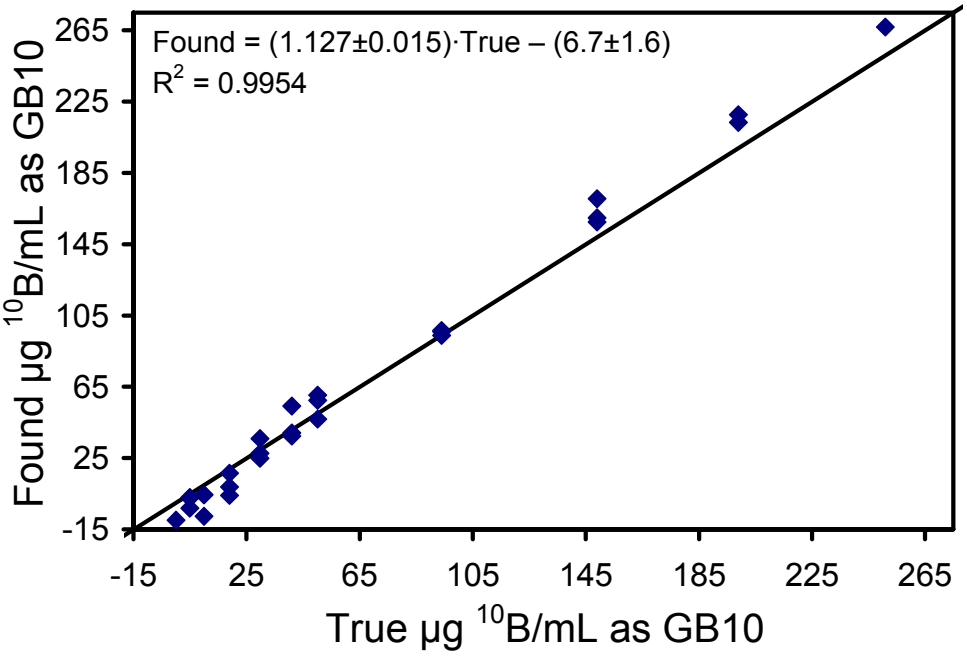

Figure 9. Determination of ^{10}B as GB10 by ATR FTIR using spectra collected on a Bruker Equinox 55 and a PLS calibration developed with spectra collected on a Digilab FTS 65 one year earlier. The black line represents a 1:1 correlation of the true and found concentrations.

be operated at rates as high as 1,000 Hz. The PulseIR and ReflectIR sources can operate at a maximum pulse rate of only about 12 Hz. The main advantage of the pulsed thermal sources over the IRLEDs is that the output power can be as high at 1.75 W. Even with the attenuation by the optical components and water, enough light reaches the detector with the pulsed thermal sources to make them a much better alternative to the IRLEDs. The miniature continuous output thermal sources can output up to 9 W, but a chopper is required to modulate the signal since most IR detectors operate in AC in order to handle the large DC backgrounds.

This year the work centered primarily upon incorporating the ReflectIR source into the system and understanding the optimum conditions under which it can be operated. The pulse is actually a two step square-wave consisting of a warm-up phase and a sustained phase. Generally, for this application, the best response was achieved with a warm-up phase of 12 ms at 2.8 A, a sustained phase of 3 ms at 0.8 A and a 18.8% duty cycle for a total of 80 ms/pulse. These parameters tend to push the source to its limit and will ultimately shorten the lifetime of the source, however, they do provide sufficient detector response so that small changes may be noted.

Initially, the ATR cell was being used, however, the noise level achievable did not seem to be accurate. Much of the problem with the ATR cell may be related to the offsets noted in the FTIR spectra. It had been noted on the FTIR that each time the ATR cell is removed to change samples and replaced onto its base, there was a baseline offset that varied by as much as ± 0.003 absorbance units. Offsets and drifting baselines are easily corrected when the whole spectrum is available. However, with only the single bandpass filter and detector, offsets and drifting

baselines of this magnitude are a limiting factor, given the ~10 μm pathlength of the ATR cell and the minimal absorbance of the analyte.

With FIA, the baseline is continuously being monitored between injection samples, removing some of the limitations associated with having only one filter and one detector. Therefore, the ATR cell was removed from the experimental setup and replaced with a flow cell equipped with CaF_2 windows. Because the absorbance of water is at a minimum near the B-H absorption band, a reasonable signal at the detector was obtainable with the pathlength expanded to 100 μm. Figure 10 is an example of a FIA run using the apparatus shown in Figure 1 with the 100 μm pathlength cell. The drifting baseline is readily apparent, but the injections of the samples are also easily noted. The peak-to-peak noise is > 0.0005 absorbance units. This noise-level is currently too high for use with the ATR cell, but may be approaching usefulness with the 100 μm transmission cell, as the 10 μg B/mL injections are readily apparent. The cause for the baseline jump near the end of the experiment is unknown, but suspected to be associated with some change in the laboratory environment. Reduction in the noise level and stabilization of the baseline is anticipated once the apparatus is fully enclosed in a housing and isolated from the variable laboratory environment.

CONCLUSIONS

The feasibility using ATR-FTIR for the determination of B with different boron compounds containing multiple B-H bonds has been demonstrated. With the multivariate processing of the IR spectra in the region of the B-H stretch, detection limits < 5 μg B/g should be routinely achievable. For monitoring blood-boron concentrations, this could be a relatively important application because it eliminates problems associated with the use of short pathlength transmission cells, eliminates the need for any sample preparation as is required for the standard ICP techniques, and it can be performed using relatively low cost Fourier transform (FT) or dispersive IR instruments which have a much smaller footprint and essentially no facility requirements as the ICP instruments do. It is conceivable that the ATR-IR instrument can be mobile enough to be placed at the patient's bedside while the B infusion and B elimination are being monitored.

An even more compact and low cost alternative to the ATR-IR technique would be a simple filter photometer that is designed specifically to detect the B-H stretch. The feasibility of this approach has been demonstrated using a low cost pulsed infrared source, a flow cell, an optical filter, and a PbSe detector. Operated in the FIA mode, this simple apparatus is currently capable of detecting B in liquids containing B compounds with B-H bonds at levels of ~10 μg B/mL or less. With some minor improvements to control noise, the detection limits for this apparatus may exceed those achieved by the ATR-FTIR as described above because the pathlength can be extended to 100 + μm. Improvements include encasing the components for climate control, and better signal conditioning, either digitally or electronically.

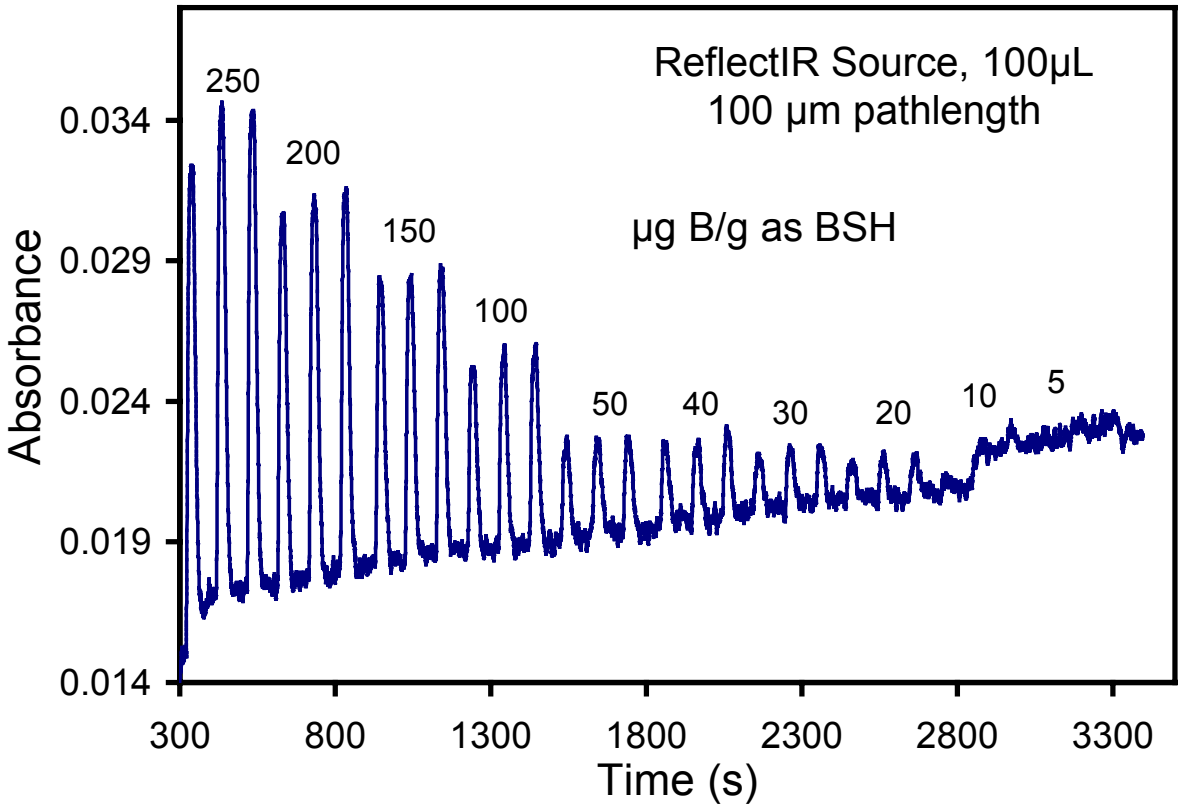

Figure 10. Flow injection analysis for B at the B-H 2500 cm^{-1} using 100 µL injections, a flow cell with CaF_2 cells windows spaced at 100 µm. The source was a pulsed ReflectIR and the detector a PbSe cooled to –30°C.

REFERENCES

1. Saini, P.; Lai, J. C. K.; Lu, D. R., "FT-IR measurement of mercaptoundecahydrododecacarborate in human plasma," *Journal of Pharmaceutical and Biomedical Analysis*, *12*, **1994,** 1091-1095.

2. Lu, D. R.; Munro, C., "Quantitative analysis of mercaptoundecahydrododecaborate by Fourier transform infrared spectroscopy," *Pharmaceutical Research*, *9*, **1992,** 1199-1202.

3. Moore, D. E.; Setiawan, Y.; Blagojevic, N.; Allen, B. J., "FTIR Spectrometry for the assay of polyhedral boron compound in plasma," In: *Advances in Neutron Capture Therapy*; Soloway, A. H., Barth, R. F., Carpenter, D. E., Eds.; Plenum Press: New York, 1993, pp 413-417.

4. Setiawan, Y.; Rise, T.; Moore, D. E., "Fourier-Transform Infrared (FTIR) Spectrometry for the Assay of Polyhedral Boron-Compounds in Plasma and Pharmaceutical Formulations," *Pharmaceutical Research*, *11*, **1994,** 723-727.

5. Moore, D. E., "A Review of Techniques for the Analysis of Boron in the Development of Neutron-Capture Therapy Agents," *Journal of Pharmaceutical and Biomedical Analysis*, *8*, **1990,** 547-553.

6. Bauer, W. F.; Jeffery, C.; Partin, J. K., "Development of a Boron Analyzer Based Upon Infrared Spectroscopy," In: INEEL BNCT Research Program Annual Report, 2000, Venhuizen, J. R., Ed., INEEL-EXT-01-00204, INEEL, March 2001, 5-14.

7. Bauer, B.; Floyd, T. A., "Monitoring of Glucose in Biological-Fluids by Fourier-Transform Infrared Spectrometry with a Cylindrical Internal Reflectance Cell," *Analytica Chimica Acta*, *197*, **1987,** 295-301.

8. Bauer, W. F.; Johnson, D. A.; Steele, S. M.; Messick, K.; Miller, D. L.; Propp, W. A., "Gross Boron Determination in Biological Samples by Inductively Coupled Plasma-Atomic Emission-Spectroscopy," *Strahlentherapie Und Onkologie*, *165*, **1989,** 176-179.

9. Bauer, W. F.; Gresham, G. L.; Gianotto, A. K., "Additional impurities identified in borocaptate sodium," In: *Cancer Neutron Capture Therapy*; Mishima, Y., Ed.; Plenum Press Div Plenum Publishing Corp: New York, 1996, pp 643.

10. Hotz, N. J.; Bauer, W. F., "Determination Of Strongly Protein-Bound Borocaptate Species By High-Performance Liquid-Chromatography With Online Inductively- Coupled Plasma-Atomic Emission-Spectroscopy Detection Of Boron," In: *Advances in Neutron Capture Therapy*; Soloway, A. H., Barth, R. F., Carpenter, D. E., Eds.; Plenum Press Div Plenum Publishing Corp: New York, 1993, pp 439.

11. Haaland, D. M.; Thomas, E. V., "Partial Least-Squares Methods for Spectral Analyses .1. Relation to Other Quantitative Calibration Methods and the Extraction of Qualitative Information," *Analytical Chemistry*, *60*, **1988,** 1193-1202.

12. Zhu, C. J.; Griffiths, P. R., "Extending the range of Beer's law in FT-IR spectrometry. Part I: Theoretical study of Norton-Beer apodization functions," *Applied Spectroscopy*, *52*, **1998a,** 1403-1408.

13. Zhu, C. J.; Griffiths, P. R., "Extending the range of Beer's law in FT-IR spectrometry. Part II: Theoretical study of continuous apodization functions," *Applied Spectroscopy*, *52*, **1998b,** 1409-1413.

14. Haaland, D. M.; Melgaard, D. K., "New classical least-squares/partial least-squares hybrid algorithm for spectral analyses," *Applied Spectroscopy*, *55*, **2001,** 1-8.

CONSTRUCTION OF AN EPITHERMAL NEUTRON BEAM FOR PRECLINICAL BNCT RESEARCH AT WASHINGTON STATE UNIVERSITY

J.R. Venhuizen[1], D.W. Nigg[1], C.A. Wemple[1], J.M. Zabriskie[1], K.D. Watts[1], R. E. Mitchell[1], G.E. Tripard[2], K. Fox[2], and S. Sharp-Dugan[2]

1. Idaho National Engineering and Environmental Laboratory, Idaho Falls, ID
2. Washington State University, Pullman, WA

INTRODUCTION

Attention[1] has been focused upon the development of a convenient, local epithermal-neutron beam facility at Washington State University (WSU) for collaborative Idaho National Engineering and Environmental Laboratory (INEEL)/WSU BNCT preclinical research and boronated pharmaceutical screening in cell and animal models. The design of the new facility, which is installed in the thermal column region of the TRIGA[a] research reactor at WSU, was performed in a collaborative effort[2,3] of WSU and INEEL scientists. This article summarizes the physical construction and assembly of the beamline components.

FACILITY DESCRIPTION

The 1 MW reactor core is suspended from a movable bridge above the pool as shown in Figure 1. It can be positioned directly adjacent to a truncated aluminum cone that extends horizontally into the reactor pool from the tank wall on the upstream side of a large shield wall penetration. This cone and the adjacent volume were originally filled with graphite, comprising what was known as the 'thermal column'. A lead wall and water-filled shield were located downstream of the graphite portion of thermal column. There was a large open floor area outside of this final shield, as shown in Figure 2. Figure 3 shows a schematic diagram of the components of the WSU epithermal-neutron beam facility that were installed in the original thermal column region of the reactor-shielding monolith. In this design, the original graphite has been removed from this region and replaced with an epithermal-neutron filtering, moderating, and collimating assembly, as shown. Neutrons emanating from the core travel into the filtering and moderating region. The spectrum is tailored in this region such that most neutrons emerge with energies in the epithermal energy range (0.5 eV – 10 keV). Downstream of the filtering and moderating region is a cadmium thermal neutron absorber, a bismuth and lead gamma shield, and a conical neutron collimator composed of bismuth surrounded by borated polyethylene. A final layer of lithiated polyethylene covers the lead face. Provision is made for several different exit port aperture sizes, as shown in Figure 3. A heavily shielded concrete beam stop and treatment room has been constructed just outside of the thermal column opening in the reactor shield wall, as shown in Figure 4.

[a] TRIGA is a trademark of General Atomics of San Diego, CA.

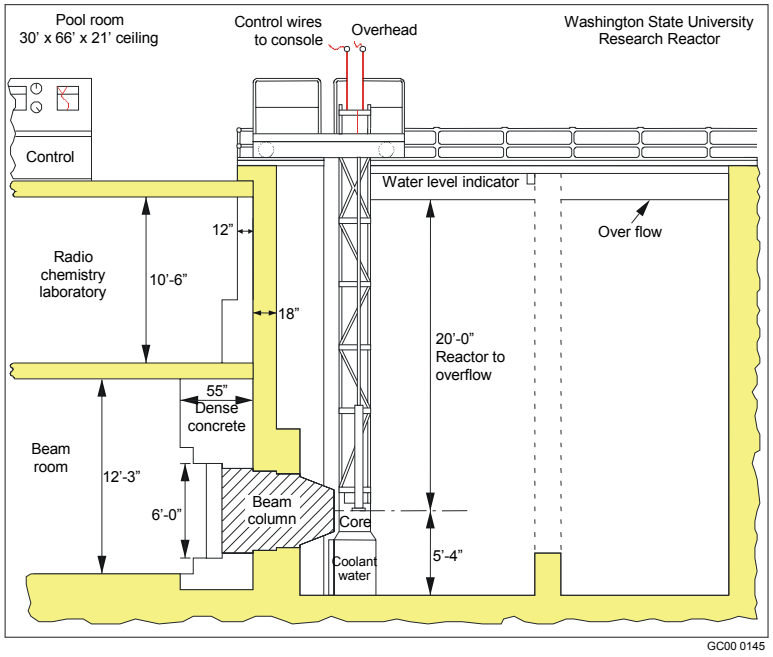

Figure 1. Elevation plan of the WSU TRIGA reactor facility.

Figure 2. Final thermal column shield (water-filled door) and adjacent floor area at the WSU TRIGA facility prior to modifications.

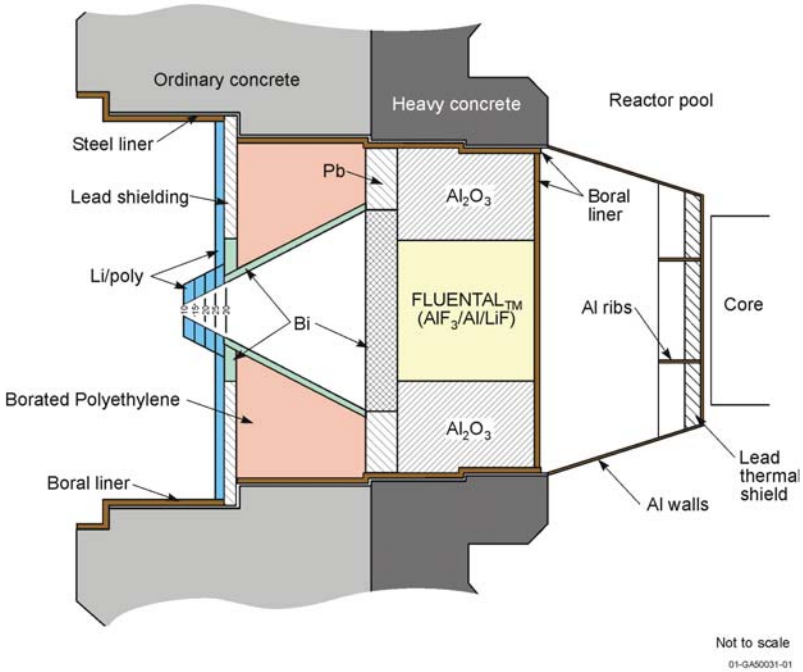

Figure 3. WSU column assembly, with epithermal-neutron filter in place.

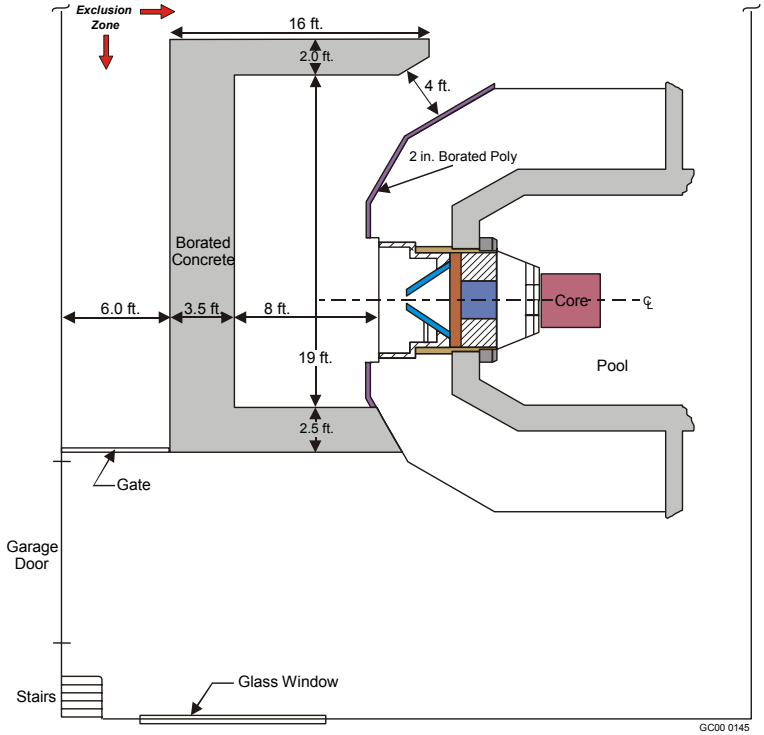

Figure 4. Approximate WSU beam stop and treatment room arrangement.

A key distinguishing feature of the WSU facility is the incorporation of a new, high-efficiency, neutron moderating and filtering material, FLUENTAL[b], into the design. FLUENTAL, developed by the Technical Research Centre of Finland[4], is manufactured by hot isostatic pressing of a powered mixture of 69% (by weight) aluminum fluoride, 30% aluminum, and 1% lithium fluoride. A block of this material, having a thickness in the beam propagation direction of 0.64 m and transverse dimensions of approximately 0.6 m, is surrounded by aluminum oxide to produce the neutron filtering and moderating region, as shown in Figure 3. MCNP[5] and DORT[6] radiation transport design calculations for the coupled core and filter-collimator assembly indicate that an epithermal-neutron flux of approximately 10^9 n/cm^2-s at a reactor power of 1 MW will be produced at the exit port of the collimator (with the reactor core optimally loaded). The background neutron KERMA factor (a measure of the fast-neutron contamination) for the beam is calculated to be approximately 3.0 x 10^{-11} cGy/n-cm^2. The computational methods used for this design were previously validated against INEEL measurements performed for a similar neutron beam facility that is in operation at the FiR 1 TRIGA research reactor in Finland[7].

An additional key feature of the WSU beam facility design is the provision for adjustable filter-moderator thickness (in 4 cm steps) to systematically explore the radiobiological consequences of increasing the fast-neutron contamination above the nominal value associated with the baseline system described above. The components shown in Figure 3 are designed for relative ease of disassembly and re-assembly, compared to other reactor-based epithermal-neutron facilities that are currently in operation. Thus, it will be possible to have a number of different filter/moderator arrangements over the life of the facility.

CONSTRUCTION

Figure 5 is a view into the original thermal column prior to assembly of the filter. The thermal column is a steel box lined with boral [aluminum-boron carbide-aluminum sandwich 0.635 cm (0.25 inches) thick]. The top and side boral sheets are held in place by the other filter components, i.e., they are not attached to the walls, so that there are no penetrations into the steel box liner.

Thermocouples and Nitrogen Vent Line

Prior to installation of the filter-moderator components, thermocouples were placed at selected locations on the primary gamma shielding at the far end of the thermal column cone housing, as shown in Figure 6. This shielding is composed of lead, and is subject to heavy gamma heating from the adjacent reactor core. Five thermocouple leads were attached to the lead via screws or inserted into spaces in the lead; the sixth lead is attached to the center of the boral sheet facing the cone. The Type K thermocouples were procured from Omega Engineering (Catalog number WTK-8-S 240-TT), and connected to a thermocouple readout meter outside the beam-stop room (Omega Model DP462). The leads from the thermocouples were brought out the bottom center of the assembly through slots cut into the first five rows of alumina bricks, and then routed to the right side of the thermal column, taking advantage of the first offset in the wall of the thermal column. These cables were then run along the bottom right side of the thermal column, out to

[b] FLUENTAL is a trademark of The Technical Research Centre of Finland.

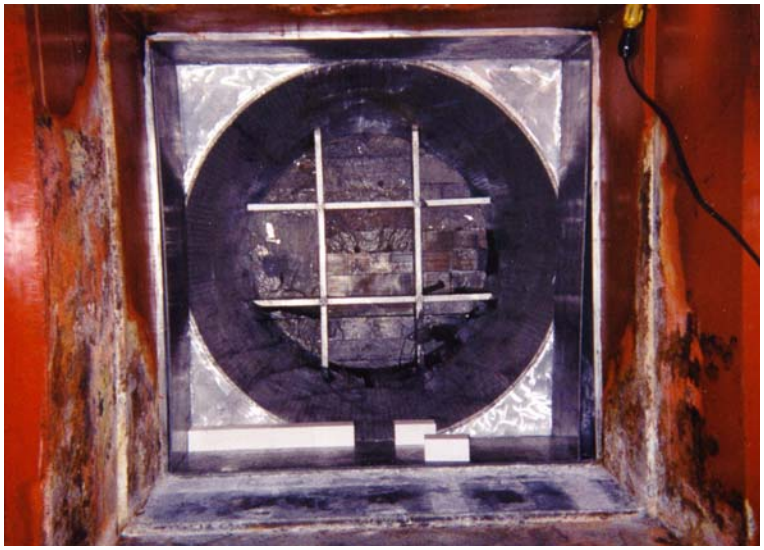

Figure 5. View into the thermal column prior to assembly. Note the sheets of boral on the sidewalls, several of the aluminum oxide bricks on the floor near the cone, and the offsets in the walls.

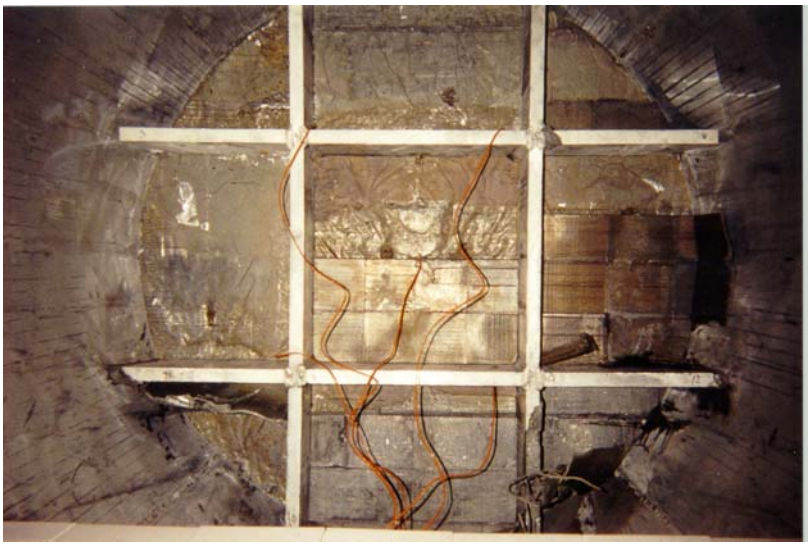

Figure 6. Thermocouple installation in the upstream gamma-shielding region of the WSU thermal column cone showing the leads brought out the center of the alumina blocks.

the cable penetration port in the beam room. Also included with the thermocouple leads was a 0.635 cm (0.25-inch) diameter nylon tube that vents into the bottom of the cone area. This vent was provided to supply a nitrogen-purge in the cone area to reduce air activation, and is typically connected to a nitrogen supply outside the beam-stop room.

Aluminum Oxide and FLUENTAL Assembly

The primary filter moderator-filter assembly was then built up from blocks of aluminum oxide and FLUENTAL, as shown in Figure 7 for the partially completed assembly, and in Figure 8 for the fully completed assembly. A sheet of boral prevents the blocks from falling into the cone area, and reduces the thermal neutron flux impinging on the upstream side of the filter-moderator region.

The FLUENTAL material consists of 17 blocks of nominal dimensions 63.5 x 22 x 8 cm, 8 blocks of 63.5 x 11 x 8 cm, and 6 blocks of 63.5 x 22 x 4 cm. This allows stacking the blocks in a cube arrangement of 8 rows measuring 63.5 x 64 x 66 cm (25 x 25.2 x 26 in) when completed. The 4 cm thick blocks make it possible to shorten the filter in 4 cm increments if desired. The alumina blocks were produced in 8 x 8 x 16 cm size by Coors Ceramics (Golden, CO.) to mate with the FLUENTAL. These blocks were stacked with an offset in both directions to minimize neutron-streaming paths. The vertical offset was established by cutting (using a diamond tile saw) 1 cm off the bottom row of alumina blocks in rows 2 and 4. Rows 6 and 8 were stacked on the floor (utilizes a step in the thermal column construction), and row 7 was elevated by using the 1 cm pieces left over from rows 2 and 4. The horizontal offset was established by offsetting the FLUENTAL blocks 1.3 cm (1/2 in) left-to-right between rows. The alumina blocks at the sides and top edges of the thermal column were cut to fit.

Figure 7. Partially completed WSU filter-moderator assembly, showing the FLUENTAL and alumina blocks, and the boral backing sheet. Note the offsets in both directions.

Figure 8. Completed WSU filter-moderator assembly.

Cadmium Assembly

Cadmium sheets, 0.12 mm (.030 in) thick, 30.5 x 183 cm (12 x 72 in), were 'hung' over the end of the above assembly by tucking the end of the cadmium sheet into the small space between the ceiling and the top alumina blocks. Figure 9 is a photo of the cadmium sheets in place.

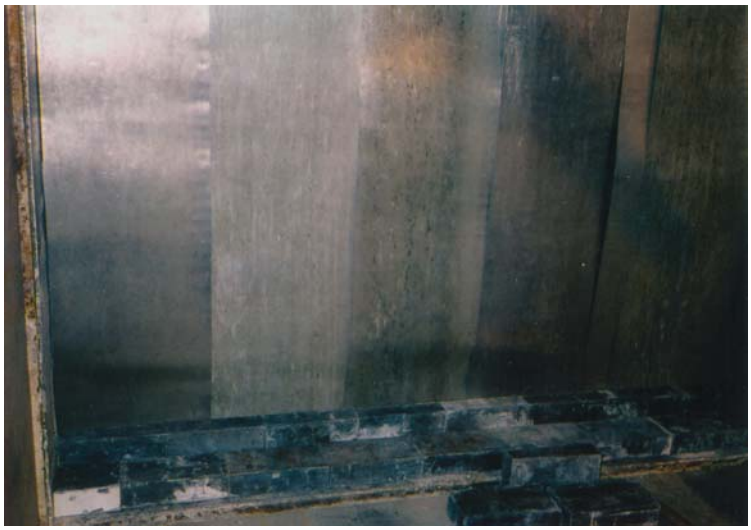

Figure 9. Cadmium thermal neutron shield.

Gamma Shield

The next assembly installed was the gamma shield. This consisted of 10 cm (4 in) of lead bricks covering the outside area of the alumina blocks, and 10 cm (4 in) of bismuth covering the FLUENTAL region. The lead bricks are stacked on edge, with an overlapping design to prevent streaming. Four interlocking bismuth shield blocks, designed to mate with the lead bricks, were cast at the INEEL. A special lifting jig was built to lift the blocks into place [they weigh about 55 kg (340 lb) ea]. An automotive engine hoist was used to supply the lifting force. Figure 10 shows the device in operation.

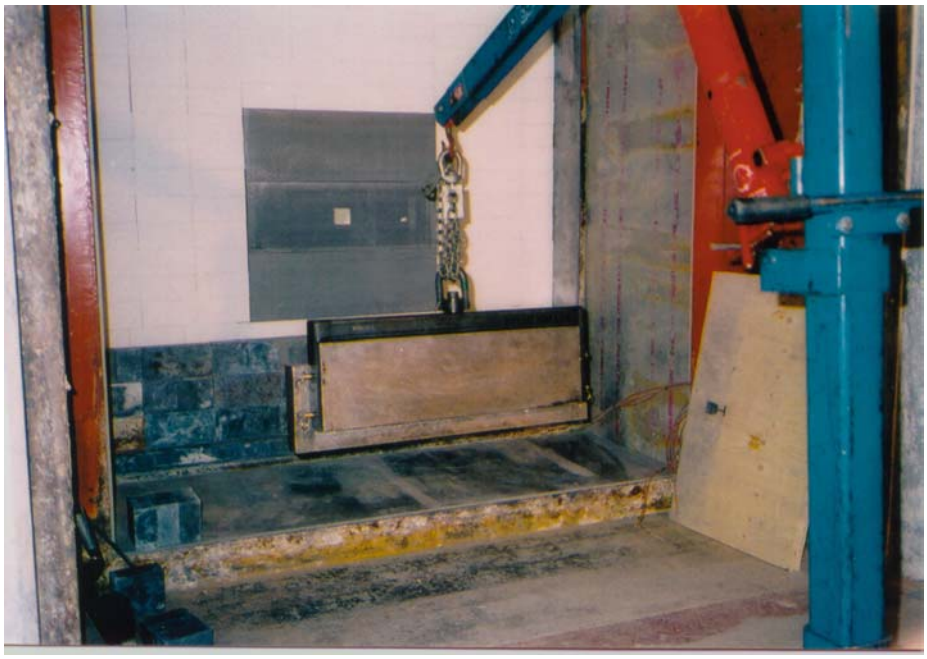

Figure 10. Bismuth gamma shield block hanging on the lifting jig. Note the offsets built into the bismuth block to mate with the lead bricks.

Figure 11 shows the detail of the offsets built into the bismuth blocks; how they mate with each other and with the lead bricks. Figure 12 shows the completed lead wall gamma shield with the bismuth blocks covering the area in front of the FLUENTAL blocks.

Figure 11. Detail of the bismuth gamma shield blocks, 5cm (2 in) offsets at the top/bottom and sides.

Figure 12. Completed gamma shield assembly.

Collimator Design

The design of the cone-shaped bismuth collimator was based on a tradeoff of cone height to maximize the collimation versus the loss of intensity of the neutrons due to increased distance from the reactor core. The final design selected was a truncated right circular cone with a base opening diameter of 91.4 cm (36 in), a height of 38.1 cm (15 in), and a wall thickness of 3 cm (1.2 in). The angle of the cone is 45 degrees, giving an opening of 15.24 cm (6 in). The final 5 cm (2 in) of the cone is fitted with a collar, designed so that various shaped apertures can be fabricated from lithiated polyethylene and inserted in a flanged opening.

The actual construction of the collimator bismuth sections presented a challenge due to the final weight [> 270 kg (600 pounds)] of the finished bismuth cone. The design decision was to make the collimator out of 16 sections, much like barrel staves. A mold was constructed of aluminum, and the sections were formed from molten bismuth. The inside surface of the individual section was the free surface of the mold, which was machined off (bismuth expands when cooled from a liquid) to provide a smooth surface. Each of the 16 pieces weighs about 18 kg (40 pounds). Figure 13 is a photograph of a finished section.

Figure 13. Bismuth collimator section.

The bismuth cone is supported by borated polyethylene (Reactor Experiments, 5% Borated Polyethylene, Catalog Number 201) for the first 28 cm (11 in), and two rows [10.16 cm (4 in)] of lead bricks. The last five cm (2 in) of the bismuth staves are fitted with a bismuth collar, as shown in Figure 15, designed to provide a transition from the cone shape to mate with the lead bricks while providing shielding for the capture gammas generated from the boron in the polyethylene.

Figure 14 is a drawing of the completed collimator, showing the interlocking features of the staves.

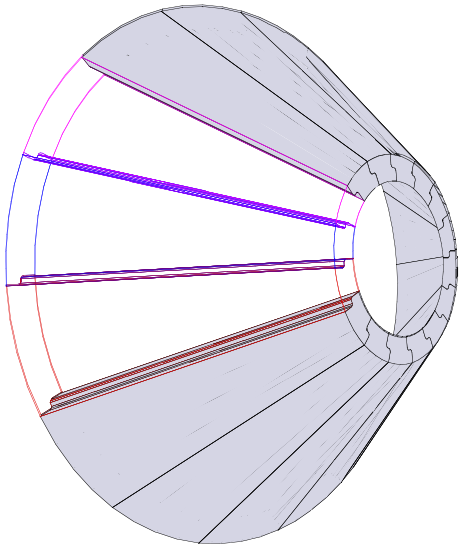

Figure 14. Bismuth collimator.

The collar was formed in a mold also, in two pieces due to the final weight (~45 kg, 100 lbs each). This bismuth collar will accommodate lithiated polyethylene final neutron beam delimiters.

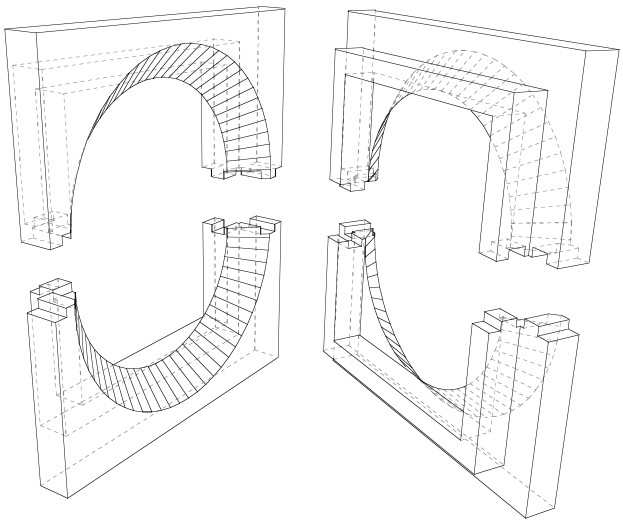

Figure 15. Collimator collar, a rear and front view. Staves fit in the tapered area, and the delimiter fits into the square flange area.

Collimator Assembly

The collimator assembly was put together in two halves, lower and upper. The poly sheets, which are numbered from 1 to 11 and have the corresponding cone shape cut in them, were bolted together with 11.4 cm (4.5 in) long, 1.6 cm (5/8 in) nylon bolts. The boltholes are designed to have a captive nut (Figure 16) on the side facing the reactor, and the bolt with fiberglass washer can be threaded through the holes and tightened with a socket wrench. The purpose of the bolts is too prevent the poly sheets from separating and sliding on each other, so the bolts are used in sheer rather than in tension. There are three sets of seven bolts required to assemble each the bottom and top halves, with the holes offset to prevent streaming paths. The final bolt heads are not recessed into the poly, and required the adjacent lead bricks to have a relief cutout to accommodate the bolt head.

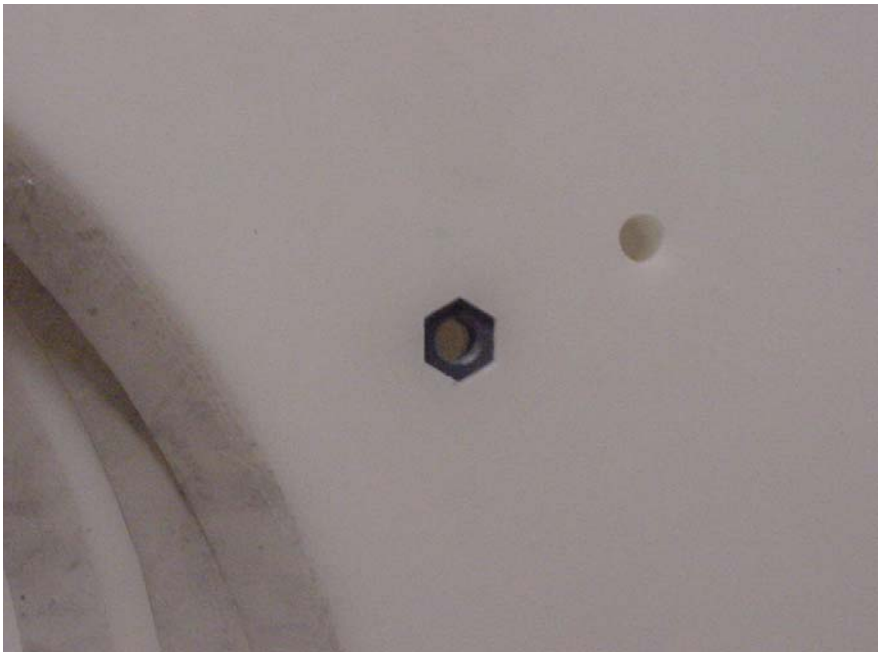

Figure 16. Captive nut inserted into polyethylene.

With the lower half of the poly in position with accompanying sidepieces (Figure 17), the front lead bricks were assembled up to the level of the collimator collar. The lower half of the collar was placed on the lead (Figure 18), and then the bismuth staves put into position. Each half of the collar weighs approximately 45 kg (100 lb), and each stave weighs approximately 18 kg (40 lb). The collimator was assembled by starting with the center bottom stave and working up either side to the halfway point. The bottom seven staves are pinned to the collar with 0.635 cm (0.25 in) diameter aluminum rod (6061) (Figure 19). At this point, a carbon fiber ring (fabricated by Spencer Composites Corp., Sacramento, CA) was put in place at the rear of the assembly, and a lexan ring inserted at the front of the assembly (Figure 20). These rings provide support for the top half of the collimator staves. With the staves all in position, (Figure 21) the

top half of the poly was assembled, bolted together as described for the bottom section. With the top half of the poly in place, the upper bismuth collar was positioned (Figure 22), and lead bricks continued up to the level of the top of the collar. The top of the collar and accompanying lead bricks are used to support the final large bismuth lintel piece (Figure 23). This lintel piece weighs about 155 kg (340 lb), and required the engine hoist and lifting jig to lift it into place. With the lintel positioned, the remainder of the lead bricks were added to complete the lead wall. The lead wall is covered with lithiated polyethylene, held in place with nylon bolts, as shown in Figure 24. Figure 25 is a cut-away cross section of the collimator section, bismuth shield, and the filter (Al_2O_3 and AlF_3).

Figure 17. Lower half of the polyethylene in position, lead bricks to the bottom half-collar.

Figure 18. Lower half of the collar in position on the lead wall.

Figure 19. First stave in position. Note the partially inserted aluminum rod used to pin the stave to the collar. The bottom seven staves were pinned to the collar.

Figure 20. Carbon fiber and lexan rings in place.

Figure 21. Top half of collimator staves in place.

Figure 22. Upper half of collar in place.

Figure 23. Lintel piece in place above the collar, showing the lead bricks carrying the load.

Figure 24. Outer face of the filter-moderator region showing lithiated polyethylene in place. The four inch collimator is in position.

DISASSEMBLY

Disassembly of the collimator/filter can be accomplished in reverse of the assembly. Careful note should be taken of the various components (lead bricks, aluminum oxide blocks) that have been 'cut-to-fit'. There will be approximately 6,273 kg (13,800 lb) of lead (500 bricks), 5,227 kg (11,500 lb) of aluminum oxide (1,300 blocks), 1,045 kg (2,300 lb) bismuth and 804.5 kg (1,770 lb) of FLUENTAL[a] to deal with.

[a] The FLUENTAL blocks will contain small, but noneligible, quantities of elemental tritium, built up during irradiation, and they should be handled accordingly.

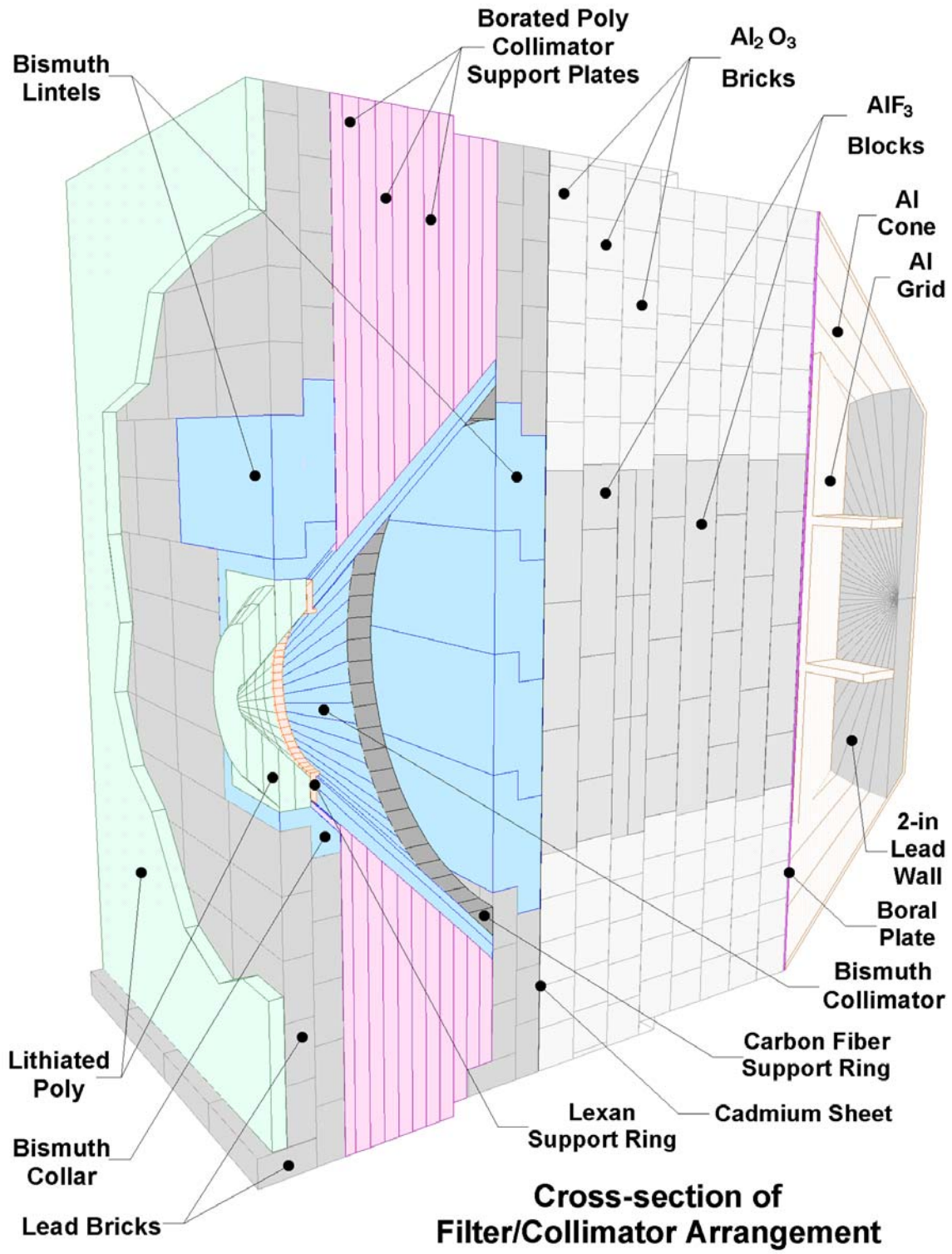

Figure 25. Cut-away cross section of the collimator section, bismuth shield, and the filter.

ACKNOWLEGEMENTS

The construction of such a complex structure could not have been accomplished without the skill and dedication of machinists to build the various parts, and the carpenters to build the shipping containers to get the parts to their destination. The INEEL Prototype Shop (T.G. Brown, R.E. Hatch, J.M. Johnson, D.R. Mechling, R.E. Mitchell and L.L. Wallace) made all the bismuth and polyethylene componenets, and the INEEL Carpenter Shop (T.A. Capson, L.J. Johnson, B.F. McMurtrey, and R.K. Walker) made two large shipping containers to transport the bismuth and poly pieces from Idaho to Washington. The WSU Tech Services shop (G. Henry and L. Frei) fabricated several additional poly and Lexan pieces, and provided the final field fitting for all the poly.

REFERENCES

1. D.W. Nigg, C.A. Wemple, J.R. Venhuizen, G.E. Tripard, S. Sharp, K. Fox, P.R. Gavin, "Preliminary Neutronic Performance Assessment of an Epithermal Neutron Beam for Preclinical BNCT Research at Washington State University," In: J.R. Venhuizen (ed.), "INEEL BNCT Research Program Annual Report – 2001," INEEL-EXT-02-00060, April, 2002.

2. F.J. Wheeler, D.W. Nigg, "Feasibility Study for an Epithermal-Neutron Beam Facility at the Washington State University Radiation Center," EGG-NRE-11296, Idaho National Engineering Laboratory, USA, 1994.

3. T.D. Burns Jr., "A Monte Carlo Model System for Core Analysis and Design at the Washington State University Radiation Center," INEL-95/0458, Idaho National Engineering Laboratory, 1996.

4. I. Auterinen, P. Hiismäki, "Epithermal BNCT Neutron Beam Design for a Triga II Reactor," Advances in Neutron Capture Therapy, Plenum Press, New York, 1993, Pages 81-84.

5. J.F. Breismeister, (1993) MCNP – A General Monte Carlo N-Particle Transport Code, Version 4A, LA-12625-M, Los Alamos National Laboratory, USA.

6. W.A. Rhoades, et. al., "TORT-DORT: Two and Three-Dimensional Discrete-Ordinates Transport," Radiation Shielding Information Center, Oak Ridge National Laboratory, CCC-543, 1993.

7. D.W. Nigg, Y.D. Harker, J.K. Hartwell, C.A. Wemple, T. Seren, I. Auterinen, P. Kotiluoto, P. Hiismaki, T. Sepala, M. Kortesniemi, S. Savolainen, R. Risler, "Collaborative Neutronic Performance Characterization of the FiR-1 Clinical Epithermal Neutron Beam Facility for BNCT," In: J.R. Venhuizen (ed.), "INEEL BNCT Research Program Annual Report – 1998," INEEL-EXT-99-00293, April, 1999.

PRELIMINARY NEUTRONIC PERFORMANCE ASSESSMENT OF AN EPITHERMAL NEUTRON BEAM FOR PRECLINICAL BNCT RESEARCH AT WASHINGTON STATE UNIVERSITY

D.W. Nigg[1], C.A. Wemple[1], J.R. Venhuizen[1], G.E. Tripard[2], S. Sharp-Dugan[2], K. Fox[2], and P.R. Gavin[2].

1. **Idaho National Engineering and Environmental Laboratory, Idaho Falls, ID**
2. **Washington State University, Pullman, WA**

INTRODUCTION

Veterinary radiation oncology researchers at the Washington State University (WSU) School of Veterinary Medicine have made major contributions to the understanding of the *in-vivo* radiobiology of Boron Neutron Capture Therapy (BNCT) over the years. For example, the large-animal model studies of normal brain tissue tolerance in BNCT conducted by this group[1] provided a key component of the radiobiological basis for the resumption of human BNCT trials in the U.S. in 1994. Those studies used the epithermal-neutron beams available at Brookhaven National Laboratory and at the Petten facility, in The Netherlands, with technical support from the Idaho National Engineering and Environmental Laboratory (INEEL) in several areas of physics, biophysics, and analytical chemistry. More recently, attention has been focused upon the construction of a more convenient and cost-effective local epithermal-neutron beam facility at WSU for collaborative INEEL/WSU BNCT preclinical research and boronated pharmaceutical screening in cell and animal models. The design[2,3] and construction[4,5] of the new facility, which has now been installed in the thermal column region of the TRIGA[a] research reactor at WSU, was performed in a collaborative effort of WSU and the INEEL. This article summarizes the results of some initial neutronic performance measurements for the WSU beam that were completed during CY 2001.

FACILITY DESCRIPTION

The 1 MW WSU reactor core is suspended from a movable bridge above the pool as shown in Figure 1. It can be positioned directly adjacent to a truncated aluminum cone that extends horizontally into the reactor pool from the tank wall on the upstream side of the filtering and moderating assembly. This cone and the adjacent thermal column area were originally filled with graphite, comprising the thermal neutron column (or thermal column) for the WSU Nuclear Radiation Center. A water-filled shield was located on the downstream of the graphite thermal column. There was a large open floor area outside of this final shield.

[a] TRIGA is a trademark of General Atomics of San Diego, CA.

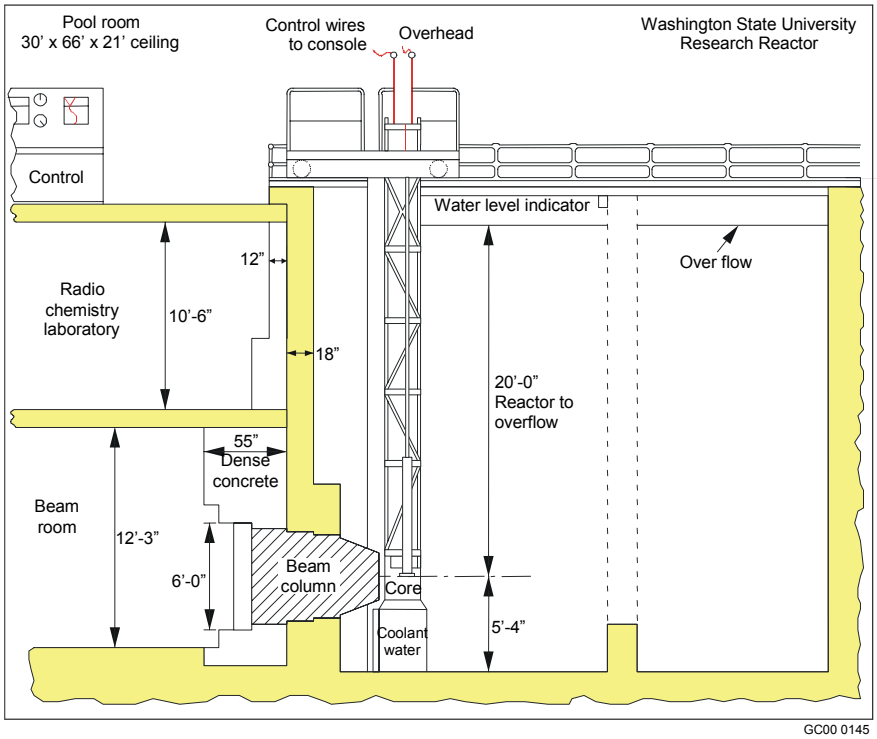

Figure 1. Elevation plan of the WSU TRIGA reactor facility.

Figure 2 shows a schematic diagram of the WSU epithermal-neutron beam facility. The new epithermal-neutron beam extraction components are located in the thermal-column region of the reactor-shielding monolith. In this design, the original graphite has been removed from this region and replaced with a new epithermal-neutron filtering, moderating, and collimating assembly as shown. Neutrons emanating from the core travel into the filtering and moderating region. The spectrum is tailored in this region such that most neutrons emerge with energies in the epithermal energy range (0.5 eV – 10 keV). Downstream of the filtering and moderating region is a bismuth and lead gamma shield, followed by a conical neutron collimator composed of bismuth surrounded by lithiated polyethylene. Provision is made for several different exit port aperture sizes as shown. A heavily shielded concrete beam stop and treatment room has been constructed just outside of the thermal column opening in the reactor shield wall as shown in Figure 3.

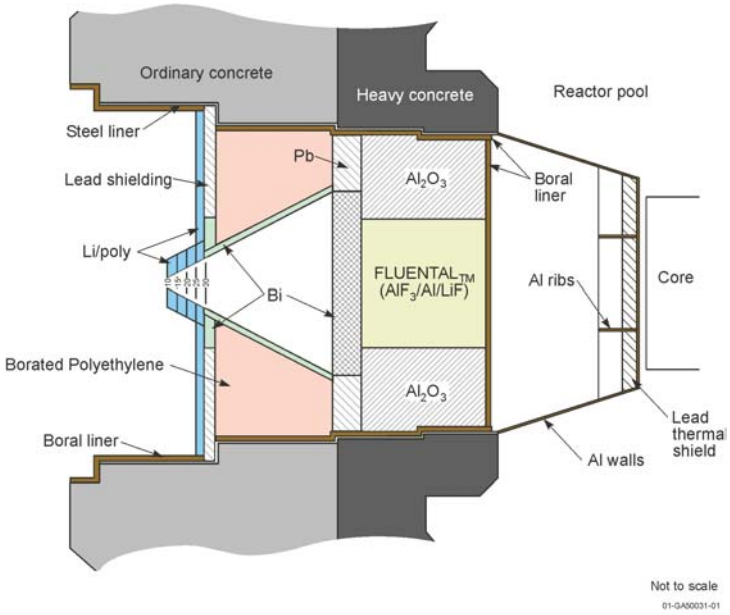

Figure 2. WSU column assembly, with epithermal neutron filter in place.

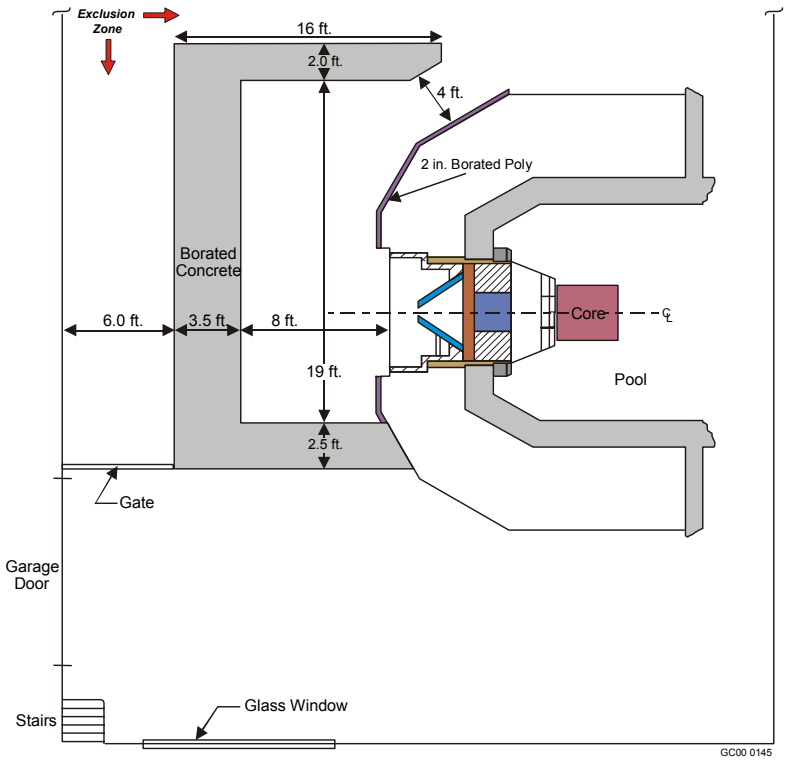

Figure 3. Approximate WSU beam stop and treatment room arrangement.

A key distinguishing feature of the WSU facility is the incorporation of a new, high-efficiency, neutron moderating and filtering material (FLUENTAL)[b] developed by the Technical Research Centre of Finland[6] into the design. FLUENTAL is manufactured by hot isostatic pressing of a mixture of 69% (by weight) aluminum fluoride, 30% aluminum, and 1% lithium fluoride. A block of this material having a thickness in the beam propagation direction of 0.64 m and transverse dimensions of approximately 0.6 m is surrounded by aluminum oxide to produce the neutron filtering and moderating region as shown in Figure 2. MCNP[7] and DORT[8] radiation transport design calculations for the coupled core and filter-collimator assembly indicate that a free-beam epithermal neutron flux of approximately 10^9 n/cm^2-s at a reactor power of 1 MW will be produced at the exit port of the collimator (with the reactor core optimally loaded). The background neutron KERMA rate per unit useful epithermal neutron flux (a measure of the fast-neutron contamination) for the beam is calculated to be approximately 3.0×10^{-11} cGy/n-cm^2. The computational methods used for this design were previously validated against INEEL measurements performed for a similar neutron beam facility that is already in operation at the FiR1 TRIGA research reactor in Finland[9].

An additional key feature of the WSU beam facility design is the provision for adjustable filter-moderator thickness to systematically explore the radiobiological consequences of increasing the fast-neutron contamination (harden the beam) above the nominal value associated with the baseline system described above. This is an important clinical issue for BNCT. Thinner filter/moderator arrangements will produce epithermal beams having correspondingly harder spectra and greater levels of fast-neutron contamination. The components shown in Figure 2 are designed for relative ease of disassembly and re-assembly compared to other reactor-based epithermal-neutron facilities that are currently in operation. Thus, it will be possible to have a number of different filter/moderator arrangements over the life of the facility.

Construction of the new WSU beam facility was initiated in 1999, and largely completed during 2001 with the installation of the final bismuth collimator and surrounding shielding as shown in Figure 4.

[b] FLUENTAL is a trademark of the Technical Research Center of Finland.

(a)

(c)

(b)

(d)

Figure 4. Final beam collimator installation at WSU showing the partially installed collimator (a), the fully installed collimator with square exit port collar and lower borated polyethylene shielding (b), the upper borated polyethylene shielding (c), and the final lead shielding (d).

The collimator, assembled from 16 identical bismuth "barrel-stave like " castings, is a truncated right circular cone with a base opening diameter of 91.4 cm (36 in), a height of 38.1 cm (15 in), and a wall thickness of 3 cm (1.2 in). The angle of the cone is 45 degrees. It is supported by borated polyethylene and two rows of lead bricks as shown in Figure 4b. The downstream end of the collimator is fitted with a bismuth collar designed to provide a transition from circular shape of the cone to the square shape required to match with the lead shielding bricks comprising the final shield wall. The collar will accommodate borated or lithiated polyethylene inserts having various beam port aperture sizes and field shaping configurations as shown in Figure 2.

INITIAL NEUTRON SPECTRUM MEASUREMENTS

After installation of the collimator assembly, some initial measurements were made to characterize the neutron spectrum in an imaginary transverse "source plane" passing through the base of the square flange on the downstream side of the bismuth collar. The source plane is a mathematical construct used for specifying the neutron source boundary conditions for the various dosimetry and treatment planning computations that will be required to support each experimental irradiation at WSU. By definition, the physical beamline components upstream of the source plane do not change from one irradiation to the next. Components downstream of this plane, such as the previously mentioned lithiated polyethylene field shaping plates, can change for each irradiation and are, therefore, explicitly modeled in dosimetry and treatment planning computations. Time-consuming beam modeling computations are thus only done once for each beamline configuration upstream of the source plane, and the results are coupled to the patient dosimetry computations for each irradiation via a computed boundary condition specified for the source plane and validated by appropriate measurements.

The measurements reported here were based on a simplified version of the activation foil protocol that was used for earlier INEEL measurements at the FiR 1 epithermal-neutron facility operated by the Technical Research Centre of Finland[9]. That protocol, in turn, was based on neutron activation analysis techniques[10] that have been adapted for BNCT applications by the INEEL through extensive experience with several other epithermal-neutron facilities in the U.S. and in Europe. Neutronically thick circular activation foils of various types were used for the measurements. The foil specifications and corresponding neutron activation interactions of interest are listed in Table 1. A very limited set of foils was used for these initial measurements compared to the FiR 1 protocol.

Table 1. Activation interactions and foils used for the INEEL/WSU preliminary epithermal-neutron beam measurements.

Neutron Interaction	Energy Range of Primary Response	Activation Gamma Energy of Interest (keV)
^{115}In (n, γ)	1 eV Resonance	1293,1097, and 416
^{197}Au (n, γ)	5 eV Resonance	411
^{63}Cu (n, γ)	1 keV Resonance	511 (Positron)
^{115}In (n,n')	430 keV Threshold	336

Positioning of Foils in the Beam

Standard 12.7-mm (0.5 in) diameter Au, Cu, and In foils were used with a lexan foil positioning plate shown in Figure 5a. A cadmium cover was placed around one foil of each type to suppress the thermal-neutron response. Thus, each foil responds largely to neutrons having energies at or

near the energy of the respective primary resonance of the foil material, as shown in the first three lines of Table 1. The three covered foils were placed in three of the outer foil positioning plate positions. An uncovered gold foil was placed in a fourth outer position of the foil plate to measure the thermal flux. The foils had nominal thicknesses in the range of 0.0254 mm (0.001 in) to 0.127 mm (0.005 in), depending on the material type.

(a) (b)

Figure 5. Activation foil plate (a) positioned in the WSU epithermal neutron beam source plane (b).

An additional foil package was used to provide spectral information in the high-energy range. A heavy (~5 g) 25.4-mm (1 in) diameter indium foil was placed in a small hollow boron sphere shown (disassembled) in Figure 6. The composition of the sphere is approximately 93% ^{10}B and 7% ^{11}B by weight, with a total boron density of 2.6 g/cm^3. This arrangement provides essentially total suppression of thermal and epithermal flux within the inner cavity of the boron sphere. Thus, an artificial threshold above the resonance energy range is imposed on the neutron capture reactions in the foil within the sphere. Since the activation gamma emissions that arise from neutron capture in indium are thereby suppressed, the relatively weak 336 keV gamma line from inelastic scatter in indium, which is of crucial interest in these measurements, is much more prominent in the spectrum of the activated indium foil. The activated indium foil is also much easier to handle when the boron sphere is used in this manner, since the induced activity is significantly lower than it would be without the sphere. The inside diameter of the boron sphere is approximately 2.8 cm (1.1 in). The outside diameter is approximately 4.75 cm (1.9 in). The boron sphere assembly was placed in the center of the foil positioning plate. as shown in Figure 5b.

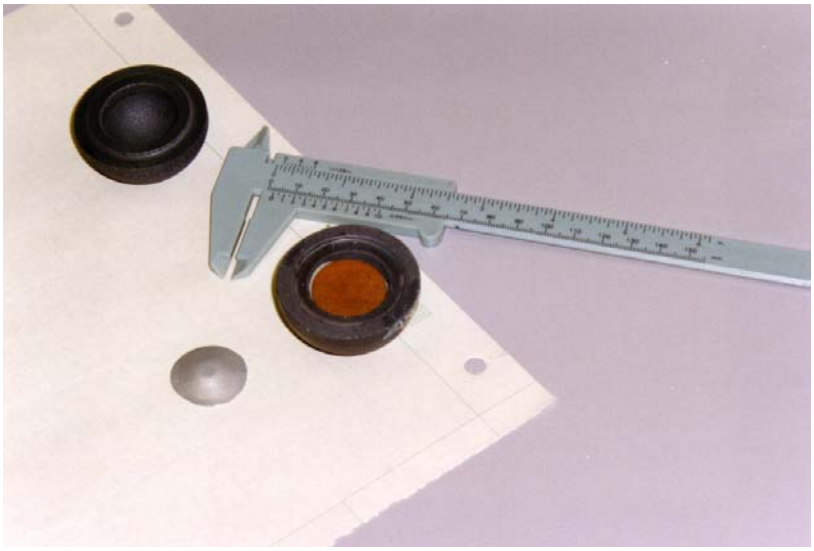

Figure 6. Boron sphere used to suppress low-energy neutron flux.

Use of the foils as described provided 5 basic neutron response functions having a useful degree of linear independence. These response functions were:

1. Resonance capture in the copper, gold, and indium foils in the foil wheel, all with thermal neutron capture suppressed by cadmium (3 responses);

2. Total neutron capture in the single uncovered gold foil in the foil wheel (1 response);

3. Inelastic scatter in the indium foil in the boron sphere (1 response).

The measurements reported here are based on the results of a one-hour irradiation at a reactor power of 770 kW.

Foil Data Acquisition and Analysis

The irradiated foils were assayed at WSU using a standard high-purity germanium (HPGe) gamma spectrometry system (Canberra/Genie). The induced activities in the free-beam foils were computed from the photopeak areas and system efficiencies based on calibration of the spectrometer using a National Institute Standards and Technology (NIST)-traceable mixed europium-antimony calibration source. The measured activity of the heavy indium foil in the boron sphere was corrected for gamma self-shielding using an escape fraction at 336 keV calculated using a combination of MCNP computations and handbook data for the specific source-detector geometry that was used for the assay. This factor was 0.90 ± 0.01. The activity of the indium foil in the cadmium cover was taken as the average of the results derived separately from the measured activities of the three primary gamma lines.

Deconvolution of the Free-Beam Neutron Spectrum from the Activation Measurements

The activation rates of the various foils were used to estimate the neutron spectrum by way of a simple direct matrix unfolding procedure, derived as follows:

The volume-average activation rate per atom for a foil dosimeter placed in a neutron flux field may be calculated as:

$$R = \int_0^\infty \sigma_f(E)\, \Psi_f(E)\, dE\,, \tag{1}$$

where $\sigma_f(E)$ is the microscopic activation cross section of interest for the foil material, as a function of neutron energy and $\psi_f(E)$ is the volume-average scalar neutron flux within the foil, again as a function of energy. Equation (1) can also be expressed as:

$$R = \int_0^\infty \sigma_f(E)\left(\frac{\Psi_f(E)}{\Psi(E)}\right)\Psi(E)\, dE = \int_0^\infty \sigma_f(E)\, P_f(E)\, \Psi(E)\, dE\,, \tag{2}$$

where $\psi(E)$ is the unperturbed neutron flux that would exist at the measurement location in the absence of the foil and any surrounding spectral modification devices (Cd covers, boron sphere, etc.)

It may be noted here that, as a practical matter, the function $P_f(E)$ in Equation 2 can be determined independently from $\Psi(E)$ if desired since it is simply a flux ratio. In this case $\Psi(E)$ on the far right hand side of Equation 2 can be any appropriate *a-priori* free-beam unperturbed flux estimate that is then modified by the self-shielding function $P_f(E)$.

Equation 1 may be written as a summation rather than as an integral by partitioning the range of the energy variable into a number of discrete contiguous energy groups:

$$R = \sum_{j=1}^{NG} a_j \phi_j\,, \tag{3}$$

where NG is the total number of groups, and

$$a_j = \frac{\int_{EL_j}^{EH_j} \sigma_f(E)\, P_f(E)\, \Psi(E)\, dE}{\int_{EL_j}^{EH_j} \Psi(E)\, dE}\,, \tag{4}$$

and

$$\phi_j = \int_{EL_j}^{EH_j} \Psi(E)\, dE\,, \tag{5}$$

where EL_j and EH_j are the lower and upper limits of energy group j.

If additional foils are placed in the beam, or if a particular foil exhibits more than one activation response, then Equation (3) may be written as a system of equations:

$$R_i = \sum_{j=1}^{NG} a_{ij}\ \phi_j\,, \tag{6}$$

where R_i is the total activation rate for interaction i, and a_{ij} is the activation constant from Equation (4) for reaction i due to neutrons in energy group j. There will be a total of NF equations, where NF is the total number of activation responses available.

Effective shielded cross sections $\sigma_f(E)$ and the corresponding shielded and unshielded neutron fluxes suitable for computing the function $P_f(E)$ in Equation 4 for this work were generated by the INEEL using MCNP models of the dosimeter packages in the positioning plate. The *a-priori* unperturbed neutron flux at the center of the source plane, computed using MCNP, was used to represent $\Psi(E)$ in Equation 2. The MCNP computation for P_f accounts for foil self-shielding as well as for the fact that the foils in the outer locations in the positioning plate are exposed to a slightly lower flux than they would if they were in the center.

It should also be noted here that in practical applications the functions $\sigma_f(E)$, $P_f(E)$, and $\Psi(E)$ are ordinarily not continuous functions. For the work reported here they are 47-group representations of the actual functions, computed using MCNP and tallied according to the BUGLE-80 neutron energy structure[11]. The integrals in Equations 4 and 5 are therefore actually summations over the fine-group structure within each broad group used for spectral unfolding.

The system of activation equations, Equation (6), may be written out in matrix form as:

$$\begin{bmatrix} a_{11} & a_{12} & a_{13} & \Lambda & a_{1\,NG} \\ a_{21} & a_{22} & a_{23} & \Lambda & a_{2\,NG} \\ a_{31} & a_{32} & a_{33} & \Lambda & a_{3\,NG} \\ \mathrm{M} & \mathrm{M} & \mathrm{M} & & \mathrm{M} \\ \mathrm{M} & \mathrm{M} & \mathrm{M} & & \mathrm{M} \\ a_{NF1} & a_{NF2} & a_{NF3} & & a_{NF\,NG} \end{bmatrix} \begin{bmatrix} \phi_1 \\ \phi_2 \\ \phi_3 \\ \mathrm{M} \\ \mathrm{M} \\ \phi_{NG} \end{bmatrix} = \begin{bmatrix} R_1 \\ R_2 \\ R_3 \\ \mathrm{M} \\ \mathrm{M} \\ R_{NF} \end{bmatrix}, \tag{7}$$

or, more compactly:

$$[A][\Phi] = [R]. \tag{8}$$

Equation (7) is exact, provided that the reaction rates R_i, the activation constants a_{ij} and the group fluxes, ϕ_j are all self-consistent. If measured reaction rates for each interaction R_i are substituted into Equation (7), a solution of the resulting new system of equations for "measured" fluxes corresponding to the measured reaction rates may also be obtained under certain conditions.

If NF = NG (as is the case for the measurements presented here), then the matrix [A] is square, its inverse will ordinarily exist, and the unknown "measured" flux vector may be obtained by any standard solution method that converges, provided that the rows of [A] are linearly-independent. In physical terms this implies that the response functions (cross sections) for the activation interactions used in the measurement must be selected such that they have different shapes as functions of energy. It may be noted that positive fluxes are not guaranteed to result from this procedure, but if the elements of [A] are computed in a sufficiently valid, physically-realistic manner for the specific measurement configuration, and if the measured reaction rates are accurately determined, a positive solution can generally be obtained.

Propagation of the measurement uncertainties in the unfolding process can be analyzed as follows:

An estimate for the variance of the unfolded flux in group j may be expressed as:

$$s_j^2 = \sum_{i=1}^{NF} \left(\frac{\partial \phi_j}{\partial R_i} \right)^2 \left[u_i^2 \right], \tag{9}$$

where u_i is the experimental uncertainty associated with reaction rate i. Thus, it is necessary to compute a matrix of derivatives of the group fluxes with respect to each reaction rate in order to evaluate the uncertainties in the unfolded fluxes from Equation (9).

If the matrix [A] is square, i.e., if NF = NG, as in the measurements presented here, the evaluation of the derivatives begins with a rearrangement of Equation (8):

$$[\Phi] = [C][R], \tag{10}$$

where [C] is defined to be the inverse of [A]. Expansion of Equation (10) yields:

$$\begin{bmatrix} \phi_1 \\ \phi_2 \\ \mathrm{M} \\ \phi_{NG} \end{bmatrix} = \begin{bmatrix} c_{11}R_1 + c_{12}R_2 \,\Lambda\, c_{1NG}\,R_{NF} \\ c_{21}R_1 + c_{22}R_2 \,\Lambda\, c_{2NG}\,R_{NF} \\ \mathrm{M} \\ c_{NG1}R_1 + c_{NG2}R_2 \,\Lambda\, c_{NG\,NG}\,R_{NF} \end{bmatrix}, \tag{11}$$

where NF = NG. Differentiating with respect to R_1 now yields

$$\begin{aligned}
\frac{\partial \phi_1}{\partial R_1} &= c_{11}\ , \\
\frac{\partial \phi_2}{\partial R_1} &= c_{21}, \\
\frac{\partial \phi_1}{\partial R_2} &= c_{12}, \\
\frac{\partial \phi_2}{\partial R_2} &= c_{22}\ , \textit{etc.}
\end{aligned} \tag{12}$$

Thus:

$$\frac{\partial[\Phi]}{\partial R_1} = [C]\begin{bmatrix} 1 \\ 0 \\ 0 \\ \mathrm{M} \\ 0 \end{bmatrix} = [C]\left[\text{column 1 of an } NG \text{ x } NG \text{ identity matrix}\right], \tag{13}$$

and, in general,

$$[A]\frac{\partial[\Phi]}{\partial R_i} = \left[\text{column i of an } NG \text{ x } NG \text{ identity matrix}\right], \tag{14}$$

since $[C] = [A]^{-1}$.

Equation (14) describes NF systems of NG simultaneous equations in NG variables that can be solved for the necessary derivatives. These are used to evaluate Equation (9).

The method outlined here, as well as the more general extension to the overdetermined case where NF > NG, have been implemented in a FORTRAN program SPECTRE, Version 5.2. This program inputs self-shielded activation cross section functions $\sigma_f(E)$ and the a-priori volume-average unperturbed and perturbed fluxes, Ψ(E) and $\Psi_f(E)$, in a user-specified fine-group structure for each activation foil interaction of interest. These, along with a user-input *a-priori* spectrum (which in the most rigorous case is the same as Ψ(E), as noted previously) are used to compute the elements of the matrix [A] for NG broad groups, each of which spans one or more specified fine groups. Solution of the various systems of equations to produce the unfolded fluxes and associated uncertainties corresponding to a user-input set of NF measured activation rates (and associated experimental uncertainties) is accomplished using standard Gauss-Seidell iterations, with linear extrapolation to accelerate convergence.

RESULTS

The measured saturation activities of the various foils are shown in Table 2. The statistical uncertainties given in this table include the uncertainty of the spectrometer calibration as well as the uncertainty of the activity measurement for each foil. These were used to derive the spectrum of the neutron flux at the measurement location using the previously-described direct few-group matrix unfolding procedure.

Table 2. Foil saturation activities measured at a WSU reactor power of 770 kW.

Neutron Interaction	Saturation Activity[4] (Bq/ atom)
^{197}Au (n, γ)[1]	4.02 x 10^{-14} (5.0%)
^{115}In (n, γ)[2]	5.02 x 10^{-14} (5.1%)
^{197}Au (n, γ)[2]	3.52 x 10^{-14} (5.0%)
^{63}Cu (n, γ)[2]	1.44 x 10^{-16} (5.6%)
^{115}In (n,n')[3]	2.80 x 10^{-19} (5.2%)

[1] Bare foil.
[2] Cadmium covered foil.
[3] Foil in boron sphere.
[4] Percentage uncertainty (1σ) given in parentheses.

Figure 7 shows an unfolded, 5-group, free-field, unperturbed neutron spectrum in the source plane, at the center of the foil positioning plate. The computed 47-group *a-priori* neutron spectrum, normalized to 770 kW, is also shown in Figure 7 for comparison. The broad group structure used for the unfolded spectrum presented in Figure 7 was selected to provide a well-conditioned unfolding matrix, and because it permits the most accurate integration of the measured spectrum in the epithermal energy range to determine the total epithermal neutron flux.

It will be observed that the propagated uncertainty associated with the thermal flux (E < 0.404 eV) in Figure 7 is quite large. This is a result of the fact that the thermal flux is very small compared to the remainder of the spectrum. The measured activities of the gold foils with and without Cd covers differ by only a few percent --- a difference comparable to the uncertainties of the activities themselves. This leads to a magnification of the uncertainty in the usual manner when the thermal flux is estimated from these foil activities in the spectral unfolding process.

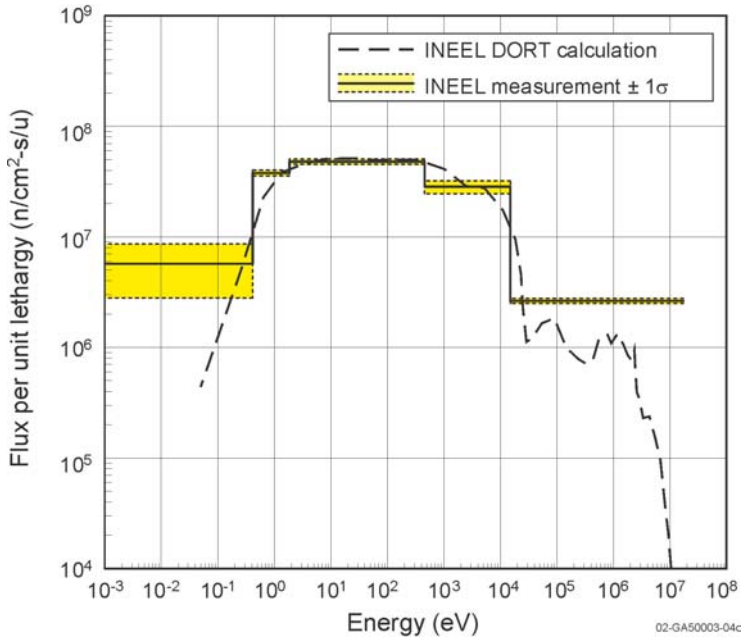

Figure 7. Unfolded free beam neutron spectrum in the source plane obtained by direct fitting for the WSU epithermal neutron beam facility. The reactor power was 770 kW.

Integrating the measured curve shown in Figure 7 between the standard epithermal energy limits of 0.414 eV and 10 keV produces a measured epithermal neutron flux of 4.1 x 10^8 n/cm^2-sec at 770 kW, with a propagated uncertainty of approximately 5% (1σ). This is well within the expected range based on the design computations. It may be noted that this flux is expected to increase by a factor of between 2 and 3 when the WSU reactor fuel element loading pattern is reconfigured for optimum beam performance.

A simple, but widely used metric for the quality of reactor-based epithermal-neutron beams is based on dividing the free-field neutron KERMA rate of the beam (integrated over all energies above thermal) by the useful epithermal-neutron flux, again measured in the free field. This parameter is an indicator of the non-selective neutron background dose that will be produced in tissue by the above-thermal spectral component of the beam itself, in the absence of any neutron capture agent that may be administered to the patient. It is computed here for WSU using the measured flux spectrum in conjunction with broad group KERMA factors based on data for the components of standard tissue available on File 27 of the BUGLE[11] cross section library that was used for the various DORT computations performed as part of this project. Fine-group neutron KERMA factors from File 27 are averaged over the broad unfolding group structure using the *a-priori* spectrum as a weighting function to produce the necessary information. This procedure yields a measured free-beam neutron contamination parameter of 2.96x10^{-11} cGy total neutron KERMA from all components per unit useful epithermal-neutron flux, with an estimated uncertainty of about 7%. This is in excellent agreement with the computed value of 2.75 x 10^{-11} cGy-cm^2. Approximately 91% of the background neutron dose results from proton recoil. The remainder is from other recoil components. Additional background dose in tissue is, of course, produced by non-selective thermal neutron induced components, primarily from neutron capture

in nitrogen and hydrogen, but these components are not directly indicative of the intrinsic biophysical quality of the incident beam. They must be taken into account in treatment planning, but they are not normally included in the free-beam quality parameter discussed here.

DISCUSSION

The WSU facility is the third clinical-scale reactor-based epithermal-neutron source for BNCT research that has been constructed in the U.S. With the recent decision to decommission the Brookhaven Medical Research Reactor, the new WSU neutron source and a recently constructed epithermal beam facility at the Massachusetts Institute of Technology[12] are the only two currently operating reactor based facilities of this type in the U.S.

REFERENCES

1. P.R. Gavin, S.L. Kraft, C.E. DeHann, C.D. Swartz, M.L. Griebenow, "Large Animal Normal Tissue Tolerance with Boron Neutron Capture," Int. J. Radiat. Oncol. Bio. Phys., **28**:1099-1106 (1994).

2. F.J. Wheeler, D.W. Nigg, "Feasibility Study for an Epithermal-Neutron Beam Facility at the Washington State University Radiation Center," EGG-NRE-11296, Idaho National Engineering Laboratory, USA, 1994.

3. T.D. Burns Jr., "A Monte Carlo Model System for Core Analysis and Design at the Washington State University Radiation Center," INEL-95/0458, Idaho National Engineering Laboratory, 1996.

4. J.R. Venhuizen et. al, "Construction Progress of an Epithermal Neutron Beam for Preclinical BNCT Research at Washington State University," In: J.R. Venhuizen (ed.), "INEEL BNCT Research Program Annual Report – 2000", INEEL-EXT-01-00204, March, 2001.

5. J.R. Venhuizen et. al, "Construction of an Epithermal Neutron Beam for Preclinical BNCT Research at Washington State University," In: J.R. Venhuizen (ed.), "INEEL BNCT Research Program Annual Report – 2001," INEEL-EXT-02-00060, April 2002.

6. I. Auterinen, P. Hiismäki, "Epithermal BNCT Neutron Beam Design for a Triga II Reactor," Advances in Neutron Capture Therapy, Plenum Press, New York, 1993, Pages 81-84.

7. J.F. Breismeister, (1993) MCNP – A General Monte Carlo N-Particle Transport Code, Version 4A, LA-12625-M, Los Alamos National Laboratory, USA.

8. W.A. Rhoades, et. al., "TORT-DORT: Two and Three-Dimensional Discrete-Ordinates Transport," Radiation Shielding Information Center, Oak Ridge National Laboratory, CCC-543, 1993.

9. D.W. Nigg, Y.D. Harker, J.K. Hartwell, C.A. Wemple, T. Seren, I. Auterinen, P. Kotiluoto, P. Hiismaki, T. Sepala, M. Kortesniemi, S. Savolainen, R. Risler, "Collaborative Neutronic Performance Characterization of the FiR-1 Clinical Epithermal Neutron Beam Facility for

BNCT", In: J.R. Venhuizen (ed.), "INEEL BNCT Research Program Annual Report – 1998," INEEL-EXT-99-00293, April, 1999.

10. Y.D. Harker, et al., "Spectral Characterization of the Epithermal Neutron Beam at the Brookhaven Medical Research Reactor," Nuclear Science and Engineering, **110**:355-368, 1992.

11. R.W. Roussin, "BUGLE-80 Coupled 47-Neutron, 20 Gamma-Ray P3 Cross Section Library," DLC-75, Radiation Shielding Information Center, 1980.

12. O.K. Harling, et al., "The Fission Converter-Based Epithermal Neutron Irradiation Facility at the Massachusetts Institute of Technology," Nuclear Science and Engineering, **140**, 223-240 (2002).

DEVELOPMENT OF ADVANCED MULTI-MODALITY RADIATION TREATMENT PLANNING SOFTWARE

D.E. Wessol[1], C.A. Wemple[1], D.W. Nigg[1], J.J. Cogliati[2], C. Frederickson[2], A. Kimmel[2], G.J. Harkin[2], C. Hartmann Siantar[3], M. A. Descalle[3]

1. **Idaho National Engineering and Environmental Laboratory, Idaho Falls, ID**
2. **Montana State University, Bozeman, MT**
3. **Lawrence Livermore National Laboratory, Livermore CA**

INTRODUCTION

The Idaho National Engineering and Environmental Laboratory (INEEL) has long been active in development of advanced Monte Carlo-based computational dosimetry and treatment planning methods and software for advanced radiotherapy, with a particular focus on Neutron Capture Therapy (NCT) and, to a somewhat lesser extent, Fast-Neutron Therapy (FTN). The most recent INEEL software system of this type is known as SERA, Simulation Environment for Radiotherapy Applications[1]. SERA is at a mature level in its life cycle, it has been licensed for research use worldwide, and it has become well established as a computational tool for research. However, along with its strengths, SERA also has some limitations in its structure and computational methodologies. More specifically, it is optimized only for neutron-based applications. Although photon transport can be computed with SERA, the simplified model that is used is designed primarily for photons produced in the neutron transport process. Thus, for example, SERA is not appropriate for applications to standard external-beam photon radiotherapy, which is far more common in the clinic than neutron based therapy.

At the same time, researchers at Lawrence Livermore National Laboratory (LLNL) have been engaged in the development of the PEREGRINE Monte Carlo code system, optimized for photon and electron therapy[2]. Now, as a logical next step in the development of modern radiotherapy planning tools to support the most advanced research, INEEL and LLNL have recently launched a new project to collaborate in the development of a "next-generation" multi-modality treatment planning software system. This effort will draw on the combined experience of the two laboratories, in their respective areas of interest to produce a new system that will be useful for all modern forms of radiotherapy. This article first provides some history of the SERA and PEREGRINE systems, followed by a discussion of the more recent new developmental effort being undertaken by INEEL and LLNL, along with a summary of current progress.

HISTORICAL BACKGROUND

INEEL

Figure 1 shows, on the left-hand side, a history of the medical treatment planning software developmental effort at the INEEL, which has been focused almost entirely on neutron-based applications.

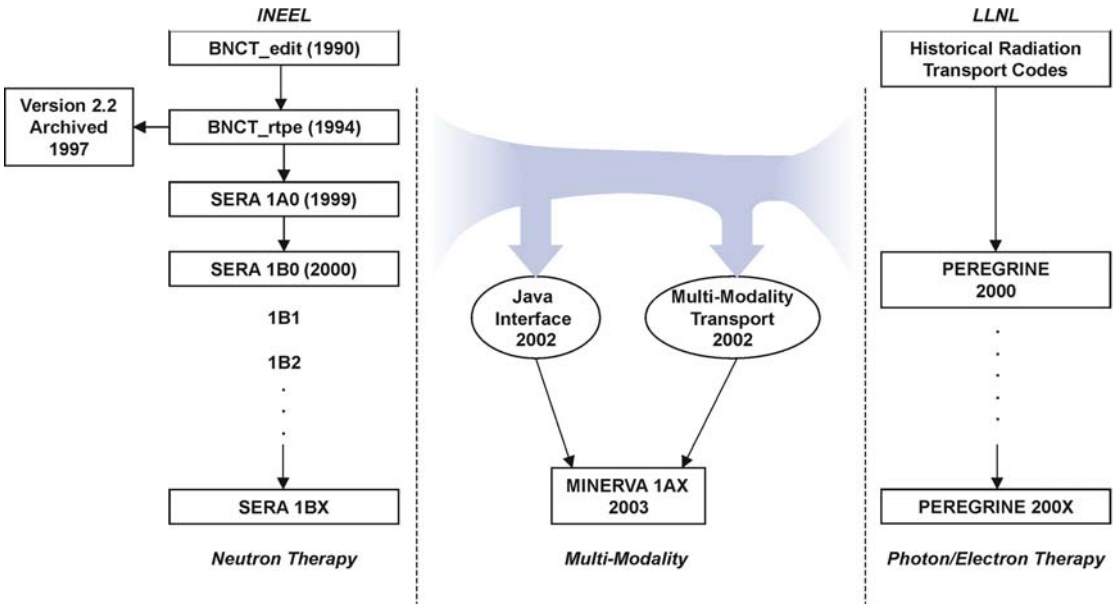

Figure 1. History of radiotherapy planning software development at the INEEL and at LLNL.

In the 1980s, it became apparent that new computational methods were required to support large animal-model preclinical NCT research, and anticipated human trials, for epithermal-neutron NCT in the U.S. Computational approximations that work well for photon-electron therapy and, to some extent, fast-neutron therapy, are not appropriate for neutron capture therapy. Complete solutions of the transport equations, with an explicit treatment of particle scattering, are required. Standard Monte Carlo radiation transport codes used in other fields of nuclear science, e.g., MCNP[3], have often been used successfully for this purpose by various investigators. In addition, specialized medical image-based geometric reconstruction and radiation dose visualization interfaces have been introduced for use with an especially tailored version of MCNP to produce a practical treatment planning system for boron neutron capture therapy (BNCT)[4,5]. Modern, three-dimensional, general-purpose discrete-ordinates codes have also sometimes been used to perform the necessary calculations[6,7].

However, MCNP and other general-purpose transport codes are designed for very broad applications. They are quite flexible, and have the advantage of dedicated maintenance and quality control by the developers, but in some situations they can tend to be slow in execution,

relative to expectations for treatment planning in clinical oncology practice (a few minutes per field, maximum), and there are limitations in the geometric detail that can be modeled. Hence, a project was initiated at the INEEL in 1988 to develop a special-purpose, medical image-based Monte Carlo system optimized specifically for radiotherapy, with epithermal-BNCT as the first anticipated application. This initial effort, conducted in collaboration with the University of Utah Department of Computer Science, resulted in the BNCT_edit system[8] as shown at the top of Figure 1. BNCT_edit was used by the INEEL in the early 1990s for various preclinical applications, but it was not used for human trials and it was never released for external use.

In 1994 BNCT_edit was replaced by a much-improved system, BNCT_rtpe (BNCT Radiation Treatment Planning Environment). The BNCT_rtpe system was introduced into clinical use in connection with the Department of Energy (DOE)-sponsored clinical trials of epithermal-neutron BNCT for glioblastoma multiforme that began at Brookhaven National Laboratory in the same year[9]. BNCT_rtpe was developed by the INEEL in collaboration with the Montana State University (MSU) Department of Computer Science. It was based on experience gained with the BNCT_edit development effort, in that it featured a sophisticated Non-Uniform Rational B-Spline (NURBS) approach to image modality-independent reconstruction of patient geometry from medical images[10]. With this method, the patient anatomy is initially reconstructed in so-called "pixel space," with subsequent rescaling to the actual computational geometry using the true field of view parameters pertinent to the image set. This allows modeling of essentially any anatomy that can be imaged, independent of the image modality, and without any computational restrictions. Furthermore, it incorporated an improved particle tracking method[11] based on a superimposed "edit mesh" that offered relatively rapid computation times (2-4 hours per field on the computer hardware of the time) compared to what had been previously possible, and vastly improved user interfaces. In addition to the Brookhaven application, BNCT_rtpe was also licensed for use in the European BNCT research programs conducted by the Technical Research Centre of Finland, and by the Commission of the European Communities Joint Research Centre at Petten, in The Netherlands.

Although BNCT_rtpe proved to be a useful and relatively efficient clinical research tool, there still was a need to reduce the computation time further-ideally to no more than a few minutes per field. Accordingly, INEEL and MSU undertook some studies in the late 1990s that were focused on achieving a significant breakthrough in execution speed via a total reformulation of the mathematical algorithms. Although it is possible to recast various standard Monte Carlo algorithms for parallel execution on specialized multi-CPU computer systems and thereby achieve increases in execution speed, INEEL and MSU researchers instead directed their efforts toward development of new and much faster algorithms. This approach was taken because most radiotherapy research centers and clinics typically operate with single-CPU desktop computer systems. The result of this developmental effort led to the introduction of the completely new SERA[1] treatment planning software in 1998.

The SERA treatment planning system incorporates an integrated method for reconstructing patient geometry from medical images and for subsequently tracking particles through this geometry during a Monte Carlo radiation transport simulation. The method, in contrast to coarse voxel reconstruction methods used with standard transport codes and the NURBS method used in BNCT_rtpe, is based on a pixel-by pixel uniform volume element ("univel") reconstruction of

the patient geometry[12]. As with the B-Spline method, construction of the patient geometry is independent of the medical image modality and field of view. Anatomical regions are defined on a selected set of two-dimensional images, and these regions are combined to produce a three-dimensional (3D) reconstruction, as shown in Figure 2. Fast scan-line rasterization methods, implemented largely with integer arithmetic, are then used to allow rapid particle tracking through the univel geometry. This is a key distinction between the univel method and standard voxel based reconstruction and tracking methods. Univels along the particle track are investigated and precise intersection points ("distance to boundary" in Monte Carlo terminology) can be rapidly calculated as the particle moves from one anatomical region to the next. Fluxes and doses are then tallied on a superimposed edit mesh in the same manner as in BNCT_rtpe.

The univel method has several attractive features. By scaling the univels to match the resolution of the original image data, the geometric fidelity of the NURBS reconstruction method is retained, but certain numerical difficulties associated with defining non-intersecting volumes in regions where the spline surfaces are very close together are eliminated. Furthermore, and most visibly, the computed fluxes and doses have the same statistical accuracy as with a NURBS model, but the execution time for the transport computations is reduced by a factor of between five and ten. This speedup factor holds even though the new univel model may consist of several million elements. Single-CPU execution times for SERA, with current desktop scientific computing hardware (e.g., 750 MHz Pentium III systems running under Linux), are in the range of a few minutes per field for neutron applications.

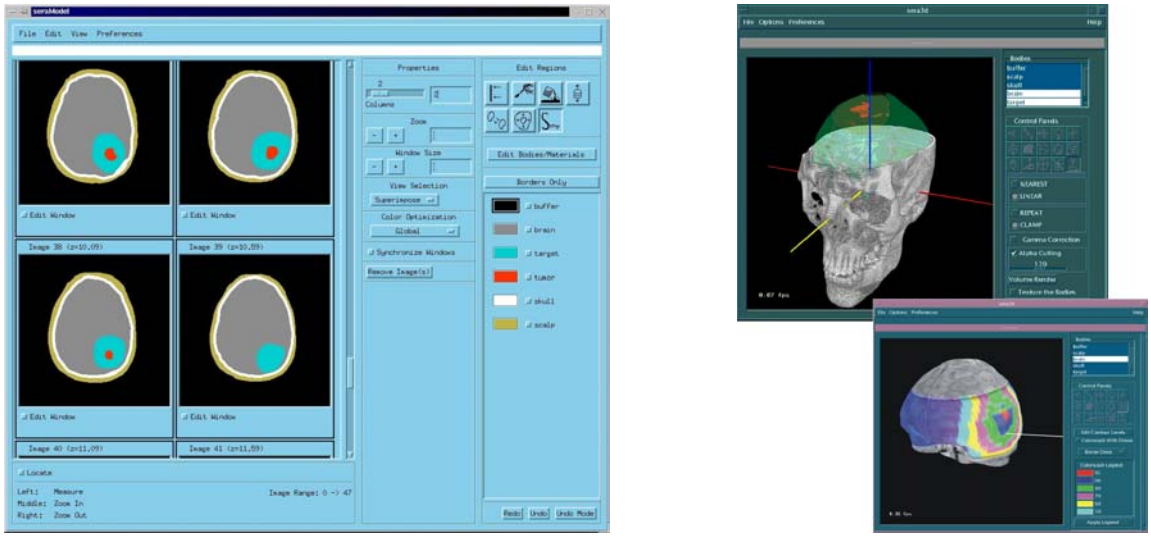

Figure 2. Univel-based anatomical reconstruction in SERA, with three-dimensional dose display.

Finally, the basic physics modules of SERA allow incident neutron energies up to 100 MeV, with an explicit (i.e., non-equilibrium) treatment of recoil proton transport[13]. This expands the utility of the SERA system into the field of FNT, with NCT augmentation[14]. Although other

clinically-useful treatment planning methodologies and tools are available for FNT[15], these are based on approximations, whereas SERA offers the capability to rigorously handle the more complex neutron transport and thermalization computations required for combined FNT/NCT applications.

SERA is licensed worldwide for research purposes and is currently in clinical testing in connection with ongoing epithermal-neutron BNCT clinical trials in Finland, Sweden, and in The Netherlands. Active SERA licensees include:

Lawrence Berkeley National Laboratory
The University of Washington
Massachusetts Institute of Technology
Purdue University
Commission of the European Communities – Joint Research Centre Petten
The Technical Research Center of Finland
Helsinki University Central Hospital
University Hospital Birmingham (United Kingdom)
Commision Nacional De Energia Atomica (Argentina)
Studsvik BV (Sweden)
Lund University (Sweden)
Kyoto University (Japan)
Medical Radiological Research Center, Russian Academy of Medical Sciences
Institute of Physics and Power Engineering (Russia)
National Tsing-Hua University

SERA licensees have agreed to serve as benchmarking and testing institutions for SERA. They have provided, and continue to provide, extremely valuable feedback and suggestions for improvement. SERA is maintained by the INEEL and MSU via an internet-based update distribution. It is anticipated that SERA will be maintained in a reasonably stable configuration for the foreseeable future, as shown on the left-hand side of Figure 1.

LLNL

Figure 1 shows, on the right hand side, the history of the PEREGRINE code at LLNL. The PEREGRINE dose calculation system[2] is primarily designed to provide Monte Carlo transport calculations fast enough for day-to-day external-beam photon-electron radiation therapy planning, although computations for other types of radiotherapy using specialized versions of PEREGRINE are also possible. It operates on low-cost commodity hardware, enables real time visualization of dose as it is simulated, and completes a full treatment simulation in minutes.

PEREGRINE simulates radiation therapy starting with a set of representative particles randomly sampled from energy, angle, and position distributions determined from offline simulations of the treatment-independent portion of the radiation source. It tracks each photon, electron, and positron through the treatment-dependent beam delivery system and then through the patient using random numbers, microscopic particle-interaction probabilities, and other standard Monte Carlo transport methods. As each particle interacts, it sets in motion other particles that are also

tracked. Photons and electrons are tracked to a minimum energy of 10 keV. The minimum energy for delta ray and bremsstrahlung production is 200 keV.

Treatment-specific beam modifiers, such as collimators, apertures, blocks, multileaf collimators and wedges, are modeled explicitly during each PEREGRINE calculation. Each component is described in terms of its physical dimensions, material composition, and density. The patient is described as a Cartesian map of material electron density determined from the patient's computed tomography (CT) scan. Each CT pixel defines the electron density of a corresponding transport mesh voxel. Material composition is determined from user-defined CT threshold values. Density is determined from a user-defined, piecewise-linear function that describes the CT number-to-density conversion. PEREGRINE records the dose deposited by each particle in a uniform Cartesian dose collection mesh that consists of packed spheres.

The PEREGRINE dose calculation system demonstrates the promise of Monte Carlo modeling for photon-electron radiation therapy. The value of stochastic simulations stems from the ability to use basic, microscopic physical data to provide practical information in arbitrarily complex systems. This power is limited only by the computational time necessary to complete sufficiently precise calculations and the creativity of the analyst. Many typical computations can be completed in minutes on hardware designed for clinical treatment planning, and faster computers will allow continued progress.

As is the case with SERA, PEREGRINE is in a relatively mature, stable status. The current release version, recently licensed for commercial applications by the NOMOS Corporation, has been approved by the U.S. Food and Drug Administration (FDA). It is anticipated that PEREGRINE will remain in a stable configuration to facilitate clinical deployment for external beam photon-electron therapy, as shown on the right-hand side of Figure 1.

THE MINERVA PROJECT

With SERA on a path to stabilization, INEEL and MSU began directing their attention to the development of a new generation of radiotherapy planning software, with a much broader range of applications in mind. More or less concurrently, the developers of PEREGRINE were thinking along the same lines. As a result, INEEL, MSU and LLNL launched, in October, 2001, a new project to collaborate in the creation of a multi-modality treatment planning software system that will draw on the combined experience of the two laboratories in their respective areas of interest. It will feature several important new functionalities made possible by recent advances in computational hardware, software, and operating system technology. The objective will be to create an integrated software system that is useful for all modern forms of radiotherapy. The new system will carry the name MINERVA (Modality-Inclusive Environment for Radiotherapeutic Variable Analysis).

Several state-of-the-art features will be incorporated into the new system, which is shown schematically in Figure 3. With the advent of the Java[a] internet-based programming language, it is now possible to produce extremely sophisticated software and graphic user interfaces with much greater portability among various computer hardware platforms. In addition, the focus will

[a] Java is a trademark of Sun Microsystems, Inc.

be on the development of a system that can be easily tailored to any radiotherapy modality, and to include multiple computational methodology options for a given therapeutic modality via an open "plug-in" based interface environment. The first version of MINERVA will include capabilities for external beam photon, electron, fast-neutron radiotherapy, neutron capture therapy, and molecular targeted radionuclide therapy. Other future anticipated additions include computational modules optimized for external-beam proton therapy, as well as for brachytherapy. Alternate computational methods based on existing transport software, such as MCNP, could also be incorporated by providing an appropriate code specific interface, as shown in Figure 3. The new system will employ multi-modality image sets for treatment plan development, and it will implement a universal data base for patient information file storage, with interfaces to accommodate standard clinical data communication protocols and formats, such as RTOG and DICOM-RT.

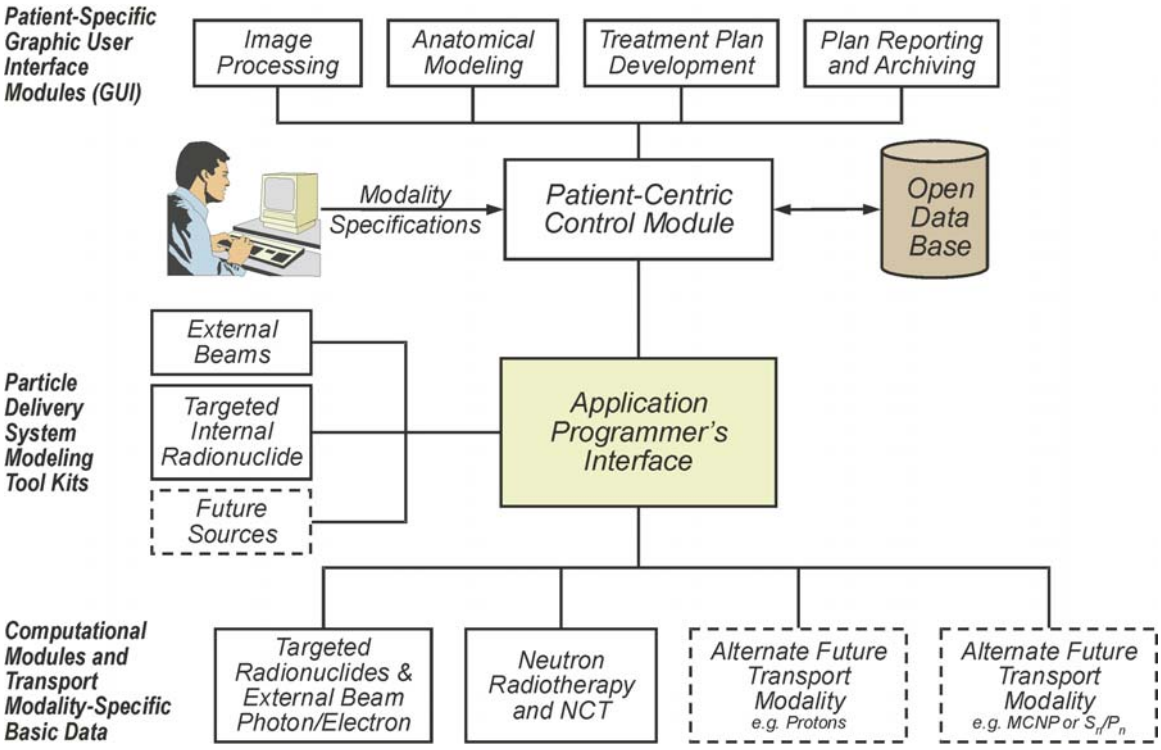

Figure 3. Schematic of the MINERVA code system.

The following three sections detail the recent progress and the current status of various aspects of the MINERVA project.

Feasibility Investigations --- The Seragrine Prototype System

In anticipation of this longer-term joint developmental program, INEEL and LLNL have completed some initial computational feasibility studies for a combined software system. These

studies employed an internet-based, *ad hoc* coupling of the functionalities in the SERA and PEREGRINE code systems as they currently stand to produce a temporary prototype, referred to as Seragrine. (See accompanying article in this report, P. 69). This exploratory system will continue to be used, on an interim basis, for various studies required to specify the design of the new system. The final product will be almost entirely based on new code, but the exercises conducted here have successfully demonstrated that there should be no fundamental difficulties with the development of the key computational and data interfacing functions that will be required in the new system. Two specific demonstration computations have been completed in this manner:

1. Calculation of the radiation dose distribution in a hypothetical patient resulting from a manually specified, spatially distributed, radionuclide-based internal photon-electron source.

2. Calculation of the radiation dose distribution in a hypothetical patient resulting from the application of photon and electron beams.

Dose Distribution from an Internal Radionuclide Source - PEREGRINE and SERA are not currently well structured for calculations involving fixed internal radiation sources. Secondary particles created by the interaction of external radiation sources within the patient anatomy are, of course, properly accounted for in both systems, but primary internal sources are not routinely accommodated. To handle this on a temporary demonstration basis, a special auxiliary univel file was created for use with SERA where the material specification for each univel was interpreted not as a physical material, but as an internal radiation source intensity (Bq per unit volume) averaged over the univel volume. For this application the source was assumed to be ^{131}I, and the spatial distribution was assumed to be uniform over a target volume that is typically associated with Glioblastoma Multiforme at presentation. This pseudo-univel file could be superimposed in SERA over the medical images used for the actual anatomical reconstruction, as shown in Figure 4, to show the assumed radionuclide distribution. The patient geometry for this demonstration was based on CT images taken from the Visible Human (VHP) data set distributed by the U.S. National Library of Medicine (http://www.nim.nih.gov).

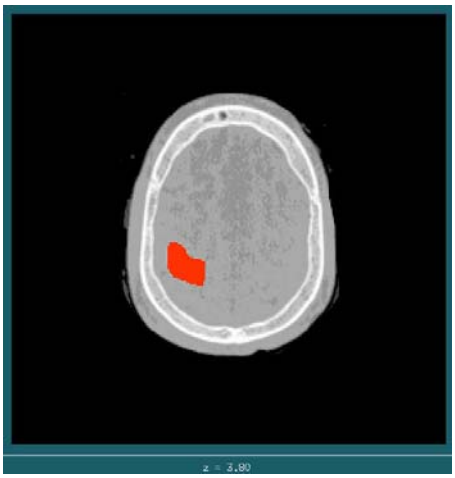

Figure 4. Radionuclide distribution superimposed over patient anatomical image.

The file describing the radionuclide distribution and the corresponding VHP anatomical image set were then passed to PEREGRINE for the photon-electron radiation transport computation. The resulting radiation doses were then passed back to SERA for contouring and display, superimposed over the original anatomical image set. The resulting dose contours (at intervals of 10%) for one axial plane are shown in Figure 5.

Dose Distribution from an External Photon-Electron Teletherapy Source - Figure 6 shows a case in which PEREGRINE was used to compute dose distributions resulting from application of standard external 6 MeV photon beams to a patient represented by the VHP anatomical data set. The resulting dose maps were then input to SERA for processing and display. The photon beam results shown here result from full photon-beam models. Figure 7 shows a dose distribution resulting from a monoenergetic 8 MeV electron point source. Once again, the ability to couple the functionalities of PEREGRINE and SERA is clearly demonstrated.

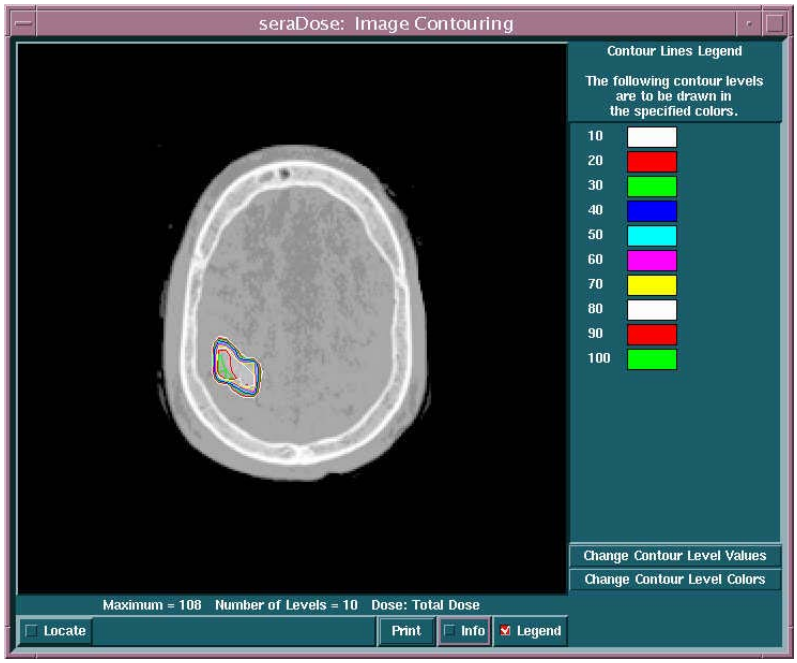

Figure 5. Total dose contours computed by PEREGRINE for the demonstration targeted radionuclide source.

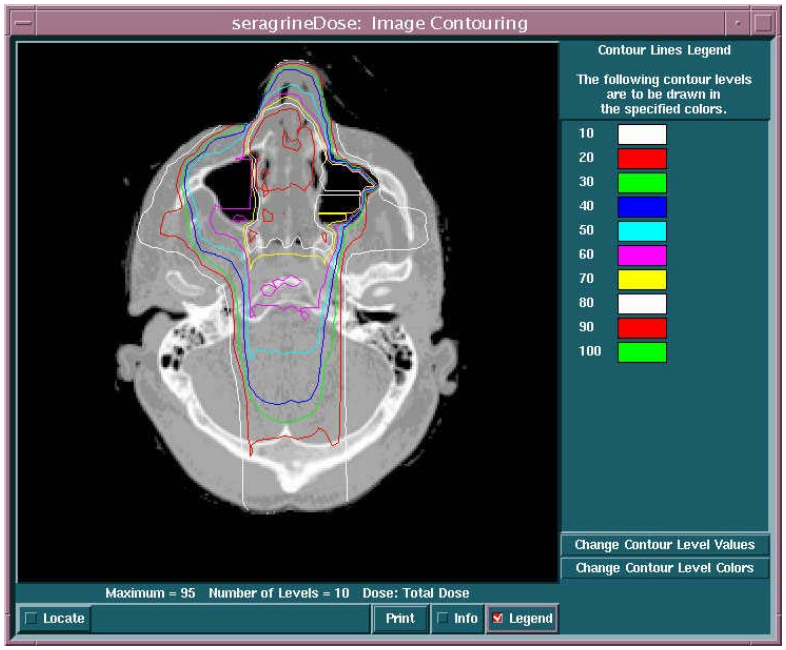

Figure 6. Dose contours resulting from a multi-field external photon source.

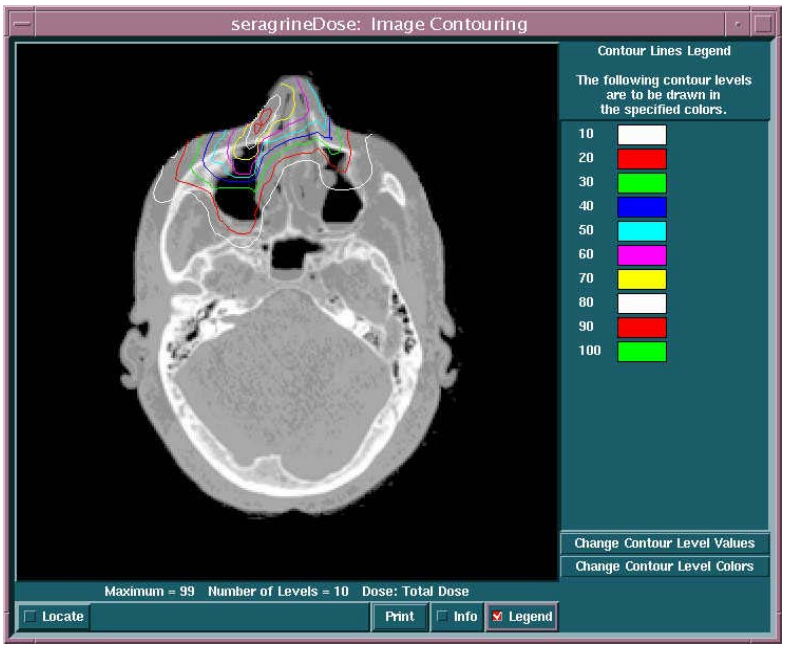

Figure 7. Dose contours from an external electron source.

Development of the Computational Module for Coupled Photon-Electron Transport

The initial emphasis in this part of the project has been focused on working with prospective users to assess the roles and key challenges in treatment planning for emerging photon/electron radiation therapy modalities[16,17]. From this, the overall functional requirements of the system for internal and external radiation sources have been developed, with an emphasis on internal radioisotope emitters, including the input of radiation source distributions from planar (2D) and single photon emission computed emission tomography (SPECT) (3D) scans[18,19]. In addition, the development and testing of the MINERVA photon-electron particle transport package, which is based on the PEREGRINE system, continued, with extensions of its capabilities to internal isotopic emitters[18] as described previously.

The initial validation approach for internal isotopic sources has been the comparison of MINERVA transport module simulations with other well-benchmarked Monte Carlo code systems and standard publications for point and spherical-volume sources consisting of monoenergetic photons and electrons, as well as commonly-used isotopes. The first phase of this benchmarking effort is complete. It was generally observed that MINERVA simulations of absorbed fractions for monoenergetic, photon and electron radiation sources distributed uniformly in standard tissue and water spheres agree with EGS4[20] to about 2% and MCNP[3] to about 5%, for sphere radii ranging from 1 to 7 cm for electrons, and 1 to 10 cm for photons. In addition, MINERVA simulations of absorbed fractions for photons emitted by ^{131}I, ^{111}In, ^{67}Cu, and ^{186}Re agree with EGS4[21] to within 1-2% for sphere radii ranging from 1 to 15 cm. For monoenergetic photon sources, MINERVA, EGS4, and MCNP predict absorbed fractions that are higher than those recommended by MIRD-3[22] and MIRD-8[23], by as much as 30-40%.

Development of User Interfaces

TIRADE (Transport Independent RADiotherapy Environment) was introduced in the INEEL BNCT Research Program Annual Report 2000[24] as a generalized multi-modality treatment planning system. With the incorporation of LLNL into the developmental effort as of October 1, 2001, the MINERVA name was adopted for the overall software system. However, since the initial development of the common interface modules and tools was performed under TIRADE acronym for the first three quarters covered by this Annual Report, the TIRADE acronym is retained in this section for this year only.

As detailed previously, MINERVA is designed to accommodate the differing modalities via plugins through the application programmer's interface (API). Each plugin, whether for a source specification module or transport application, will provide its own graphical user interface (GUI). For the targeted radionuclide modality, MSU/INEEL will be developing the source specification module, and LLNL will be developing the transport plugin as well as specifying interfaces and dose reporting requirements.

Patient Module - The patient module, the focal point of the system shown in Figure 3, manages the entire treatment planning process. In addition to running and managing all of the independent modules, the patient module creates, edits, and retrieves patient information. The ability to access the new patient database has been added to the patient module in CY 2001.

Image Processing Module - The image module is at the beginning of the treatment planning pipeline. It prepares and processes the images for use by the other TIRADE modules. During the last year, an image registration system based on the use of mutual information[25] to determine the best 3D fit between two image sets was completed. This method is marker-independent and relies only on the content of the images to produce a registration, making it easier for users and less invasive for patients. More importantly, patients that are imaged, either without markers, or with a non-standard marker system, all can have their image sets registered. The optimal fit is based on a line optimization with parabolic interpolation to improve the speed and reduce the likelihood of being side-tracked by local minima. This system is currently being tested and refined for integration into the image module.

A filter was added to the image module to remove the random noise from an image so that the outer edges are more sharply defined, and image noise and unwanted information are removed in the space outside of the image object. This should improve the accuracy and performance of the image registration algorithm, particularly when working with images from positron emission tomography (PET) scanners.

Anatomical Modeling Module - The modeling module provides tools for creation of the anatomical geometry of the patient and target based on the image data. The model module is used to either create a new univel geometry file or edit an existing model.

During CY 2001, several changes were made to the modeling module. Several programming errors were corrected. To facilitate modeling, a 3x3x3 median filter was added to better define structures within an image. This filter treats each image pixel as having an intensity value equal to the average of the pixel and its 26 nearest neighbors in three dimensions, which smoothes the intensity distribution and improves the threshold functionality. The ability to save and load data into and out of the database was added to the model module.

Reporting and Display Modules - Formerly, the SERA reporting module included two separate interfaces: the plotting module and the dose module. The plotting module provides the functionality for displaying, comparing, and manipulating dose-volume histograms (DVH) and dose-depth plots (DDP). The dose module allows the user to load and display contours on individual images and entire image sets. Over the past year, the plotting and dose contouring modules were integrated into a single interface. The decision to combine plotting and contouring functionality will allow the development of tools that better show the relationship between DVH and DDP and the contours displayed on the image sets.

Currently, the display module is in the early stages of development, but will eventually provide the user with powerful tools to compare and assess the treatment plans generated by the modules in the TIRADE treatment planning pipeline.

Figure 8 is an example of a dose volume histogram using the display module.

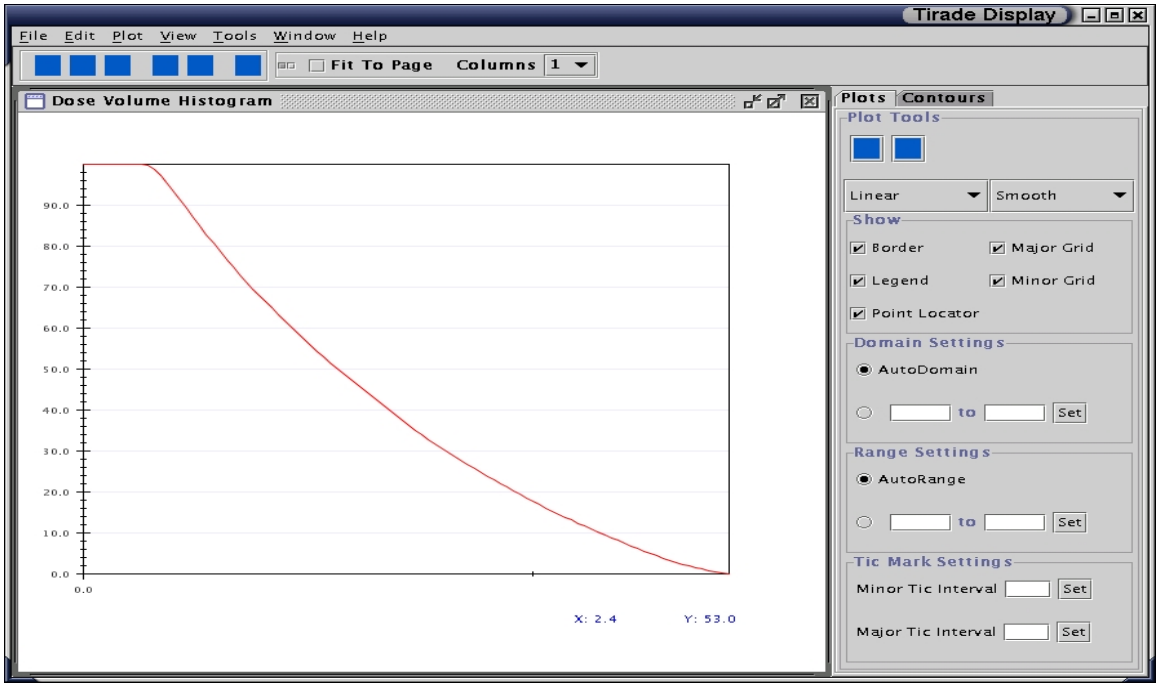

Figure 8. TIRADE display of dose-volume histogram.

Three-Dimensional Methods - Several 3D classes and methods have been developed, including methods to display, scale, and rotate 3D objects using the mouse or keyboard. A 3D geometry class has been created for displaying image, geometry, and dose data. The methods of the geometry class can display the geometry data as points, lines, and polygons, similar to that which was provided in SERA. The geometry class also allows the user to specify which regions to display, and the attributes (color, transparency, etc) used to display these regions. This class can be added to the image, model, and reporting modules to display the appropriate data.

Design and Development Tools

The system is being designed with the Unified Modeling Language (UML) and coded with the Java[26] language. Researchers have examined two new Java design and development tools, Together Control Center[a] and NetBeans[b], which are described in the next two subsections. While the design and development policies do not require the use of these two tools, they are highly recommended. Coding standards and policies can be found at the developer's web site, which is described in the last section of this particular report.

[a] TogetherSoft is a trademark of TogetherSoft Corporation (www.togethersoft.com)

[b] Netbeans is a Trademark of Sun Microsystems (www.netbeams.org)

Unified Modeling Language / Together Control Center - The UML has been used extensively in the design and development of the TIRADE project. During the past year, the Together Control Center software package for UML modeling and diagramming has been used extensively. This software uses the UML specifications for creating diagrams showing the relationships between packages, classes, and objects. Together Control Center also provides CVS[a] support and the capabilities to generate source code templates directly from diagrams, generate diagrams for code already written, and generate project documentation and diagrams in hyper-text markup language (HTML) format.

NetBeans - The NetBeans Integrated Development Environment (IDE) is a software package that combines many useful development tools for Java, such as a source code editor, compiler, and debugger, into one piece of software. NetBeans software was chosen as the recommended development environment for the TIRADE project because, along with basic IDE tools, it offers many useful features, such as CVS support, JavaDoc index searching, and the ability to create source code templates. NetBeans is an open-source project written entirely in Java, which makes it platform independent and easily obtainable by everyone involved in the TIRADE project.

Database

Database support has been added to the patient, image, and model modules. The database part of TIRADE has undergone significant redesign in the last four months of CY 2001. Even the understanding of how Java applications use the Java Database Connectivity (JDBC) to access information stored in a database has changed. Previously, it was understood that all Open Database Connectivity (ODBC) compliant Database Management Systems (DBMS) wrote their files to a common specification, allowing one DBMS to read database files produced by any other ODBC compliant DBMS. In practice, only the DBMS that wrote the database is able to read it (see Figure 9). Several database drivers (MySQL, Postgress) will be supported. Currently, tools are provided to exchange information among supported databases. TIRADE will also provide the capability to export the database information to flat files.

Steps have been taken to ensure that the database integrity is maintained by storing a patient's information in several smaller tables and by supporting transactional tables. The latter guards against a patient's data being partially updated during a save and therefore corrupted. If, for some reason, data corruption did occur, the damage would be largely localized through the database design.

The main focus of database development during the reporting period has been developing a common set of tools for accessing the database. One of these is a tool that will convert the database to flat files and back again. This ability is provided for transport plugin developers who prefer to read and write flat files.

Transport Plugins

Development began on a tool to calculate digitally reconstructed radiographs (DRR) from the patient anatomical model. A DRR is simply a projection of monoenergetic, monodirectional

[a] Concurrent Version System, freeware (see reference 28).

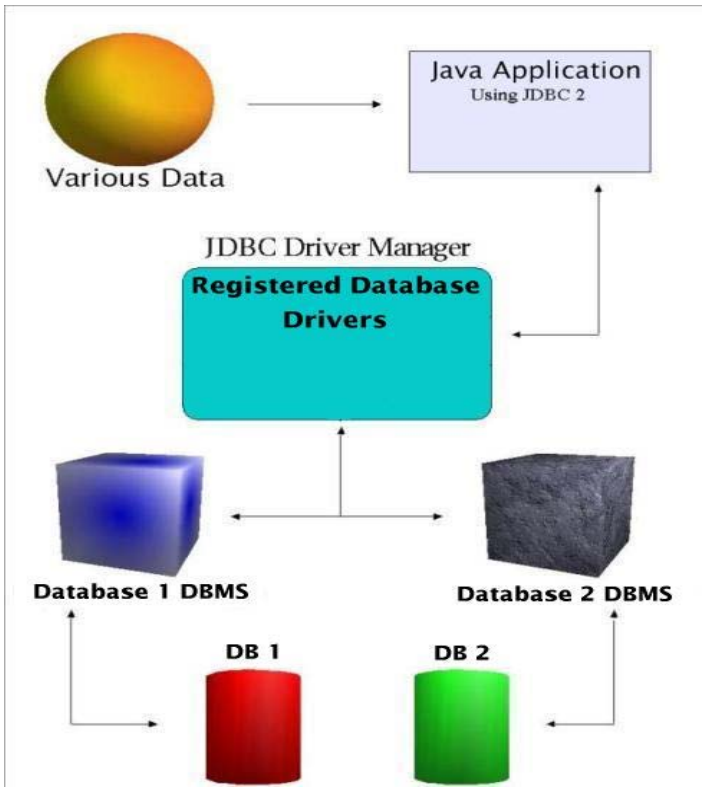

Figure 9. TIRADE database design.

photons from a plane source through the patient geometric model. The resulting images are useful for various verification processes in treatment planning. The photon transport model used was a simple attenuation function, which assumes that any interaction results in a loss of the photon. This methodology also has applications for molecular targeted radiotherapy, as the calculation engine for attenuation correction of initial internal source distributions in a semi-iterative approach. Requirements for this module will be developed with guidance from LLNL.

The TIRADE DRR tool was developed using both the Java and C programming languages to compare language dependent performance. The Java version achieved 50% to 66% of the speed of the optimized C version in our tests. This, along with evidence that IBM has achieved 90% of the speed of optimized Fortran in their Watson Research Center NINJA[a] project for certain BLAS[b] routines, suggests that Java may be a viable candidate language for developing numerically intense transport applications as well as for visualization applications. This presents certain advantages over conventional software development and deployment using C and/or Fortran, as Java is inherently more portable, and the resulting transport plugin can then be more easily integrated into the TIRADE system (e.g., direct database access.) With this in mind,

[a] Numerically Intensive Java (http://www.research.ibm.com/ninja/)

[b] Basic Linear Algebra Subprograms

design of the neutron transport module for the MINERVA package has begun, with the intent of developing the code using the Java programming language and the development methods outlined in Section 2 above.

Website

The developers' website (http://boron.csnet.montana.edu) for the INEEL/MSU Advanced RadioTherapy Project (ARTP) was created to provide documentation, programming standards, and design information. This website includes the CVS repository mailing list archives, which allows browsing of the changes made to the TIRADE source code and data. The ARTP website contains links to the TIRADE development resources, including the TIRADE JavaDoc and UML diagrams and documentation. Also included is bugzilla (http://www.mozilla.org/bugs/), a bug tracking database. Bugzilla allows bugs to be recorded, annotated, assigned, and resolved.

REFERENCES

1. D.W. Nigg, C.A. Wemple, D.E. Wessol, F.J. Wheeler, "SERA-An Advanced Treatment Planning System for Neutron Therapy and BNCT," *Trans. ANS* 80:66-68, 1999.

2. C.L. Hartmann-Siantar, et al., "Description and Dosimetric Verification of the PEREGRINE Monte Carlo Dose Calculation System for Photon Beams Incident on a Water Phantom," *Medical Physics* 28:1322-1337, 2001.

3. Briesmeister, J.F. (1993), "MCNP – A General Monte Carlo N-Particle Transport Code, Version 4A," LA-12625-M, Los Alamos National Laboratory, USA.

4. R.G Zamenhof, E. Redmond, G. Solares, D. Katz, K. Riley, S. Kiger, O. Harling, "Monte Carlo Based Treatment Planning for Boron Neutron Capture Therapy Using Custom Designed Models Automatically Generated from CT Data," *Int. J. Rad. Onc. Biol. Phys.* 35:383-397, 1996.

5. T. Goorley, G. McKinney, K. Adams, G. Estes, "MCNP Enhancements, Parallel Computing, and Error Analysis for BNCT," In: Hawthorne et al. (Editors), *Frontiers in Neutron Capture Therapy*, Volume 1, Kluwer Academic/Plenum Publishers, New York, 2001.

6. D.W. Nigg, P.D. Randolph, F.J. Wheeler, "Demonstration of Three-Dimensional Deterministic Radiation Transport Theory Dose Distribution Analysis for Boron Neutron Capture Therapy," Medical Physics 18:43-53, 1991.

7. J.M. Moran, D.W. Nigg, F.J. Wheeler, W.F. Bauer, "Macroscopic Geometric Heterogeneity Effects in Radiation Dose Distribution Analysis for Boron Neutron Capture Therapy," *Medical Physics* 19:723-732, 1992.

8. D.W. Nigg, "Methods for Radiation Dose Distribution Analysis and Treatment Planning in Boron Neutron Capture Therapy," *Int. J. Rad. Onc. Biol. Phys*. 28:1121-1134, 1994.

9. D.W. Nigg, F.J. Wheeler, D.E. Wessol, J. Capala, M. Chadha, "Computational Dosimetry and Treatment Planning for Boron Neutron Capture Therapy of Glioblastoma Multiforme," *Journal of Neuro-Oncology*, 33:93-104, 1997.

10. D.E. Wessol, F.J. Wheeler, "Methods for Creating and Using Free-Form Geometries in Monte Carlo Particle Transport," *Nuclear Science and Engineering* 113:314-323, 1993.

11. F.J. Wheeler, D.W. Nigg, "Three Dimensional Radiation Dose Distribution Analysis for Boron Neutron Capture Therapy," *Nuclear Science and Engineering*, 110:16-31, 1992.

12. M.W. Frandsen, D.E. Wessol, F.J. Wheeler, D.Starkey, "Rapid Geometry Interrogation for Uniform Volume Element-Based BNCT Monte Carlo Particle Transport Simulation," Proceedings of the 1998 ANS Radiation Protection and Shielding Division Topical Conference – *Technologies for the New Century*, American Nuclear Society, Chicago, Illinois, Volume II, pp. 84-94, 1998.

13. C.A. Wemple, F.J. Wheeler, D.W. Nigg, "Modifications to rtt_MC for Fast-Neutron Therapy Treatment Planning," Proceedings of the Eighth International Symposium on Neutron Capture Therapy – *Frontiers in Neutron Capture Therapy*, Plenum Press, New York, Volume 1, pp. 715-722, 2001.

14. G.E. Laramore, P Wootton, J.C. Livesey, D.S. Wilbur, R. Risler, M. Phillips, J. Jacky, T.A. Bucholtz, T.W. Griffin, S. Brossard, "Boron Neutron Capture Therapy - A mechanism for achieving a concomitant tumor boost in fast neutron radiotherapy," *Int. J. Rad. Onc. Biol. Phys*. 28:1135-1142, 1994.

15. I.J. Kalet, J.P. Jacky, M.M. Austin-Seymour, S.M. Hummel, K.J. Sullivan, J.M. Unger, "PRISM: A New Approach to Radiotherapy Planning Software," *Int. J. Rad. Onc. Biol. Phys*. 36:451-461, 1996.

16. Gerald L. DeNardo, Christine L. Hartmann-Siantar, Sally J. DeNardo, "Radiation dosimetry for radionuclide therapy in a nonmyeloablative strategy," Cancer Biotherapy and Radiopharmaceuticals, 17(1), 107-118 (2002).

17. C. L. Hartmann-Siantar, K. Vetter, G. L. DeNardo, S. J. DeNardo "Treatment planning for molecular targeted radionuclide therapy," (in press), In: Cancer Biotherapy and Radiopharmaceuticals.

18. C.L. Hartmann-Siantar, M.A. Descalle, D.W. Nigg, and G.L. DeNardo, "Applications of Monte Carlo methods in molecular targeted radiation therapy," In: Proceedings of 12th Biennial Topical Meeting of the American Nuclear Society, Radiation Protection and Shielding Division, Santa Fe NM, Apr 14-18, 2002, American Nuclear Society, Chicago, Illinois.

19. D.W. Nigg and C. L. Hartmann-Siantar, "Development of advanced multi-modality radiation treatment planning software," In: Proceedings of 12th Biennial Topical Meeting of the

American Nuclear Society, Radiation Protection and Shielding Division, Santa Fe, NM, Apr 14-18, 2002, American Nuclear Society, Chicago, Illinois.

20. M. Stabin, M. Konijnenberg, "Evaluation of absorbed fractions for photons and electrons in spheres of various sizes," J. Nucl. Med. 41:1, 149-160 (2000).

21. E. E. Furhang, G. Sgouros, and C-S Chui, "Radionuclide photon dose kernels for internal emitter dosimetry," Med. Phys. 23(5) 759-764 (1996).

22. G. Brownell, W. Ellett, R. Reddy, "Absorbed fractions for photon dosimetry," MIRD Pamphlet No. 3, New York, NY, Society of Nuclear Medicine (1968).

23. W. Ellett, R. Humes, "Absorbed fractions for small volumes containing photon-emitting radioactivity," MIRD Pamphlet No. 8, New York, NY; Society of Nuclear Medicine (1972).

24. D.E. Wessol, et al., "Radiation Treatment Planning Software Development," In: J. R. Venhuizen (ed.), "INEEL BNCT Research Program Annual Report 2000," INEEL EXT-01-00204, March 2001.

25. Paul Viola and William M. Wells, "Alignment by Maximization of Mutual Information," International Journal of Computer Vision, 24 (2), 137-154, 1997.

26. James Gosling, Bill Joy, and Guy Steele, *The Java Language Specification*, Addison-Wesley, September 1996.

27. Per Cederqvist, *Version Management with CVS*: ASIN 0595149219.

MOLECULAR TARGETED RADIOTHERAPY DEMONSTRATION SOFTWARE

C.A. Wemple

Idaho National Engineering and Environmental Laboratory, Idaho Falls, ID

INTRODUCTION

As part of the Idaho National Engineering and Environmental Laboratory/Lawrence Livermore National Laboratory (INEEL/LLNL) radiotherapy software development collaboration, a demonstration tool was required to verify that molecular targeted radiotherapy (MTR) dose distributions could be calculated in the PEREGRINE[1] code. This tool should allow processing of medical images, designation of anatomical structures on the images, assignment of radionuclides to multiple organs, and display isodose contours on the medical images, with data passed in a form compatible with that employed in PEREGRINE[2]. The SERA code system[3] already provided many of these tools, so it was seen as a logical starting point for development of such a demonstration tool. Thus, in order to provide a testbed for future developments, and enable development of the MTR calculation mode, a modified, special purpose version of the SERA code was created to provide a link to the PEREGRINE code. The name adopted for this demonstration tool was Seragrine.

SERA MODIFICATIONS

Several modifications were required to the SERA modules, mostly involving reading and writing data in forms compatible with PEREGRINE. First, the Image, Model, and Dose modules needed to read medical images in the PEREGRINE format, and the Image module needed to also write them in this form. The Dose module had to be modified to read and process the PEREGRINE dose formats. The Model module required modifications to assign radionuclides to various body structures, and write the resulting univel[4] data as an activity map for PEREGRINE. An additional parameter was defined in the body_data structure within the Model module, to allow the user to define the uniform radionuclide concentration in a given structure.

EXPERIENCES

Initial testing of the Seragrine tools was performed using a uniform radionuclide concentration in the tumor region only for a standard test image set with an artificially created tumor region. Dose results for calculations with a concentration of 0.17 □Ci/g of ^{131}I in the tumor are displayed Figure 1. Testing of cases with the radionuclide deposited in multiple, disjoint locations is presently underway at LLNL.

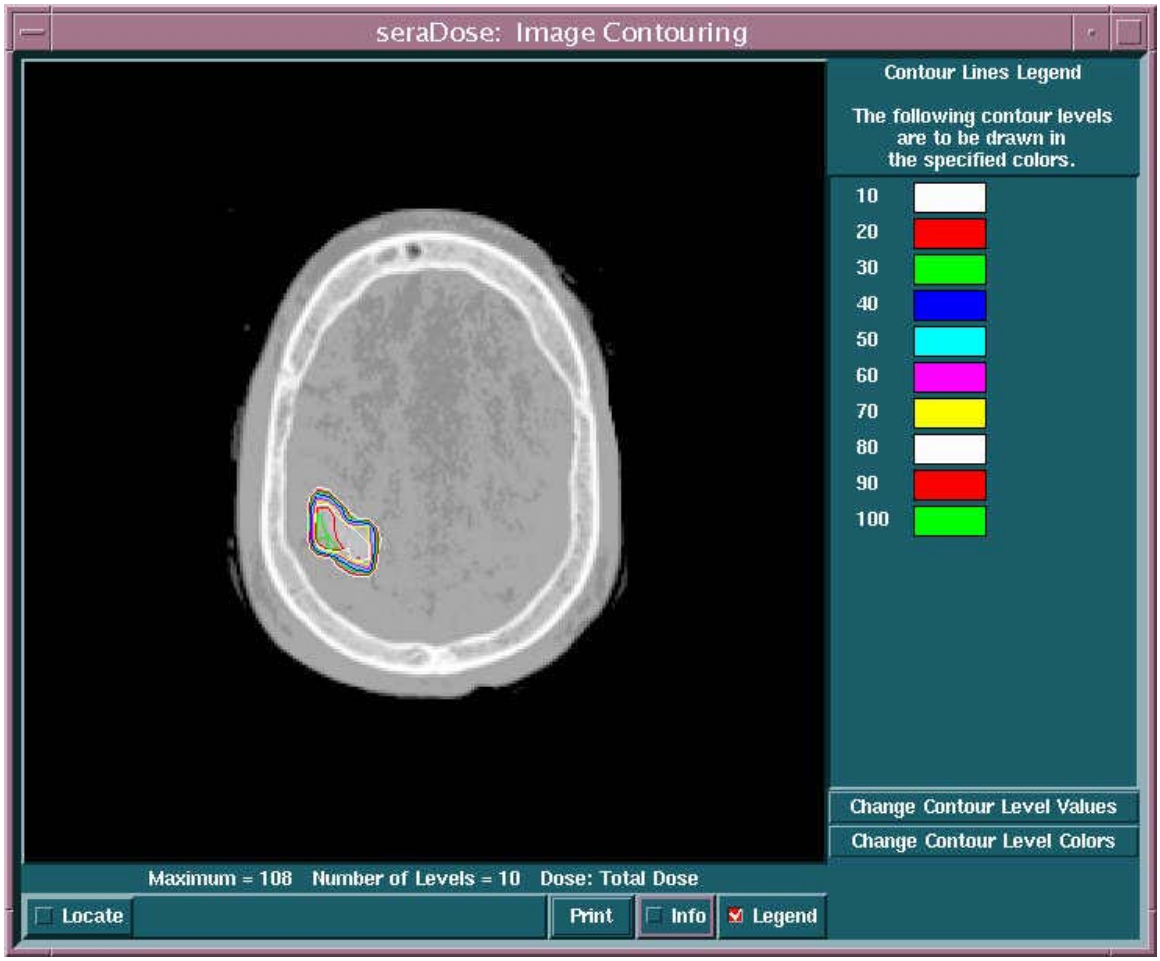

Figure 1. Dose results for calculations with a concentration of 0.17 □Ci/g of ^{131}I in the tumor.

CONCLUSION

The capability to perform MTR dose calculations using a demonstration tool, Seragrine, has been successfully developed and exhibited. This will form the experience basis for future development of more sophisticated tools, under the auspices of the TIRADE portion of the program.

REFERENCES

1. C.L. Hartmann-Siantar, P.M. Bergstrom, W.P. Chandler, L. Chase, L.J. Cox, et. al., XIIth International Conference on the Use of Computers in Radiation Therapy, p. 19-22, Medical Physics Publishing, Madison, Wisconsin (1997).

2. PEREGRINE I/O Description, LLNL Document PG-0076v1, Lawrence Livermore National Laboratory, June 2000.

3. D.E Wessol, C.A. Wemple, F.J. Wheeler, M.T. Cohen, M.B. Rossmeier, J. Cogliati, "SERA: Simulation Environment for Radiotherapy Applications Users Manual Version 1B0," http://www.cs.montana.edu/~bnct, INEEL External Report, October 1999.

4. M.W. Frandsen, D.E. Wessol, F.J. Wheeler, D. Starkey, "Rapid Geometry Interrogation for Uniform Volume Element-Based BNCT Monte Carlo Particle Transport Simulation," Proceedings of the Eighth International Symposium on Neutron Capture Therapy, Plenum Press, New York (2001).

FILTERED EPITHERMAL PHOTONEUTRON BEAM PARAMETER STUDIES FOR NEUTRON CAPTURE THERAPY APPLICATIONS

D.W. Nigg[1], C.A. Wemple[1], W. Scates[2], and J. F. Harmon[2]

1. **Idaho National Engineering and Environmental Laboratory, Idaho Falls, ID**
2. **Idaho State University, Pocatello, ID**

INTRODUCTION

The Idaho National Engineering and Environmental Laboratory (INEEL) has been investigating the feasibility of a concept for an accelerator-based source of epithermal neutrons for Boron Neutron Capture Therapy (BNCT) and other applications that is based on the use of a two-stage photoneutron production process driven by an electron accelerator[1]. In this concept, shown in Figures 1 and 2, electron beams impinge upon heavily shielded tungsten targets located at the outer radius of a small cylindrical tank of circulating heavy water (D_2O), possibly with a beryllium insert to enhance the neutron yield. A fraction of the energy of the electrons is converted in the tungsten targets into radially-inward directed bremsstrahlung radiation. Neutrons subsequently generated by photodisintegration of deuterons in the D_2O and Be within the tank are directed to the patient through a suitable beam tailoring system. The entire assembly could be constructed as part of a standard, shielded, hospital radiotherapy facility. The activities described in this article represent the completion of a multi-year INEEL effort, in collaboration

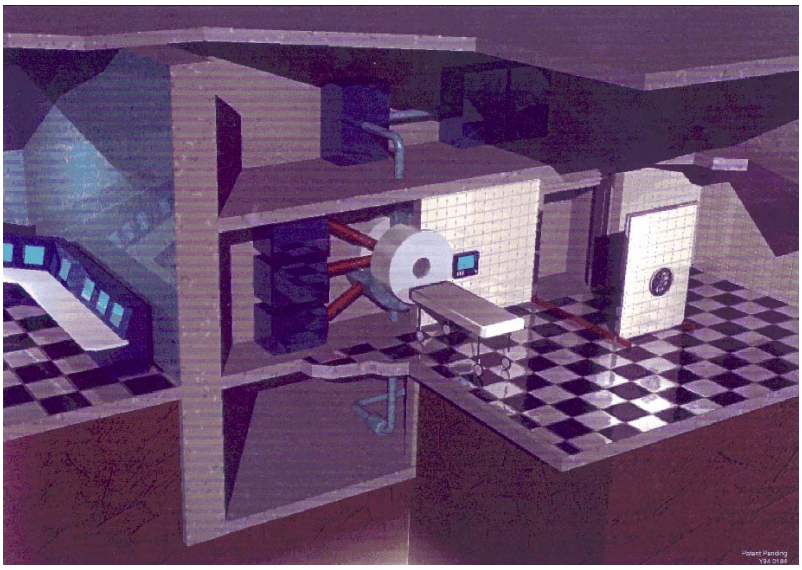

Figure 1. Artist's conception of the epithermal photoneutron source concept for BNCT.

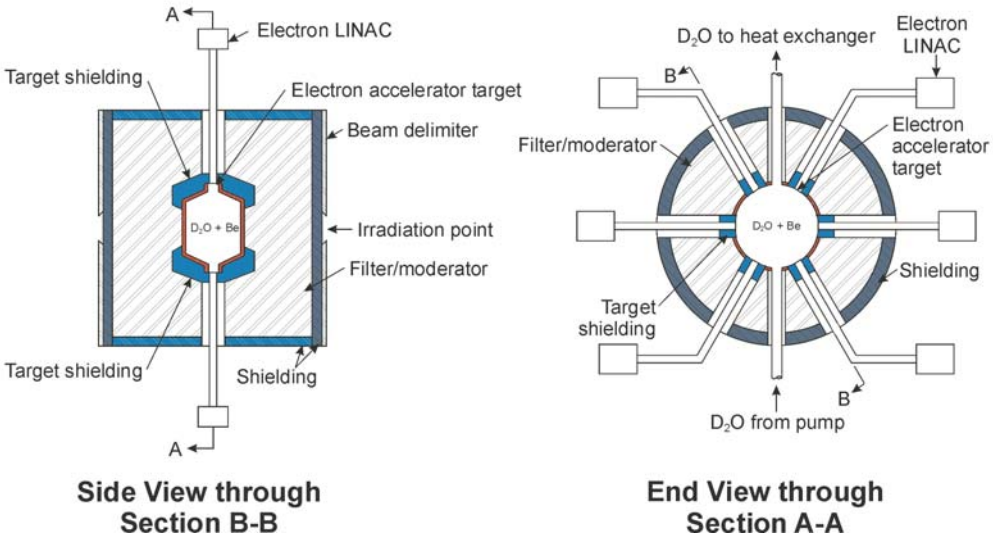

Figure 2. Schematic design of the epithermal photoneutron source concept for BNCT.

with the Idaho Accelerator Center (IAC) at Idaho State University (ISU), to experimentally demonstrate the feasibility of the concept using a realistic prototype. With some simple design changes, the device could also be adapted to the production of thermal neutrons for various purposes, including treatment of certain shallow lesions.

Initial proof-of-principal tests using a low-current, benchtop prototype of the filtered photoneutron source concept were conducted in 1994 and 1995. Testing included extensive measurements of the unfiltered photoneutron source[2], as well as initial measurements of filtered epithermal-neutron spectra produced using two different advanced neutron filtering assemblies[3,4]. In the early experiments, a tunable electron linear accelerator, manufactured by the Varian Corporation, was used to drive the experimental apparatus shown in Figure 3. The electron beam energy was established at a nominal average value of 6 MeV with an approximately gaussian distribution in energy (FWHM[a] = 2 MeV). The forward-peaked bremsstrahlung radiation from the tungsten accelerator target was collimated by a cylindrical tungsten shield and subsequently directed into a sealed cylindrical Lucite™ container of D_2O, where a well-characterized source of photoneutrons was produced. Neutron filtering and moderating structures were placed downstream of the heavy water photoneutron source region. This arrangement would not be typical of an actual clinical device, where the axis of the neutron beam would be at right angles to that of the electron beam to reduce photon contamination at the patient irradiation point. For these early experiments, however, it was desired to have a simple geometry that could be easily modeled in theoretical calculations. In addition, it was necessary to have a high photon flux at the measurement point as an independent quantitative indicator of the electron current impinging on the accelerator target, because of difficulties that were experienced with obtaining a direct measurement of the current to ground from the target itself.

[a] FWHM – full width-half maximum.

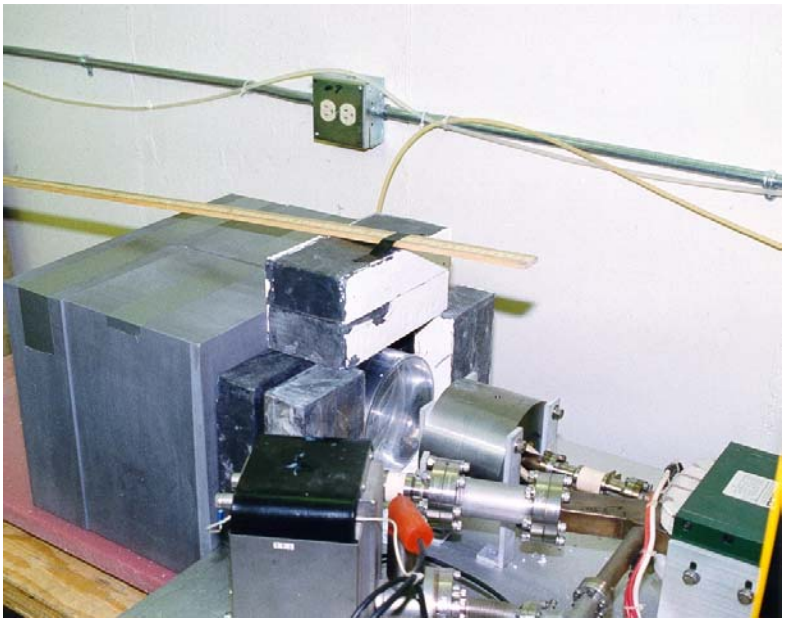

Figure 3. Early apparatus for filtered photoneutron source experiments.

The neutron filtering and moderating assembly of primary interest was constructed of a composite material (69% AlF_3, 30% Al, and 1% natural LiF, trade name FLUENTAL[a]), developed by the Technical Research Center of Finland (VTT)[5], and provided for this work to the INEEL by VTT under a research agreement. The dimensions of the filter region were 30x30x40 cm. The filter thickness along the beam axis was 30 cm. The measured density of the VTT filtering material was 3.01 g/cm^3. The entire filter was surrounded by 2.54 cm of borated polyethylene to provide a degree of isolation from room return of neutrons. A second filter assembly, composed of laminated polytetrafluoroethylene (Teflon^{TM}) and aluminum, was also tested.

Neutron intensity and spectral measurements using standard resonance and threshold activation foil techniques were performed in the early experiments. The results were generally as expected, and it was concluded that the proposed photoneutron device could offer, on the basis of neutronic performance, a promising alternate approach to the production of epithermal neutrons for BNCT. However, the measurements were performed at rather low electron currents, leading to somewhat large uncertainties in the results and, more importantly, the geometry was, by intent, not prototypical. Thus, the next stage of the development effort for this concept was focused on construction of a new experimental prototype using a much higher-power L-band electron linear accelerator (LINAC) that was concurrently being brought into operation at the IAC (Figure 4). A series of neutronic performance measurements for the new prototype has now been completed and the results are presented in this article.

[a] FLUENTAL is a trademark of the Technical Research Center of Finland.

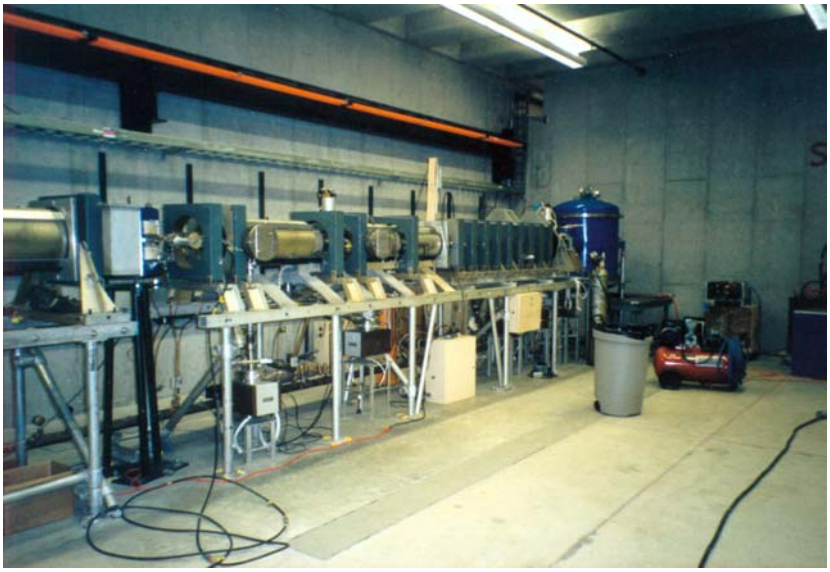

Figure 4. L-Band electron LINAC at the Idaho Accelerator Center.

METHODS AND MATERIALS

The new experimental apparatus features a more prototypical system geometry, with the irradiation point on an axis at right angles to the electron beam axis. The higher power of the L-Band LINAC has permitted neutron spectral measurements with significantly smaller experimental uncertainties. Furthermore, the right-angle geometry permits a more realistic measurement of the photon content of the source at the irradiation point. Control of photon contamination at the irradiation point is a key to the success of the overall concept.

Figure 5 shows several steps in the construction of the experimental neutron production and filtering assembly. The accelerator is on the opposite side of the concrete shielding wall in the background of Figure 5a. Electrons from the accelerator are magnetically directed through an evacuated drift tube that passes through a hole in the shield wall. A water cooled tungsten target is located at the end of the drift tube, slightly recessed in the hole in the shielding wall (Figure 5b). A cylindrical aluminum tank of heavy water, approximately 30.5 cm in diameter and 15.24 cm in height, is positioned with its curved surface tangent to the wall, in front of the accelerator target, as shown in Figure 5c. Hence, the bremsstrahlung photons produced in the target impinge radially onto the tank. The previously-described block of FLUENTAL filtering material, placed adjacent to the face of the tank, with the 40-cm dimension aligned perpendicular to the electron beam axis, is also shown. Neutrons emanating from the tank are thus filtered and moderated through 40 cm of filter/moderator material before emerging on the downstream (in the sense of neutron flow) side of the filter-moderator, toward the left side of Figure 5c. The entire assembly is surrounded by a reflecting region composed of aluminum oxide and lead blocks, as shown in Figure 5d. Finally, Figure 6 shows a view of the electron drift tube passing into one side of the shield wall, with the filter/moderator assembly on the other side.

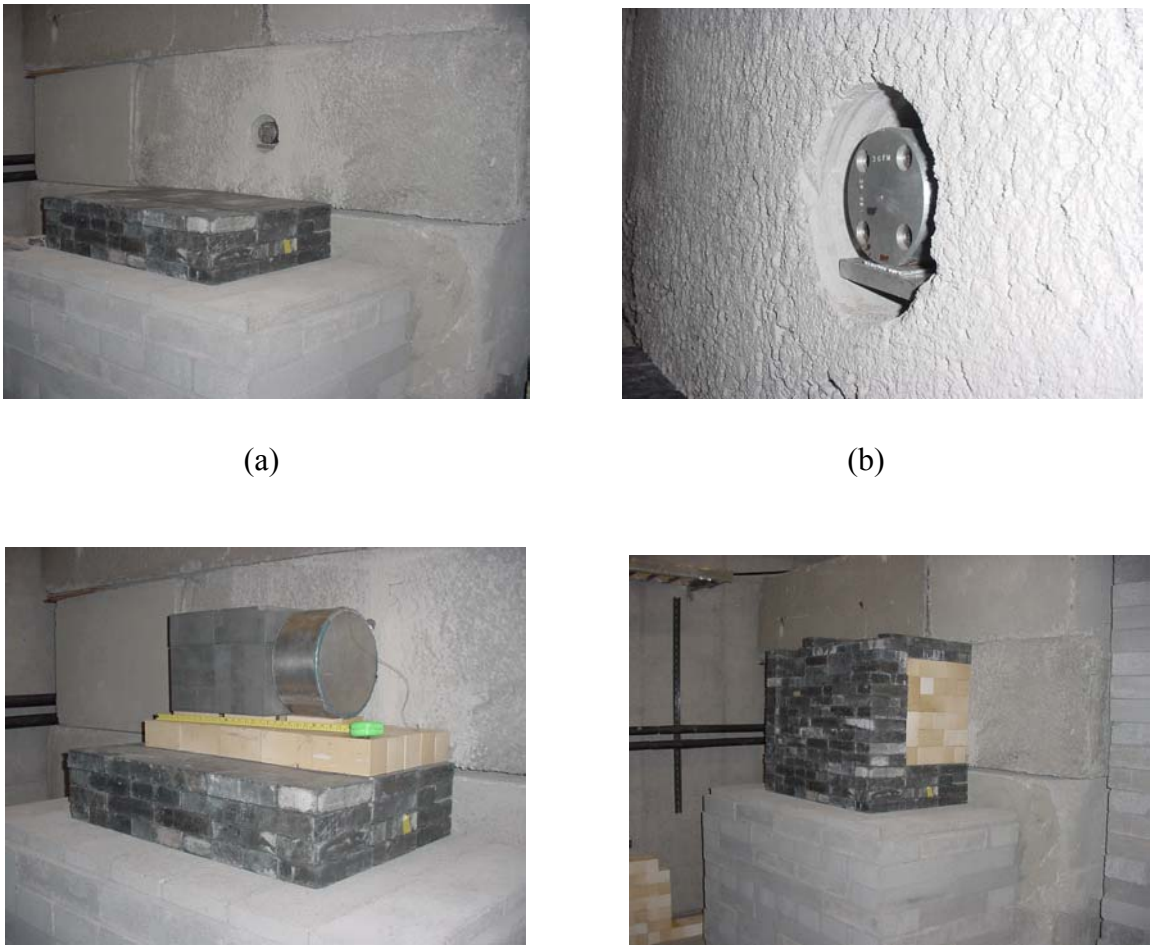

(a) (b)

(c) (d)

Figure 5. Photoneutron production and filtering assembly showing; (a) the shielding wall through which the electron drift tube passes; (b) a close-up of the accelerator target assembly; (c) a view filtering assembly, with the FLUENTAL filter-moderator blocks on the left (downstream) side of the heavy water tank; and (d) the complete assembly surrounded by a lead reflector/shield region, with aluminum oxide reflector blocks on the back side of the heavy water tank.

Neutron spectrum measurements were performed using simplified extensions of neutron activation analysis techniques[6,7] that have been adapted for BNCT applications by the INEEL through extensive experience with several other epithermal-neutron facilities in the U.S. and in Europe. Neutronically thick circular foils of various types were used. The foil specifications and corresponding neutron activation interactions of interest are listed in Table 1.

Figure 6. View perpendicular to the electron beam axis, showing the shielding wall, the accelerator drift tube on the right, and the filter/moderator/reflector assembly on the left.

Table 1. Activation interactions and foils used for the filtered epithermal photoneutron measurements.

Neutron Interaction	Nominal Foil Mass (g)	Nominal Foil Thickness (cm)	Energy Range of Primary Response	Activation Gamma Energy of Interest (keV)
^{115}In (n, γ)	0.30	0.0127	1 eV Resonance	1293,1097, and 416
^{197}Au (n, γ)	0.18	0.00254	5 eV Resonance	411
^{63}Cu (n, γ)	8.0	0.2	1 keV Resonance	511 (Positron)
^{115}In (n,n')	9.0	0.4	430 keV Threshold	336

Duplicate foils of each type were placed in a borated polyethylene positioning assembly, as shown in Figure 7. The foils were all approximately 2 cm in diameter. The central cavity of the positioning assembly was lined with cadmium. Indium, gold, and copper foils, as described in Table 1, were placed in cadmium covers and arranged around the periphery of the central cavity as shown. Bare gold foils wrapped in aluminum foil were also placed as shown. A calibrated ion chamber with buildup cap (Radcal^{TM} 1510) was placed at the top of the central cavity to indicate the photon dose rate at the measurement location. (This chamber is also somewhat sensitive to neutrons, but, as will be seen later, the neutron dose rate is significantly smaller than the photon dose rate in this particular experimental setup).

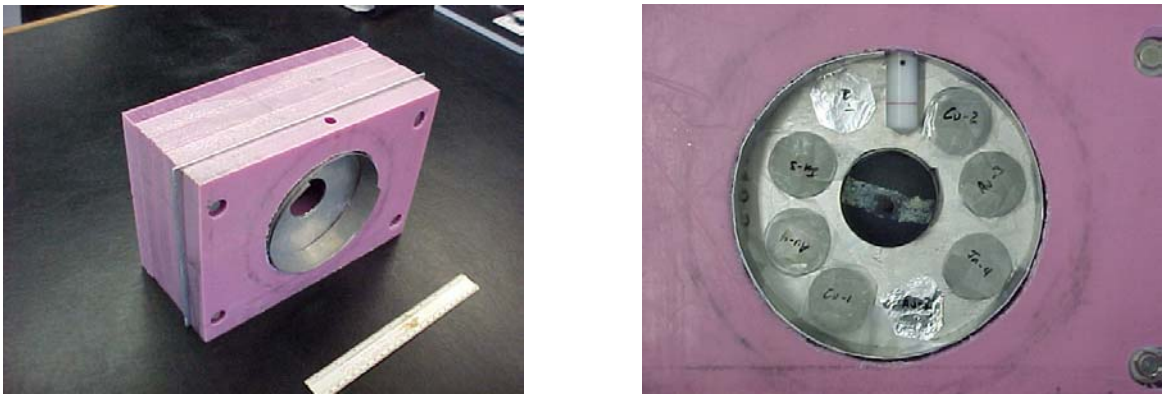

Figure 7. Detail of foil positioning and shielding assembly.

Finally, heavy indium foils with properties shown in the last line of Table 1 were placed in a small hollow boron sphere located in the center of the cavity. The composition of the sphere is approximately 93% ^{10}B and 7% ^{11}B by weight, with a total boron density of 2.6 g/cm^3. The inside diameter of the boron sphere is approximately 2.8 cm (1.1 in). The outside diameter is approximately 4.75 cm (1.9 in). This arrangement provides essentially total suppression of thermal and epithermal flux within the inner cavity of the boron sphere. Thus, an artificial threshold above the resonance energy range is imposed on the neutron capture reactions in the foil within the sphere. Since the activation gamma emissions that arise from neutron capture in indium are thereby suppressed, the relatively weak 336 keV gamma line from inelastic scatter in indium, which is of crucial interest in these measurements, is much more prominent in the spectrum of the activated indium foil. The activated indium foil is also much easier to handle when the boron sphere is used in this manner, since the induced activity is significantly lower than it would be without the sphere.

Use of the foils as described provided 5 basic neutron response functions with a useful degree of linear independence. These response functions were:

1. Resonance capture in the copper, gold, and indium foils in the foil wheel, all with thermal neutron capture suppressed by cadmium (3 responses);

2. Total neutron capture in the single uncovered gold foil in the foil wheel (1 response);

3. Inelastic scatter in the indium foil in the boron sphere (1 response).

Figure 8 shows the downstream (in the sense of neutron flow) side of the completed filtering assembly, surrounded by an aluminum oxide and lead reflector, with bismuth photon shielding blocks (thickness = 10 cm) placed on the downstream face of the FLUENTAL neutron filtering and moderating region. The borated polyethylene enclosure for positioning the various radiation measuring devices is shown adjacent to the center of the face of the bismuth shielding blocks.

Figure 8. Downstream side of the completed neutron filtering assembly, with foil positioning shield in place.

The results reported here are for three different average electron beam energies within the operating range of the L-Band LINAC. The three irradiations were designed to obtain data from about 4 MeV to about 15 MeV to provide a characterization of the system performance as a function of electron beam energy, and to thereby experimentally estimate the optimum electron energy. An optimum electron energy, believed to be in the range of 6-10 MeV, will exist since higher electron energies produce a higher total neutron yield, but at the same time more high energy neutrons are produced. Thus, additional neutron filtration and moderation is required to produce an epithermal neutron spectrum having the desired suppression of the above-epithermal neutron flux. The increased filter-moderator thickness that is required with increasing electron energy counteracts the higher neutron yield.

Figure 9 shows the measured electron beam spectra for each of the three irradiations. These spectra were measured by sweeping the electron beam across the target using an analyzing magnet and measuring the relative electron current to ground from the target in the usual manner. The three average electron beam energies obtained were 4.6 MeV ("Low"), 8.0 MeV ("Nominal"), and 11.7 MeV ("High"), with distributions of electron energy about these mean values as shown in Figure 9. The spectra have relatively large full widths at half-maximum. This is a characteristic of the electron LINAC at the operating currents used.

The irradiated foils were assayed by the ISU Environmental Radiation Measurements Laboratory using standard high-purity germanium (HPGe) gamma spectrometry systems (Canberra/Genie^{TM}) calibrated against National Institute of Standards and Technologies (NIST)-traceable standards. The induced activities in the free-beam foils were estimated from the net

photo peak areas and system efficiencies per standard procedures for the Genie™ system. The measured activities of

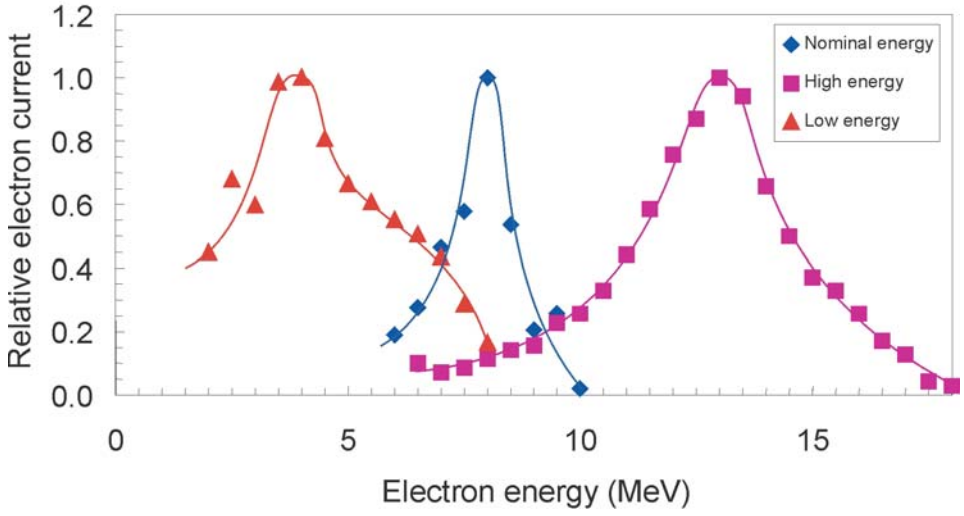

Figure 9. Electron energy spectra for the three accelerator energies examined.

the heavy indium foils in the boron sphere were corrected for gamma self-shielding using an escape fraction at 336 keV, calculated using a combination of MCNP[9] numerical computations and handbook data for the specific source-detector geometry that was used for the assay. The escape fraction used for these foils was 0.85 ± 0.02. The other foils had much higher escape fractions, greater than 0.95. Finally, the measured induced activities of the foils were then converted to equivalent saturation activities using the standard radioactive isotope buildup and decay formulas.

RESULTS

The measured saturation activities of the various foils are shown in Tables 2-4. Some entries in these tables are listed as "Not Available" for various reasons. In the case of the 336 keV line from inelastic scatter in indium, the activity was so low that sometimes reliable results could not be measured, especially in the case of the lowest electron beam energy. In a few other cases, the calibration of the spectrometer was suspect. In any event, enough usable data was obtained for each case to produce a reasonable result for the neutron spectrum at the irradiation point. The statistical uncertainties given in Tables 2-4 include the uncertainty of the spectrometer calibration, as well as the uncertainty of the activity measurement for each foil.

In each case, the measured activation results were used to derive the neutron spectra of the photoneutron flux at the measurement location using a direct, few-group, overdetermined, least-squares matrix unfolding procedure, adapted by the INEEL for this type of measurement as discussed in Reference 8. All theoretical system performance computations and effective foil activation cross section computations that were required to support the unfolding process described in the reference were performed using the MCNP[9] and ITS[10] codes. Figures 10-12

show the unfolded, few-group, free-field neutron spectra at the downstream face of the bismuth shield for each case.

Table 2. Foil saturation activities measured at an electron energy of 4.6 MeV and an electron current of 94 microamperes.

Neutron Interaction		Saturation Activity[4] – First Foil (Bq/atom)	Saturation Activity- Second Foil (Bq/atom)
^{197}Au (n, γ)[1]		3.40×10^{-17} (5.5%)	Not Available
^{115}In (n, γ)[2]	1293 keV	2.37×10^{-17} (5.1%)	2.18×10^{-17} (5.1%)
	1097 keV	2.52×10^{-17} (5.1%)	2.26×10^{-17} (5.1%)
	416 keV	2.37×10^{-17} (5.1%)	2.30×10^{-17} (5.1%)
^{197}Au (n, γ)[2]		3.04×10^{-17} (5.5%)	3.04×10^{-17} (5.8%)
^{63}Cu (n, γ)[2]		9.80×10^{-20} (5.7%)	1.19×10^{-19} (5.9%)
^{115}In (n,n')[3]		Not Available	5.94×10^{-22} (42.7%)

1. Bare foil.
2. Cadmium covered foil.
3. Foil in boron sphere.
4. Percentage uncertainty (1σ) given in parentheses.

Table 3. Foil saturation activities measured at an electron energy of 8.0 MeV and an electron current of 64.6 microamperes.

Neutron Interaction		Saturation Activity[4] – First Foil (Bq/atom)	Saturation Activity- Second Foil (Bq/atom)
^{197}Au (n, γ)[1]		Not Available	7.37×10^{-17} (5.1%)
^{115}In (n, γ)[2]	1293 keV	4.70×10^{-17} (5.0%)	4.46×10^{-17} (5.0%)
	1097 keV	4.87×10^{-17} (5.0%)	4.61×10^{-17} (5.0%)
	416 keV	4.74×10^{-17} (5.0%)	4.64×10^{-17} (5.0%)
^{197}Au (n, γ)[2]		6.86×10^{-17} (5.1%)	6.60×10^{-17} (5.1%)
^{63}Cu (n, γ)[2]		2.36×10^{-19} (5.2%)	2.47×10^{-19} (5.3%)
^{115}In (n,n')[3]		6.24×10^{-22} (7.1%)	5.17×10^{-22} (8.4%)

1. Bare foil.
2. Cadmium covered foil.
3. Foil in boron sphere.
4. Percentage uncertainty (1σ) given in parentheses.

Table 4. Foil saturation activities measured at an electron energy of 11.7 MeV and an electron current of 112.6 microamperes.

Neutron Interaction	Saturation Activity[4] – First Foil (Bq/atom)	Saturation Activity- Second Foil (Bq/atom)
^{197}Au (n, γ)[1]	Not Available	1.17 x 10^{-16} (5.3%)
^{115}In (n, γ)[2] 1293 keV	Not Available	Not Available
^{115}In (n, γ)[2] 1097 keV	Not Available	Not Available
^{115}In (n, γ)[2] 416 keV	Not Available	Not Available
^{197}Au (n, γ)[2]	1.08 x 10^{-16} (5.2%)	1.01 x 10^{-17} (5.4%)
^{63}Cu (n, γ)[2]	3.70 x 10^{-19} (5.5%)	3.96 x 10^{-19} (5.9%)
^{115}In (n,n')[3]	4.60 x 10^{-21} (5.5%)	4.35 x 10^{-21} (7.7%)

1. Bare foil.
2. Cadmium covered foil.
3. Foil in boron sphere.
4. Percentage uncertainty (1σ) given in parentheses.

The unfolding method produces the imputed unperturbed spectrum at the location of the center of the boron sphere, corrected for self-shielding and corrected for the effect of the radial flux distribution across the foil holding plate, because not all of the foils were actually located at the center. The computed *a-priori* neutron spectra, normalized to produce the same total integrated flux corresponding to the measurement, are also shown in Figures 10-12 for comparison. The unfolding group structures used to represent the measured spectra were selected to provide well-conditioned unfolding matrices, and to permit the most accurate integration of the measured spectra in the epithermal energy range to determine the total epithermal neutron flux.

It will be observed that the propagated uncertainties associated with the thermal fluxes (E < 0.404 eV) in Figures 10-12 are quite large. This is because, by design, the thermal flux is very small compared to the remainder of the spectrum in each case. The measured activities of the gold foils with and without Cd covers differ by only a few percent --- a difference that is comparable to the uncertainties of the activities themselves. This leads to a magnification of the uncertainty when the thermal flux is estimated from these foil activities in the spectral unfolding process. The propagated uncertainty associated with the high-energy neutron flux in the case of the lowest electron beam energy, is also quite large. This is because the high-energy flux is so low in this case.

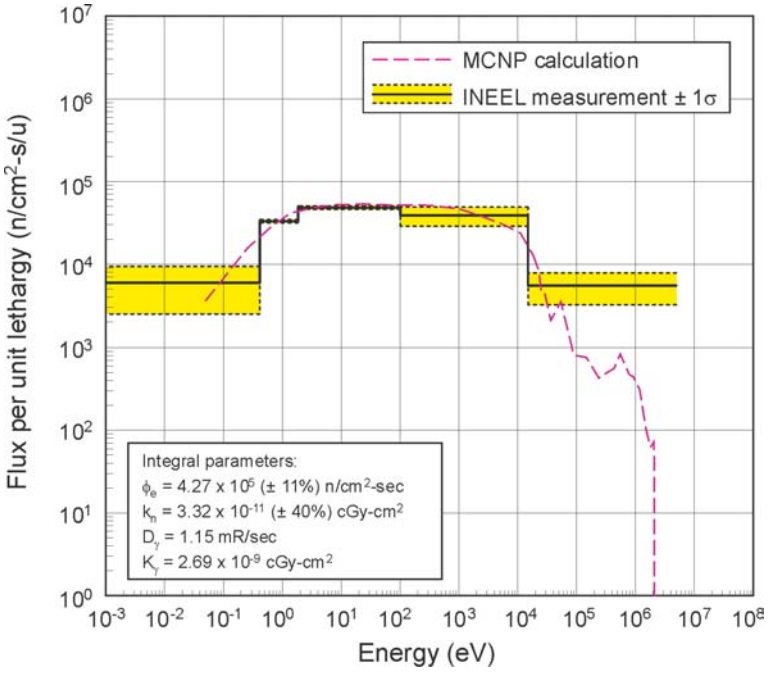

Figure 10. Unfolded neutron flux spectrum obtained by direct fitting of least-squares fitting of foil activation data for E_e = 4.7 MeV and J_e = 94 microamperes.

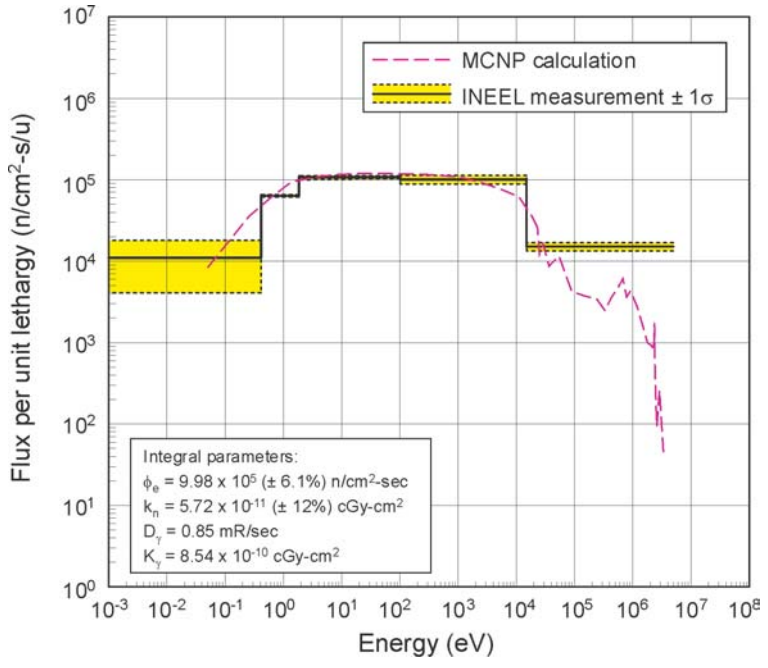

Figure 11. Unfolded neutron flux spectrum obtained by direct least-squares fitting of foil activation data for E_e = 7.97 MeV and J_e = 64.6 microamperes.

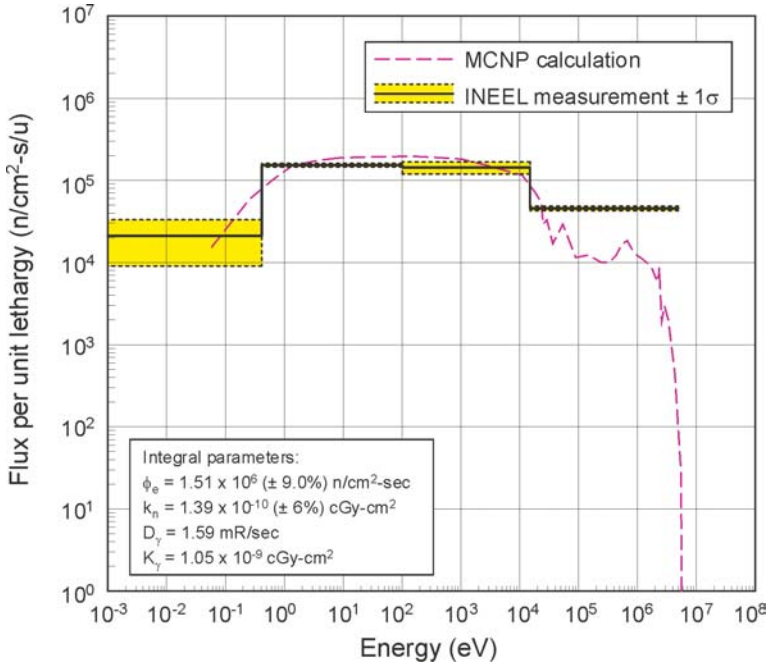

Figure 12. Unfolded neutron flux spectrum obtained by direct least-squares fitting of foil activation data for E_e = 11.7 MeV and J_e = 112.6 microamperes.

Table 5 shows some integrated parameters computed from the unfolded spectrum data. In particular, the integrated fast (E > 10 keV) and epithermal (0.414 < E < 10 keV) fluxes, normalized to a current of 1 milliampere in each case, are given. As anticipated, there is an optimum near 8 MeV electron beam energy. Lower electron beam energies produce lower epithermal fluxes because of the lower overall neutron yield. Higher electron beam energies produce a higher yield, but there is a larger fast-neutron component in the source, at the expense of the epithermal component if the filter/moderator thickness is held constant.

Table 5. Integral flux parameters for the measured photoneutron spectra.

Electron Energy (MeV)	Electron Current (mA)	Fast Neutron Flux (n/cm^2-s-mA)	Epithermal Neutron Flux (n/cm^2-s-mA)
4.6	0.094	4.27 x 10^5 (33%)	4.54 x 10^6 (11%)
8.0	0.065	1.81 x 10^6 (12%)	1.53 x 10^7 (6%)
11.7	0.113	2.94 x 10^6 (9%)	1.34 x 10^7 (9%)

Note: Percentage uncertainty (1σ) given in parentheses.

Additional neutron moderating and filtering material would reduce this fast neutron component, but the additional filtering thickness would increase the geometric divergence of the neutron source. Multiplying the measured epithermal neutron flux for the medium energy case by the design current for a full-scale device (100 mA) yields a useful epithermal flux of 1.5 x 10^9 n/cm^2-s. This flux level is comparable to that of typical research reactor-based epithermal neutron sources used for recent clinical trials of BNCT[5-7].

A simple, but widely used, metric for the quality of epithermal-neutron beams is based on dividing the free-field neutron KERMA rate of the beam (integrated over all energies above thermal) by the useful epithermal-neutron flux, again measured in the free field. This parameter is an indicator of the non-selective background dose that will be produced in tissue by the above-thermal spectral component of the beam itself, in the absence of any neutron capture agent that may be administered to the patient. It can be computed using the measured flux spectrum in conjunction with broad group KERMA factors based on standard data for the components of biological tissue[11]. This procedure yields the results shown in Table 6 for all three electron beam energies. In this table, the neutron KERMA rate is first normalized to the electron current. For the medium electron energy case, the measured free-beam neutron contamination is 5.7 x 10^{-11} cGy total neutron KERMA from all components per unit useful epithermal-neutron fluence (estimated uncertainty approximately 10%). This is within the range that has historically been considered clinically acceptable, although a few more centimeters of filtering to bring this component of the beam down to the range of about 2.0 x 10^{-11} cGy per unit flux would be desirable in a clinical device. Approximately 91% of the background neutron dose results from proton recoil. The remainder is from other recoil components. Additional background dose in tissue is, of course, produced by non-selective thermal-neutron induced components, primarily from neutron capture in nitrogen and hydrogen, but these components are not directly indicative of the intrinsic biophysical quality of the incident beam. They must be taken into account in treatment planning, but they are not normally included in the free-beam quality parameter discussed here.

Table 6. Neutron KERMA parameters for the measured photoneutron spectra.

Electron Energy (MeV)	Electron Current (mA)	Neutron KERMA Rate (mrad/mC)	Neutron Contamination (cGy-cm^2)
4.6	0.094	0.15	3.32 x 10^{-11}
8.0	0.065	0.88	5.72 x 10^{-11}
11.7	0.113	1.86	1.39 x 10^{-10}

Finally, the photon contamination of the neutron source can be estimated by dividing the measured photon dose rate (from the ion chamber shown in Figure 7) by the measured electron current. For the measurements presented here, this procedure yields the results shown in Table 7 for all three electron beam energies. The dose rates are approximately three orders of magnitude smaller than was measured in the earlier experiments, where the electron beam axis passed through the neutron flux measurement location (Figure 3). Thus, the objective of significantly reducing the photon contamination of the neutron beam using an arrangement with the neutron beam axis at right angles with the electron beam axis was achieved by a combination of geometry and shielding at the measurement location.

Table 7. Photon dose and KERMA parameters for the measured photoneutron spectra.

Electron Energy (MeV)	Electron Current (mA)	Photon Dose Rate (mrad/mC)	Photon Contamination (cGy-cm^2)
4.6	0.094	12.2	2.69×10^{-9}
8.0	0.065	13.2	8.54×10^{-10}
11.7	0.113	14.1	1.05×10^{-9}

Dividing the photon dose rates in Table 7 by the useful epithermal neutron flux provides estimates of the free-beam photon contamination in each case. In the case of the 8 MeV electron beam, this produces a value of 8.5×10^{-10} gamma dose per unit useful epithermal neutron fluence. This is approximately 40 times higher than is clinically desirable, but Monte Carlo computations using the MCNP code show that the incident photon dose rate at the irradiation point can be reduced as needed by the appropriate placement of additional shielding around the electron accelerator target, as shown in Figure 2. Such shielding was not installed in the apparatus discussed here because of difficulties associated with the constraints imposed by a fixed electron drift tube length, in combination with the fixed configuration of the concrete shielding between the accelerator and the neutron production assembly. Finally, it can be seen that there is a minimum in the photon contamination at an electron beam energy in the range of 8 MeV, as expected. This is because higher electron beam energies produce a higher gamma dose rate without a commensurate increase in the epithermal neutron flux, as discussed previously.

DISCUSSION

The results presented here provide experimental validation of the expected performance of the electron accelerator-based concept for production of medically useful epithermal-neutron sources for neutron capture research research. The efficiency (in terms of useful neutrons produced per initial accelerated charged particle) of the electron accelerator-based approach presented here is somewhat smaller than is typical for various light-ion accelerator-based schemes (see, for example, Reference 12). However, the complicated target cooling schemes

associated with such systems are not required for the electron-based system. Furthermore, the accelerator target (or multiple targets) can be integrated into the central D_2O containment structure in such a manner that the heavy water also serves as a target coolant, with circulation of the D_2O through a heat exchanger via a closed system to contain the tritium that is produced by neutron capture in deuterium.

REFERENCES

1. W.Y. Yoon, J.L. Jones, D.W. Nigg, Y.D. Harker, "Accelerator-Based Neutron Source for Boron Neutron Capture Therapy (BNCT) and Method," United States Patent 5903622, May, 1999.

2. D.W. Nigg, H.E. Mitchell, W.Y. Yoon, Y.D. Harker, J.L. Jones, "An Accelerator-Based Epithermal Photoneutron Source for BNCT," In: Mishima Y (ed), Cancer Neutron Capture Therapy, Plenum Press, NY, 1996, pp 425-430.

3. D.W. Nigg, H.E. Mitchell, Y.D. Harker, J.F. Harmon, "Experimental Investigation of Filtered Epithermal Photoneutron Beams for BNCT," In: Larsson, et al. (eds.), Advances in Neutron Capture Therapy, Volume I, Medicine and Physics, Elsevier Science BV, 1997, pp 477-481.

4. H.E. Mitchell, "An Accelerator-Based Epithermal Photoneutron Source for Boron Neutron Capture Therapy," PhD Thesis, Georgia Institute of Technology, UMI Dissertation Services, Ann Arbor, MI, April 1996.

5. I. Auterinen, P Hiismäki, T Serén, T. Seppälä, "Creating an Epithermal-Neutron Field for BNCT Using a TRIGA Reactor and an Aluminum Fluoride Composite as Neutron Moderator," In: Proceedings of the 1998 ANS Radiation Protection and Shielding Division Topical Conference, Technologies for the New Century, April 19-23, 1998, Nashville, Tennessee, USA, ANS 1998, Vol 2.

6. D.W. Nigg, et al., "Collaborative Neutronic Performance Characterization of the FiR 1 Clinical Epithermal-Neutron Beam Facility for BNCT," In: J.R. Venhuizen (ed,), INEEL BNCT Research Program Annual Report 1998, INEL/EXT-99-00293, April 1999, pp 13-38.

7. Y.D. Harker, et al., "Spectral Characterization of the Epithermal Neutron Beam at the Brookhaven Medical Research Reactor," Nuclear Science and Engineering, **110**:355-368, 1992.

8. D.W Nigg, C.A. Wemple, R. Risler, J.K. Hartwell, Y.D. Harker, G.E. Laramore, "Modification of the University of Washington Neutron Radiotherapy Facility for Optimization of Neutron Capture Enhanced Fast-Neutron Therapy," Medical Physics, **27**:359-367, 2000.

9. J.F. Briesmeister, MCNP - A General Monte Carlo Code for Neutron and Photon Transport, 1986, LA-7396 (Rev 2).
10. J.A. Hablieb, et. al., "ITS- The Integrated Tiger Series of Coupled Electron/Photon Transport Codes," SAND84-05873, Sandia National Laboratory, November, 1984.

11. D.W. Nigg, P.D. Randolph, F.J. Wheeler, "Demonstration of Three-Dimensional Deterministic Radiation Transport Theory Dose Distribution Analysis for Boron Neutron Capture Therapy," Medical Physics 18:43-53, 1991.

12. C-K. C. Wang, T.E. Blue, R. Gahbauer, "A Neutronic Study of an Accelerator-Based Neutron Irradiation Facility for Boron Neutron Capture Therapy," Nuclear Technology, **84**:93-107, 1989.